Antenna Laboratory Report No. 66-15

Scientific Report No. 8

THE THEORETICAL AND EXPERIMENTAL DETERMINATION OF THE INPUT IMPEDANCE OF A SMALL LOOP OF ELECTRIC CURRENT IMMERSED IN AN ANISOTROPIC PLASMA

G. L. Duff and R. Mittra

October 1966

Sponsored by the National Aeronautics

and Space Administration under Grant Ns G-395

Department of Electrical Engineering

Engineering Experiment Station

University of Illinois

Urbana, Illinois

ABSTRACT

In this study the exact expression for the input impedance of a small loop of uniform electric current is derived for the case when the loop is immersed in an infinite, homogeneous, cold, anisotropic plasma. Due to the nature of the exact expressions, the loop impedance is calculated by two methods of approximation for the case where the imposed steady magnetic field is normal to the plane of the loop. The first method uses the quasi-static approximation, for which a first order correction term is also calculated. The second approximate method involves the assumption that the medium is uniaxial.

The loop impedance is also calculated under the uniaxial approximation for the case where the imposed steady magnetic field is parallel to the loop.

A discussion of the experimental techniques in measuring the loop impedance is given. A brush-cathode discharge chamber was used in the experimental program.

The theoretically derived impedance formulae are numerically evaluated for a wide range of the plasma parameters and the measured loop impedance is compared to the theory. There is good general agreement between the theoretical and measured loop impedance.

ACKNOWLEDGMENT

The authors wish to acknowledge the support of the National Aeronautics and Space Administration through their Grant No. NsG 395.

TABLE OF CONTENTS

CHAPTER Page

LIST OF FIGURES

CHAPTER 1 INTRODUCTION

A considerable amount of attention has been directed recently to the study of the anisotropic magneto-plasma. Extensive studies have been carried out regarding the electromagnetic properties of electric dipoles in such media, (Balmain, 1963, Mittra and Duff, 1965).

Some initial studies of the electromagnetic properties of an infinitesimal loop of electric current have been made, (Wu, 1963, Duff, 1965). The radiation resistance of an infinitesimal magnetic dipole has been calculated by Weil, Walsh (1965).

It would be most useful to obtain expressions for the input impedance of a loop immersed in an anisotropic plasma. Because of the complex nature of solving Maxwell's equations for a current distribution, the loop in this study was assumed to be small and an uniform current distribution has been assumed. The plasma is also assumed to be cold to avoid the complexities of dealing with the acoustic phenomena of a warm plasma.

In Chapter 2 the medium is described and the general impedance formula for the steady magnetic field normal to the loop is derived by means of the induced e.m.f. method. The loop of current is described and the Fourier transformed Maxwell's equations are solved. The impedance of the loop is then given in terms of the transformed magnetic field.

In Chapter 3 the quasi-static approximation is introduced to facilitate the solution of the loop impedance. Chapter 4 gives a first order correction term

to the quasi-static result.

Chapter 5 introduces the use of the uniaxial approximation and the loop impedance is derived under these conditions.

In Chapter 6 the steady magnetic field is turned 90^{o} so that it is parallel to the loop and the impedance is again calculated using the uniaxial approximation.

Chapter 7 deals with construction and operation of the brush cathode plasma chamber and all the associated equipment used in the experimental determination of the loop impedance.

Chapter 8 gives a description of the numerical techniques used to evaluate the theoretical formulae derived in the earlier chapters.

Chapter 9 gives a discussion of the theoretical results and the kind of results that should be expected in the experimental measurements.

In Chapter 10 the computed numerical results for a wide range of electron density and imposed steady magnetic field are presented and discussed.

Chapter 11 presents the loop impedance measured under a variety of plasma conditions, along with a discussion of the results. All of these numerical results are presented on Smith Charts for the sake of clairty.

Finally Chapter 12 presents the conclusions of the study.

CHAPTER 2 DERIVATION OF THE EXACT THEORY; $\overline{B}_o$ NORMAL TO THE LOOP

2.1 The Magneto-Ionic Medium

The medium that will be considered in this study is known as an anisotropic plasma. Certain assumptions regarding the medium have been made. It is considered to be electrically neutral, that is the electron density is equal to the ion density. In addition, a steady D.C. magnetic field, $\overline{B}_o$, is assumed to exist in the positive $\hat{z}$-direction of the Cartesian co-ordinate system. The ions, being so much heavier than the electrons, are considered to be stationary and the electrons move with velocity $\overline{v}$ due to the forces exerted by the D.C. magnetic field, $\overline{B}_o$, and the r.f. electric field, $\overline{E}$. The force due to the r.f. magnetic field is relatively small and is neglected. If one assumes the medium to be homogeneous and infinite in extent and solves the force equation for the electrons, including frictional forces due to electron collisions with gas molecules and ions, one obtains the following familiar constitutive relations for the medium.

$$\overline{D} = \varepsilon_o \overline{\overline{K}}\,\overline{E} \quad \text{and} \quad \overline{B} = \mu_o \overline{H} \tag{2.1.1}$$

The relative permittivity tensor $\overline{\overline{K}}$ is

$$\overline{\overline{K}} = \begin{bmatrix} K_1 & jK_{11} & 0 \\ -jK_{11} & K_1 & 0 \\ 0 & 0 & K_o \end{bmatrix} \tag{2.1.2}$$

where
$$K_1 = 1 - \frac{XU}{U^2 - Y^2} \tag{2.1.3}$$

$$K_o = 1 - \frac{X}{U} \tag{2.1.4}$$

$$K_{11} = \frac{XY}{U^2 - Y^2} \tag{2.1.5}$$

and
$$X = \frac{\omega_N^2}{\omega^2}, \quad \omega_N^2 = \frac{Ne^2}{m\varepsilon_o} \tag{2.1.6}$$

$$Y = \frac{\omega_H}{\omega}, \quad \omega_H = \frac{eBo}{m} \tag{2.1.7}$$

$$U = 1 - jZ, \quad Z = \frac{\nu}{\omega} \tag{2.1.8}$$

The following is a list of symbols used throughout.

ω = r.f. radian frequency.

μ_o = magnetic permeability of free space.

ε_o = dielectric constant of free space.

ko = $\omega\sqrt{\mu_o\varepsilon_o}$ = free space wave number.

N = electron density.

e = magnitude of electron charge.

m = electron mass.

ν = collision frequency of electrons.

$\overline{Bo}$ = D. C. magnetic flux density.

Rationalized M. K. S. units are used throughout this study.

Maxwell's first and second equations are

$$\bar{\nabla} \times \bar{H} = j\omega \varepsilon_o \bar{\bar{K}} \bar{E} + \bar{J} \qquad (2.1.9)$$

$$\bar{\nabla} \times \bar{E} = -j\omega \mu_o \bar{H} \qquad (2.1.10)$$

The r.f. fields are assumed to be monochromatic and an $e^{j\omega t}$ time convention is used. $\bar{J}$ is the impressed electric current density of the source in the medium.

2.2 Lorentz' Reciprocity Theorem for an Anisotropic Medium

In this section the "induced e.m.f." method of impedance calculation will be derived from Lorentz' relation, (Harrington, 1961).

Consider sources $(\bar{J}_a, \bar{M}_a)$ which produce fields $(\bar{E}_a, \bar{H}_a)$ in a medium characterized by the constitutive parameters $(\varepsilon_o \bar{\bar{K}}_a, \mu_o)$. Now consider a second set of sources and fields in a second medium using subscript "b". If both sets of sources are of the same frequency, ω, then Maxwell's equations are

$$\bar{\nabla} \times \bar{E}_a = -j\omega \mu_o \bar{H}_a - \bar{M}_a \qquad (2.2.1)$$

$$\bar{\nabla} \times \bar{H}_a = j\omega \varepsilon_o \bar{\bar{K}}_a \bar{E}_a + \bar{J}_a \qquad (2.2.2)$$

and

$$\bar{\nabla} \times \bar{E}_b = -j\omega \mu_o \bar{H}_b - \bar{M}_b$$

$$\bar{\nabla} \times \bar{H}_b = j\omega \varepsilon_o \bar{\bar{K}}_b \bar{E}_b + \bar{J}_b \qquad (2.2.4)$$

Using a well known vector identity, it is easily shown that

$$\bar{\nabla} \cdot (\bar{H}_a \times \bar{E}_b - \bar{H}_b \times \bar{E}_a) = j\omega \varepsilon_o (\bar{E}_b \cdot \bar{\bar{K}}_a \bar{E}_a - \bar{E}_a \cdot \bar{\bar{K}}_b \bar{E}_b) + (\bar{E}_b \cdot \bar{J}_a - \bar{E}_a \cdot \bar{J}_b) + (\bar{H}_a \cdot \bar{M}_b - \bar{H}_b \cdot \bar{M}_a) \qquad (2.2.5)$$

Taking a volume integral of both sides of (2.2.5) and invoking the divergence theorem we have

$$\iint_{\Sigma} (\bar{H}_a \times \bar{E}_b - \bar{H}_b \times \bar{E}_a) \cdot \hat{n}\, da = j\omega\varepsilon_o \iiint_V (\bar{E}_b \cdot \bar{\bar{K}}_a \bar{E}_a - \bar{E}_a \cdot \bar{\bar{K}}_b \bar{E}_b)\, dv$$
$$+ \iiint_V (\bar{E}_b \cdot \bar{J}_a - \bar{E}_a \cdot \bar{J}_b + \bar{H}_a \cdot \bar{M}_b - \bar{H}_b \cdot \bar{M}_a)\, dv \qquad (2.2.6)$$

where Σ is the surface of the volume V, and $\hat{n}$ is the outward pointing unit vector normal to the surface Σ.

If the volume V excludes all the sources, then the second volume integral on the right hand side of (2.2.6) is zero.

Thus,

$$\iint_{\Sigma} (\bar{H}_a \times \bar{E}_b - \bar{H}_b \times \bar{E}_a) \cdot \hat{n}\, da = j\omega\varepsilon_o \iiint_V (\bar{E}_b \cdot \bar{\bar{K}}_a \bar{E}_a - \bar{E}_a \cdot \bar{\bar{K}}_b \bar{E}_b)\, dv \qquad (2.2.7)$$

The right hand side of (2.2.7) will be zero if

$$\bar{E}_b \cdot \bar{\bar{K}}_a \bar{E}_a = \bar{E}_a \cdot \bar{\bar{K}}_b \bar{E}_b \qquad (2.2.8)$$

that is

$$\bar{E}_b{}^T \bar{\bar{K}}_a \bar{E}_a = \bar{E}_a{}^T \bar{\bar{K}}_b \bar{E}_b \qquad (2.2.9)$$

but

$$\bar{E}_a{}^T \bar{\bar{K}}_b \bar{E}_b = (\bar{E}_b{}^T \bar{\bar{K}}_b{}^T \bar{E}_a)^T \qquad (2.2.10)$$

Thus, (2.2.8) will be true if $\bar{\bar{K}}_b{}^T = \bar{\bar{K}}_a$ (2.2.11)

This will be true if the direction of the magnetic field is of the opposite sense in medium "a" as compared to medium "b". In this event

$$\iint_{\Sigma} (\bar{H}_a \times \bar{E}_b - \bar{H}_b \times \bar{E}_a) \cdot \hat{n}\, da = 0 \qquad (2.2.12)$$

If we assume that the radiation condition is satisfied, then the surface integral of (2.2.12) reduces to an integral over the surface of the sources. Imposing the boundary conditions for a perfect conductor,

$$\overline{J}_a = \hat{n}x\overline{H}_a \tag{2.2.13}$$

$$\overline{M}_a = -\hat{n}x\overline{E}_a \tag{2.2.14}$$

and (2.2.12) becomes $$\iint_{\Sigma'} (\overline{E}_b \cdot \overline{J}_a - \overline{H}_b \cdot \overline{M}_a)\, da = 0 \tag{2.2.15}$$

where Σ' is the surface of the sources.

If the currents are assumed to be excited by voltages across a very small gap of width ℓ, then

$$\overline{M}_a = -\hat{n}x\overline{E}_a = -\hat{n}x\frac{V_a}{\ell} \tag{2.2.16}$$

and $$\oint \overline{H}_b \cdot d\ell = I_b = 2\pi\delta\overline{H}_b \tag{2.2.17}$$

The wire has a radius of δ. Now since $\hat{n}x\overline{E}_a$ is zero except at the gap,

$$\iint_{\Sigma'} \overline{H}_b \cdot \overline{M}_a d_a = \iint_{\Sigma''} \left(\frac{I_b}{2\pi\delta}\right)\left(\frac{-V_a}{\ell}\right) da \tag{2.2.18}$$

where Σ'' is the surface of the gap. But in this case $$da = 2\pi\delta\ell \tag{2.2.19}$$

so that $$\iint_{\Sigma'} \overline{H}_b \cdot \overline{M}_a d_a = -V_a I_b \tag{2.2.20}$$

Thus, (2.2.15) becomes $$V_a I_b = -\iint_{\Sigma'} \overline{E}_b \cdot \overline{J}_a da \tag{2.2.21}$$

Setting $$\overline{J}_a = \overline{J}_b = \overline{J} \tag{2.2.22}$$

We have $$Zin = \frac{V}{I} = -\frac{1}{I^2}\iint_{\Sigma'} \overline{E} \cdot \overline{J} da \tag{2.2.23}$$

It must be remembered that $\overline{E}$ must be calculated under the conditions of reversed steady magnetic field, as shown by (2.2.11). However, it will be demonstrated later that the electric field very near to the sources is not a func-

tion of the sense of the D. C. magnetic field and so we can calculate the input impedance of the source in the magneto-plasma using (2. 2. 23), without reversing the sense of the magnetic field.

2. 3 The Loop Geometry and the Current Density

The loop of electric current used in this chapter is assumed to be in the x-y plane. It carries a uniform current I. The radius of the loop is ρ_o and the radius of the filamentary conductor is δ. Because the radius δ is very small, the current density is mathematically approximated by a line source as

$$\bar{J} = \hat{\phi} I \delta(\rho - \rho_o)\delta(z) \qquad (2.3.1)$$

where $\delta(\rho - \rho_o)$ and $\delta(z)$ are the Dirac-Delta Functions and $\hat{\phi}$ is the unit direction vector tangent to the loop in the x-y plane. It should be noted that the conductor radius, δ, cannot be set equal to zero throughout the study, because, as will be seen, the integral representation for the impedance would not converge. The loop radius ρ_o is assumed to be very small in terms of free-space wavelengths. That is

$$k_o \rho_o \ll 1 \qquad (2.3.2)$$

2. 4 The Impedance Expression for a Small Loop

If the expression for the loop current $\bar{J}$ is substituted into the impedance expression of (2. 2. 23) one obtains,

$$Zin = -\frac{I}{I^2} \iint_{\Sigma'} \bar{E} \cdot \hat{\phi} \delta(\rho - \rho_o)\delta(z)\, da \qquad (2.4.1)$$

that is,

$$Zin = -\frac{1}{I} \iint_{\Sigma'} \hat{\phi} \cdot \bar{E}\, \delta(\rho - \rho_o)\delta(z)\, \rho\, d\rho\, d\phi \qquad (2.4.2)$$

where ρ and ϕ and the usual cylindrical co-ordinates. Using the property of the Dirac-Delta Function and integrating on ρ one obtains,

$$Zin = -\frac{\rho_o}{I}\int_0^{2\pi} \hat{\phi}\cdot\overline{E}\,\delta(z)d\phi \qquad (2.4.3)$$

which is a line integral, where

$$d\overline{l} = \hat{\phi}\rho_o\delta(z)d\phi \qquad (2.4.4)$$

Thus, (2.4.3) becomes

$$Zin = \frac{1}{I}\int_0^{2\pi} \overline{E}\cdot d\overline{l} \qquad (2.4.5)$$

Applying Stokes' theorem this becomes

$$Zin = -\frac{1}{I}\iint_{\Sigma''} \overline{\nabla}x\overline{E}\cdot\overline{dA} \qquad (2.4.6)$$

where Σ'' is the area enclosed by the loop.

Using (2.1.10), Maxwell's second equation, we have

$$Zin = \frac{j\omega\mu_o}{I}\iint_{\Sigma'''} \overline{H}\cdot d\overline{a} \qquad (2.4.7)$$

or

$$Zin = \frac{j\omega\mu_o}{I}\int_0^{2\pi}\int_0^{\rho_o} H_z\rho\, d\rho d\phi \qquad (2.4.8)$$

In this expression H_z must be calculated at $z=\delta$, the radius of the filamental wire in order that (2.4.8) yield a finite result, as discussed in the previous section.

Equation (2.4.7) is the familiar expression for the impedance of a "magnetic dipole." It is clear that the $\overline{H}$-field normal to the plane of the loop must

be obtained for the impedance calculation.

2.5 The Fourier Transform Pair and the Transformed Maxwell's Equations

The following equations define the Fourier transform pair to be used in this study.

$$\underline{\underline{\tilde{A}}}(\bar{k}) = \iiint_{-\infty}^{+\infty} \bar{A}(\bar{r}) e^{-j\bar{k}\cdot\bar{r}} d^3r \qquad (2.5.1)$$

$$\bar{A}(\bar{r}) = \frac{1}{(2\pi)^3} \iiint_{-\infty}^{+\infty} \underline{\underline{\tilde{A}}}(\bar{k}) e^{j\bar{k}\cdot\bar{r}} d^3k \qquad (2.5.2)$$

Here $\underline{\underline{\tilde{A}}}(\bar{k})$ is "the Fourier transform of the vector $\bar{A}(\bar{r})$,"

where $$\bar{r} = x\hat{x} + y\hat{y} + z\hat{z} \qquad (2.5.3)$$

and $$\bar{k} = k_1\hat{x} + k_2\hat{y} + k_3\hat{z} \qquad (2.5.4)$$

If one assumes that there are slight losses in the medium, so that the fields at infinity are zero, and the radiation condition is satisfied, Maxwell's transformed equations are

$$j\bar{k} \times \tilde{\bar{E}} = -j\omega\mu_0 \tilde{\bar{H}} \qquad (2.5.5)$$

$$j\bar{k} \times \tilde{\bar{H}} = +j\omega\varepsilon_0 \underline{\underline{K}}\tilde{\bar{E}} + \tilde{\bar{J}} \qquad (2.5.6)$$

The advantage of introducing the Fourier transform is now apparent because (2.5.5) and (2.5.6) are purely algebraic equations as opposed to the differential-equation form of Maxwell's equations in real space. The transformed $\bar{E}$ and $\bar{H}$ fields are now expressed in the Fourier domain as functions of $\bar{k}$.

It is worth noting that $\underline{\underline{K}}$ was not affected by the transformation because the medium is assumed to be infinite in extent, and homogeneous.

Solving (2.5.5) and (2.5.6) for $\tilde{\bar{H}}$ yields,

$$\bar{\bar{L}}\tilde{\bar{H}} = -j\bar{\bar{kx}}\bar{\bar{K}}^{-1}\tilde{\bar{J}} \qquad (2.5.7)$$

when $\bar{\bar{L}}$ is a tensor operator and

$$\bar{\bar{L}} = (\bar{\bar{kx}}\bar{\bar{K}}^{-1}\bar{\bar{kx}} + ko^2\bar{\bar{I}}) \qquad (2.5.8)$$

Here $\bar{\bar{I}}$ is the identity operator and ko is the free space wave number. $\bar{\bar{kx}}$ is an operator represented by

$$\bar{\bar{kx}} = \begin{bmatrix} 0 & -k_3 & k_2 \\ k_3 & 0 & -k_1 \\ -k_2 & k_1 & 0 \end{bmatrix} \qquad (2.5.9)$$

Solving (2.5.7) one obtains

$$\tilde{\bar{H}} = -j\bar{\bar{L}}^{-1}\bar{\bar{kx}}\bar{\bar{K}}^{-1}\tilde{\bar{J}} \qquad (2.5.10)$$

Inverting $\bar{\bar{L}}$ one obtains

$$\bar{\bar{L}}^{-1} = -\frac{[\bar{\bar{N}}_o + ko^2\bar{\bar{N}}_1 + ko^4\bar{\bar{N}}_2]}{ko^2(a+ko^2b+ko^4c)} \qquad (2.5.11)$$

Before proceeding any farther, the cylindrical co-ordinates of $\bar{k}$ are defined as

$$k_1 = K\cos\phi \qquad (2.5.12)$$

$$k_2 = K\sin\phi \qquad (2.5.13)$$

and therefore,

$$K^2 = k_1^2 + k_2^2 \qquad (2.5.14)$$

In (2.5.11) $\bar{\bar{N}}_o$ has components $N_{o,ij} = (K_1K^2 + K_o k_3^2)\bar{k}\bar{k}^T$ (2.5.15)

and $\bar{\bar{N}}_1$ has components $N_{1,ij}$ (illegible) (illegible)

where

$$N_{1,11} = -K_oK_1k^2 - k_1^2(K_1^2 - K_{11}^2) \qquad (2.5.16)$$

$$N_{1,12} = -jK_o K_{11} k_3^2 - (K_1^2 - K_{11}^2) k_1 k_2 \tag{2.5.17}$$

$$N_{1,13} = -K_o K_1 k_1 k_3 + jK_o K_{11} k_2 k_3 \tag{2.5.18}$$

$$N_{1,21} = jK_o K_{11} k_3^2 - (K_1^2 - K_{11}^2) k_1 k_2 \tag{2.5.19}$$

$$N_{1,22} = -K_o K_1 k^2 - k_2^2 (K_1^2 - K_{11}^2) \tag{2.5.20}$$

$$N_{1,23} = -K_o K_1 k_2 k_3 - jK_o K_{11} k_1 k_3 \tag{2.5.21}$$

$$N_{1,31} = -K_o K_1 k_1 k_3 - jK_o K_{11} k_2 k_3 \tag{2.5.22}$$

$$N_{1,32} = -K_o K_1 k_2 k_3 + jK_o K_{11} k_1 k_3 \tag{2.5.23}$$

$$N_{1,33} = -(K_1^2 - K_{11}^2) K^2 - 2K_o K_1 k_3^2 \tag{2.5.24}$$

and $$\overline{\overline{N}}_2 = K_o (K_1^2 - K_{11}^2) \overline{\overline{I}} \tag{2.5.25}$$

In the denominator, which is the determinant of $\overline{\overline{L}}$

$$a = -k^2 (K_1 K^2 + K_0 k_3^2) \tag{2.5.26}$$

$$b = (K_1^2 - K_{11}^2) K^2 + K_1 K_0 (k^2 + k_3^2) \tag{2.5.27}$$

and $$c = -K_o (K_1^2 - K_{11}^2) \tag{2.5.28}$$

It should be noted that $\overline{\overline{N}}_o \overline{\overline{kx}} = \overline{\overline{0}}$, the zero operator. Thus, upon substitution, (2.5.10) becomes

$$\underset{\sim}{H} = j \frac{[\overline{\overline{N}}_1 + ko^2 \overline{\overline{N}}_2] \overline{\overline{kxK}}^{-1} \underset{\sim}{J}}{(a + ko^2 b + ko^4 c)} \tag{2.5.29}$$

and using (2.5.2) to invert the transformed $\overline{H}$ field

$$H_z = \hat{z}\cdot\bar{H} = \frac{\hat{z}\cdot}{(2\pi)^3}\iiint_{-\infty}^{\infty}\tilde{\tilde{H}}e^{j\bar{k}\cdot\bar{r}}d^3k \qquad (2.5.30)$$

2.6 The Transformed Current Density

All of the algebraic factors of (2.5.29) have been given except for the transformed current density.

Using (2.5.1) .

$$\tilde{\tilde{J}} = \iiint_{-\infty}^{\infty}\hat{\rho}I\delta(\rho-\rho_o)\delta(z)e^{-j\bar{k}\cdot\bar{r}}d^3r \qquad (2.6.1)$$

Expressing $\bar{k}$ and $\bar{r}$ in polar co-ordinates where

$$x = \rho\,\mathrm{Cos}\,\phi \qquad (2.6.2)$$

$$y = \rho\,\mathrm{Sin}\,\phi \qquad (2.6.3)$$

$$k_1 = K\,\mathrm{Cos}\,\xi \qquad (2.6.4)$$

$$k_2 = K\,\mathrm{Sin}\,\xi \qquad (2.6.5)$$

and setting $$\hat{\phi} = -\hat{x}\,\mathrm{Sin}\,\phi+\hat{y}\,\mathrm{Cos}\,\phi \qquad (2.6.6)$$

We have

$$\tilde{\tilde{J}} = I\int_{-\infty}^{\infty}\int_{0}^{2\pi}\int_{0}^{\infty}(-\hat{x}\,\mathrm{Sin}\,\phi+\hat{y}\,\mathrm{Cos}\,\phi)\delta(\rho-\rho_o)\delta(z)e^{-j[k\rho\,\mathrm{Cos}(\phi-\xi)+k_3z]}\rho\,d\rho\,d\phi\,dz \qquad (2.6.7)$$

Integration on z and then on ρ, and using the properties of the Dirac-Delta Function yields

$$\tilde{\tilde{J}} = I\rho_o\int_{0}^{2\pi}(-\hat{x}\,\mathrm{Sin}\,\phi+\hat{y}\,\mathrm{Cos}\,\phi)e^{-jk\rho_o\,\mathrm{Cos}(\phi-\xi)}d\phi \qquad (2.6.8)$$

A familiar identity that will be useful in this study is

$$2\pi(j)^n J_n(z) = \int_0^{2\pi} e^{jnt} e^{jz \cos t} dt \qquad (2.6.9)$$

$J_n(z)$ is the Bessel's function of the first kind of integer order, n.

Expanding $(-\hat{x} \sin\phi + \hat{y} \cos\phi)$ into exponential representation allows the use of (2.6.9) to evaluate (2.6.8).

The results is

$$\tilde{\bar{J}} = 2\pi j I \rho_o J_1(K\rho_o)[\hat{x} \sin\zeta - \hat{y} \cos\zeta] \qquad (2.6.10)$$

CHAPTER 3 THE QUASI-STATIC APPROXIMATION; $\overline{B}_o$ NORMAL TO THE LOOP

3.1 Introduction

Once $\tilde{\tilde{H}}$ is determined as in (2.5.29), the inverse Fourier transform of $\tilde{\tilde{H}}$ will yield H_z by using (2.5.30). Upon examination of the denominator, $(a+ko^2b+ko^4c)$, of (2.5.29), where

$$(a+ko^2b+ko^4c) = [-k^2(K_1K^2+K_ok_3^2)+ko^2\{(K_1^2-K_{11}^2)K^2+K_1K_o(k^2+k_3^2)\}$$

$$+ko^4\{-K_o(K_1^2-K_{11}^2)\}] \qquad (3.1.1)$$

it becomes evident that the difficulty of solving (2.5.30) is extensive and some kind of approximation must be introduced.

It is important to recall that, according to (2.2.23), the $\hat{z}$-directed magnetic field will be integrated over the area enclosed by the loop, and thus, we are essentially interested in the <u>near field</u> representation of H_z.

The approximation that will be used to facilitate the solution of (2.5.30) is known as the quasi-static approximation, which, in essence, yields the low frequency approximate solution of the $\hat{z}$-component of the magnetic field. However, a difficulty arises when one considers that the constitutive parameters K_1, K_o, and K_{11} are frequency dependent, thus, one must assume that a constant permittivity tensor, $\varepsilon_o\overline{\overline{K}}$, is a valid description of the medium at low frequencies. Since $ko^2 = \omega^2\mu_o\varepsilon_o$, taking the limit of (2.5.29) as ko approaches zero corresponds to a low frequency approximation. One must remember that

the radius of the current loop is assumed to be very small compared to the free-space wavelength, so it is a reasonable approximation to consider that the wavelength approaches infinity as far as the near fields of this very small loop are concerned.

One might well ask if it is true that the wave-length in the plasma approaches infinity, especially considering the fact that the dispersion surfaces in an anisotropic plasma are anisotropic too, and infinite in some directions in a lossless plasma. The answer is found by assuming very slight losses in the medium. Under these conditions, the dispersion surfaces are finite and letting k_o^2 approach zero corresponds to assuming an infinite wavelength in all directions in the plasma.

Now letting k_o^2 approach zero in (2.5.30), one obtains

$$H_{z_{Q.S.}} = \frac{\hat{z}\cdot}{(2\pi)^3}\int_{-\infty}^{\infty}\int_{0}^{2\pi}\int_{0}^{\infty} j\frac{\overline{\overline{N}}_1 \overline{kxK}^{-1}\tilde{J}e^{j[K\rho\ \mathrm{Cos}(\xi-\phi)+k_3 z]}K\,dK\,d\xi\,dk_3}{a} \qquad (3.1.2)$$

3.2 The Evaluation of the Quasi-Static Impedance

Upon evaluation of the integrand of (3.1.1) one obtains the following form.

$$H_{z_{Q.S.}} = \frac{I\rho_o}{(2\pi)^2}\int_{-\infty}^{\infty}\int_{0}^{2\pi}\int_{0}^{\infty}\frac{K^2 J_1(K\rho_o)e^{j[K\rho\ \mathrm{Cos}(\xi-\phi)+k_3 z]}dK\,d\xi\,dk_3}{(K^2+k_3^2)} \qquad (3.2.1)$$

The fact that none of the plasma parameters appear in this quasi-static representation is important. One would, therefore, expect that the impedance calculated from this $H_{z_{Q.S.}}$ will be the impedance of a small loop in free

[illegible] is in the same with [illegible].

space. That this is the case will now be shown.

The integration on ξ can be performed by using the identity (2.6.9). This yields.

$$H_{z_{Q.S.}} = \frac{I\rho_o}{2\pi}\int_{-\infty}^{\infty}\int_{0}^{\infty}\frac{K^2 J_1(\rho_o K)J_o(\rho K)e^{jk_3 z}dKdk_3}{(K^2+k_3^2)} \qquad (3.2.2)$$

Since we are interested in the value of $H_{z_{Q.S.}}$ over the loop, z is set equal to δ, the radius of the wire.

A contour integration is now performed in the complex $\bar{k}_3$-plane and is closed in the upper half plane. The result is

$$H_{z_{Q.S.}} = \frac{I\rho_o}{2}\int_0^{\infty} KJ_1(K\rho_o)J_o(K\rho)e^{-K\delta}dK \qquad (3.2.3)$$

The impedance formula is therefore,

$$Zin_{Q.S.} = \frac{j\omega\mu_o\rho_o}{2}\int_0^{2\pi}\int_0^{\rho_o}\int_0^{\infty} KJ_1(\rho_o K)J_o(\rho K)e^{-K\delta}\rho\, dK d\rho d\phi \qquad (3.2.4)$$

Integration on ϕ introduces a factor 2π. Employing the following identity

$$\int_o^{\rho_o}\rho J_o(\rho_o K)d\rho = \frac{\rho_o}{K}J_1(K\rho_o) \qquad (3.2.5)$$

(3.2.4) becomes

$$Zin_{Q.S.} = j\omega\mu_o\rho_o^2\pi\int_0^{\infty} J_1^2(\rho_o K)e^{-K\delta}dK \qquad (3.2.6)$$

It is quite apparent that if δ is set equal to zero, the integral of (3.2.6) will not

where $K = \frac{x}{\rho_o}$ (3.2.7)

converge. Setting $\rho_o K = x$ (3.2.7)

(3.2.6) becomes

$$Zin_{Q.S.} = j\omega\mu_o\rho_o\pi\int_0^\infty J_1^2(x)e^{-Rx}dx \quad (3.2.8)$$

where $$R = \frac{\delta}{\rho_o} \ll 1 \quad (3.2.9)$$

R is dimensionless and is the ratio of the wire radius to the loop radius. Luke (1962) gives the following integral

$$I(\mu,\nu,\lambda) = \int_0^\infty e^{-Rx}x^\lambda J_\mu(ax)J_\nu(bx)dx \quad (3.2.10)$$

Thus, $$Zin_{Q.S.} = j\omega\mu_o\rho_o\pi I(1,1,0) \quad (3.2.11)$$

Luke also gives $$I(1,1,0) = \frac{2}{\pi\alpha_1}\left[\left(1-\frac{\alpha_1^2}{2}\right)K(\alpha_1)-E(\alpha_1)\right] \quad (3.2.12)$$

where K and E are elliptic integrals of the first and second kind, and

$$\alpha_1^2 = (1+R^2/4)^{-1} \quad (3.2.13)$$

Collins (1960) gives the self-impedance of a small loop in free space as

$$Zin = j\omega\mu_o\rho_o(2-R)\left[\left(1-\frac{\alpha_2}{2}\right)K(\alpha_2)-E(\alpha_2)\right] \quad (3.2.14)$$

where $$\alpha_2^2 = \left(1+\frac{R^2}{4(1-R)}\right)^{-1} \quad (3.2.15)$$

These results agree and thus, the quasi-static impedance of the small loop is equal to the free space impedance, as was anticipated in (3.2.1).

CHAPTER 4 A FIRST ORDER CORRECTION TERM TO THE QUASI-STATIC IMPEDANCE; $\bar{B}_o$ NORMAL TO THE LOOP

Since the derivation of the quasi-static impedance yielded a result independent of plasma parameters, it is desirable to find a first order correction term. We repeat equation (2.5.29) for the $\bar{H}$ field.

$$\underset{\sim}{\bar{H}} = j\frac{[\bar{\bar{N}}_1+ko^2\bar{\bar{N}}_2]\bar{\bar{kxK}}^{-1}\underset{\sim}{\bar{J}}}{(a+ko^2b+ko^4c)} \tag{4.1.1}$$

If the denominator is divided by long division into the numerator, one obtains

$$\underset{\sim}{\bar{H}} = j[\bar{\bar{N}}_1+ko^2\bar{\bar{N}}_2](\frac{1}{a}-\frac{ko^2b}{a^2}+\frac{ko^4}{a}\left\{\frac{b^2}{a^2}-\frac{c}{a}\right\})\bar{\bar{kxK}}^{-1}\underset{\sim}{\bar{J}} \tag{4.1.2}$$

Retaining only the zero order and first order terms in ko^2, (4.1.2) becomes

$$\bar{H} = j[\frac{\bar{\bar{N}}_1}{a}+ko^2(\frac{\bar{\bar{N}}_2}{a}-\frac{b\bar{\bar{N}}_1}{a^2})]\bar{\bar{kxK}}^{-1}\underset{\sim}{\bar{J}} \tag{4.1.3}$$

The first term in (4.1.3) is just the quasi-static term that was used in (3.1.1). Let us call the $O(ko^2)$ term $\bar{H}_c$, the correction term.

That is

$$\underset{\sim}{\bar{H}}_c = j\frac{ko^2}{a}(\bar{\bar{N}}_2-\frac{b\bar{\bar{N}}_1}{a})\bar{\bar{kxK}}^{-1}\underset{\sim}{\bar{J}} \tag{4.1.4}$$

The first term in (4.1.3) is just the quasi-static term that was used in (3.1.1).

$$\tilde{H}_{zc} = -2\pi\frac{ko^2}{a}I\rho_o J_1(K\rho_o)[-K_oK_1K$$

$$-b\left\{K(K_1K^2+K_ok_3^2)(\sin\xi+\cos\xi)+jK_{11}K^3(\sin\xi-\cos\xi)\right\}] \tag{4.1.5}$$

Note that all the plasma parameters appear in this expression.

Using the expressions for impedance and applying the inverse Fourier transform, we conclude that

$$Zin_{corr.} = j\frac{\omega\mu_o}{I}\int_0^{2\pi}\int_0^{\rho_o}\left[\frac{1}{(2\pi)^3}\int_{-\infty}^{\infty}\int_0^{2\pi}\int_0^{\infty}\tilde{H}_{z_c}\, e^{j[K\rho\cos(\xi-\phi)+k_3 z]}K\,dK\,d\xi\,dk_3\right]\rho\,d\rho\,d\phi \tag{4.1.6}$$

Upon substitution and rearrangement, we have

$$Zin_{corr.} = \frac{j\omega\mu_o\rho_o k_o^2}{(2\pi)^2}\int_0^{2\pi}\int_0^{\rho_o}\int_{-\infty}^{\infty}\int_0^{2\pi}\int_0^{\infty}\frac{KJ_1(K\rho_o)\rho\left[-K_o K_1 K - b\left\{K(K_1K^2+K_o k_3^2)(\sin\xi+\cos\xi)\cdot\right.\right.}{(K^2+k_3^2)(K_o k_3^2+K_1K^2)}$$

$$\left.\left.\cdot + jK_{11}K^3(\sin\xi-\cos\xi)\right\}\right]e^{j[K\rho\cos(\xi-\phi)+k_3 z]}\,dK\,d\xi\,dk_3\,d\rho\,d\phi \tag{4.1.7}$$

Again we set $z=\delta$, the radius of the wire. Integration on ϕ is performed using the identity (2.6.9). It is obvious that only the factor $-K_o K_1 K$ will persist upon integration over ξ because of the $\sin\xi$ and $\cos\xi$ terms in the factor multiplied by b.

It is at this point that the plasma parameter K_{11} disappears from the first order correction term to the impedance.

Integration of ρ is done using (3.2.5).

Thus,

$$Zin_c = -j\omega\mu_o\rho_o^2 k_o^2 K_1 K_o\int_{-\infty}^{\infty}\int_0^{\infty}\frac{KJ_1^2(K\rho_o)e^{jk_3\delta}\,dK\,dk_3}{(K^2+k_3^2)(K_1K^2+K_o k_3^2)} \tag{4.1.8}$$

Define

$$I_{k_3} = \int_{-\infty}^{\infty}\frac{e^{jk_3\delta}\,dk_3}{(k_3^2+K^2)(k_3^2+\beta^2K^2)} \tag{4.1.9}$$

where $$\beta^2 = K_1/K_o \qquad (4.1.10)$$

Breaking the integrand into partial fractions (4.1.9) is written as

$$I_{k_3} = \frac{1}{K^2(\beta-1)}\left[\int_{-\infty}^{\infty} \frac{e^{jk_3\delta}}{(k_3^2+K^2)}dk_3 - \int_{-\infty}^{\infty} \frac{e^{jk_3\delta}dk_3}{(k_3^2+\beta^2K^2)}\right] \qquad (4.1.11)$$

The integral is now in such a form that contour integration can be performed in the complex $\bar{k}_3$-plane. Assuming slight losses in the medium, so that the poles are never pure real, we see that

$$I_{k_3} = \frac{\pi}{K^3(\beta^2-1)}\left[e^{-K\delta} - \frac{e^{-\beta K\delta}}{\beta}\right] \qquad (4.1.12)$$

Thus, $$Zin_c = \frac{-j\omega\mu_o\rho_o^2 k_o^2 K_1 \pi}{(\beta^2-1)}\int_0^{\infty} \frac{J_1^2(K\rho_o)}{K^2}\left[e^{-K\delta} - \frac{e^{-\beta K\delta}}{\beta}\right]dK \qquad (4.1.13)$$

Setting $K\rho_o = x$ (2.8.13) becomes

$$Zin_c = -\frac{j\omega\mu_o\rho_o^3 k_o^2 K_1 K_o \pi}{(K_1-K_o)}\int_0^{\infty} \frac{J_1^2(x)}{x^2}\left[e^{-Rx} - \frac{e^{-\beta Rx}}{\beta}\right]dx \qquad (4.1.14)$$

where R is defined by (3.2.9).

At this point it is useful to introduce the following definition

$$k_o\rho_o = \frac{2\pi\rho_o}{\lambda_o} = \frac{C}{\lambda_o} = C_\lambda \ll 1 \qquad (4.1.15)$$

C_λ is the circumference of the loop in free-space wavelengths and is very small. Thus, (4.1.14) is

$$Zin_c = \frac{-j\omega\mu_o\rho_o C\lambda^2 K_1 K_o \pi}{(K_1 - K_o)} \int_0^\infty \frac{J_1^2(x)}{x^2} [e^{-Rx} - \frac{e^{-\beta Rx}}{\beta}] dx \qquad (4.1.16)$$

β should be chosen with a positive real part in order that (4.1.16) should converge.

An analysis of this result will be made later on.

CHAPTER 5 THE UNIAXIAL APPROXIMATION; $\overline{B}_o$ NORMAL TO THE LOOP

5.1 Introduction

As was shown in the previous chapter neither the quasi-static impedance nor the first order correction term for impedance were functions of K_{11}. This is justification of the argument that the transposed medium need not be used in the impedance expression given earlier in this report. K_{11} is the only parameter which is a function of the sense of the imposed steady magnetic field, Bo. K_1 and K_o are functions of Y^2 and thus, only functions of Bo^2.

It is most likely that, if higher order terms in ko^2 were calculated for the impedance, the factor K_{11} would eventually appear in some or all of the terms. But the fact that the loop is small and only the near fields are required leads to the conclusion that it would be useful to consider that K_{11} is identically zero. There is no reason to assume that, in this event, the result for the loop impedance would not be just as good an approximation, or better, than the quasi-static approximation.

Setting
$$K_{11} = 0 \qquad (5.1.1)$$
results in making $\overline{\overline{K}}$ a diagonal matrix. But the most important result is that the determinant of $\overline{\overline{L}}$ is factorable into two simple factors. This permits the evaluation of the inverse Fourier transform of $\underline{\underline{\tilde{H}}}$ yielding a result that is in closed form and which contains ko^2.

5.2 The Transformed Magnetic Field in the Uniaxial Medium

5.2 The Transformed Magnetic Field in the Uniaxial Medium

If one sets $K_{11} = 0$ in (2.5.8) and solves for the $\hat{z}$-component of $\tilde{\tilde{H}}$, the result is

$$\tilde{H}_z = \frac{j[k_2\tilde{J}x - k_1\tilde{J}y][K_1K^2 + K_o k_3^2 - K_1K_o ko^2]}{(a + ko^2 b + ko^4 c)} \qquad (5.2.1)$$

But $$(a + ko^2 b + ko^4 c) = -[K^2 + k_3^2 - K_1 ko^2][K_1K^2 + K_o k_3^2 - K_1K_o ko^2] \qquad (5.2.2)$$

This result is quite convenient because the second term of the denominator cancels with a factor in the numerator.

Thus, $$\tilde{H}_z = -\frac{j[k_2\tilde{J}x - k_1\tilde{J}y]}{[K^2 + k_3^2 - K_1 ko^2]} \qquad (5.2.3)$$

$\tilde{J}x$ is the x-component of the transformed current density. Expressing (5.2.3) in the cylindrical Fourier co-ordinates and substituting $\tilde{J}x$ and $\tilde{J}y$ from (2.6.10) yields

$$\tilde{H}_z = \frac{+2\omega I \rho_o J_1(K\rho_o)K}{(K^2 + k_3^2 - K_1 ko^2)} \qquad (5.2.4)$$

and $$H_{z_{uniax.}} = \frac{I\rho_o}{(2\pi)^2}\int_{-\infty}^{\infty}\int_0^{2\pi}\int_0^{\infty} \frac{K^2 J_1(K\rho_o)e^{j[K\rho\,\mathrm{Cos}\,(\xi-\phi)+k_3 z]}}{(K^2 + k_3^2 - K_1 ko^2)}\,dK\,d\xi\,dk_3 \qquad (5.2.5)$$

Comparing this result with (3.2.1), it is seen that

$$\lim_{ko^2 \to 0}\left\{H_{z_{uniax.}}\right\} = H_{z_{Q.S.}} \qquad (5.2.6)$$

Examination of (5.2.5) shows that it is a function only of K_1 and not of K_o. This is somewhat disconcerting at first until one solves for Ez in the uniaxial

case and finds that is is equal to zero. Since the role of K_o is found in (2.1.1) as part of the constitutive relation

$$\overline{D} = \varepsilon_o \overline{\overline{K}} \overline{E} \tag{5.2.7}$$

it is clear that since $$Ez = 0 \tag{5.2.8}$$

K_o plays no role and thus, the fields are functions only of K_1.

5.3 The Impedance of the Loop in the Uniaxial Medium

Upon substitution of (5.2.5) into the impedance formula (2.4.8), one obtains

$$Zin_{uniax.} = \frac{j\omega\mu_o\rho_o}{(2\pi)^2}\int_0^{2\pi}\int_0^{\rho_o}\int_{-\infty}^{\infty}\int_0^{2\pi}\int_0^{\infty}\rho\frac{K^2 J_1(K\rho_o)e^{j[K\rho\,\mathrm{Cos}\,(\xi-\phi)+k_3 z]}\,dK\,d\xi\,dk_3\,d\rho\,d\phi}{(K^2+k_3^2-K_1 ko^2)} \tag{5.3.1}$$

Integrating on ξ using identity (2.6.9) yields

$$Zin_{uniax.} = \frac{j\omega\mu_o\rho_o}{2\pi}\int_0^{2\pi}\int_0^{\rho_o}\int_{-\infty}^{\infty}\int_0^{\infty}\rho\frac{K^2 J_1(K\rho_o)J_o(K\rho)e^{jk_3 z}\,dK\,dk_3\,d\rho\,d\phi}{(K^2+k_3^2-K_1 ko^2)} \tag{5.3.2}$$

Again z is set equal to δ and integration on ϕ introduces a factor of 2π. The next integration on ρ using identity (3.2.5) results in

$$Zin_{uniax.} = j\omega\mu_o\rho_o^2\int_{-\infty}^{\infty}\int_0^{\infty}\frac{KJ_1^2(K\rho_o)e^{jk_3\delta}\,dK\,dk_3}{(K^2+k_3^2-K_1 ko^2)} \tag{5.3.3}$$

The next integration is performed as a contour integral in the complex $\overline{k}_3$-plane which is closed in the upper half plane. In this integral the poles of the integrand will never lie on the real axis if there are slight losses in the medi-

um, making K_1 complex. After integration on k_3 is performed

$$Zin_{uniax.} = j\omega\mu_o\rho_o^2\pi \int_0^\infty \frac{KJ_1^2(K\rho_o)e^{-\delta\sqrt{K^2-K_1ko^2}}}{\sqrt{K^2-K_1ko^2}}\,dK \qquad (5.3.4)$$

and again setting

$$K\rho_o = x \qquad (5.3.5)$$

and rearranging (5.3.4) becomes

$$Zin_{uniax.} = j\omega\mu_o\rho_o\pi \int_0^\infty \frac{xJ_1^2(x)e^{-R\sqrt{x^2-K_1C_\lambda^2}}}{\sqrt{x^2-K_1C_\lambda^2}}\,dx \qquad (5.3.6)$$

where C_λ is defined by (4.1.15) and R by (3.2.9). Of course, as $\lambda \rightarrow \infty$ (5.3.6) reduces to the free-space impedance of a small loop. An analysis of the impedance expression will be made later on in this study.

CHAPTER 6 THE UNIAXIAL APPROXIMATION; $\overline{B}_o$ PARALLEL TO THE LOOP

6.1 The Permittivity Matrix for a $\hat{y}$-Directed D. C. Magnetic Field

Up to this point the impedance of the loop has been calculated for the case of the D. C. magnetic field normal to the plane of the loop.

Let us now assume the same current loop configuration as before, but assume that

$$\overline{Bo} = \hat{y}\, Bo \tag{6.1.1}$$

This case can be represented by interchanging the y-z dependancy of $\overline{\overline{K}}$. Thus, the $\overline{\overline{K}}$ is

$$\overline{\overline{K}} = \begin{bmatrix} K_1 & O & jK_{11} \\ O & K_o & O \\ -jK_{11} & O & K_1 \end{bmatrix} \tag{6.1.2}$$

6.2 The Transformed Magnetic Field

Again the $\hat{z}$-component of the magnetic field is needed to calculate the loop impedance. Rewriting (2.5.10) we have

$$\tilde{\overline{H}} = -j\overline{\overline{L}}^{-1}\overline{\overline{kxK}}^{-1}\tilde{\overline{J}} \tag{6.2.1}$$

$$\overline{\overline{L}} = (\overline{\overline{kxK}}^{-1}\overline{\overline{kx}} + ko^2\overline{\overline{I}}) \tag{6.2.2}$$

$\overline{\overline{L}}^{-1}$ must now be recalculated using the new representation of $\overline{\overline{K}}$ from (6.1.2). The inversion of $\overline{\overline{L}}$ is a tedious process at best. This is especially true in the case when $K_{11} \neq 0$. In view of the argument presented in the last section, K_{11} will again be set equal to zero and the impedance of the loop in a

uniaxial medium will be calculated. Therefore, we set,

$$\overline{\overline{K}} = \begin{bmatrix} K_1 & O & O \\ O & K_o & O \\ O & O & K_1 \end{bmatrix} \qquad (6.2.3)$$

It can be shown that

$$\overline{\overline{L}} = \frac{-ko^2}{K_1^2 K_o}(a' + ko^2 b' + ko^4 c') \qquad (6.2.4)$$

where a', b', and c' are the same as defined by (2.5.2), (2.5.2), and (2.5.2) except that k_2^2 and k_3^2 are interchanged everywhere.

Upon completing the inversion of $\overline{\overline{L}}$ and evaluation of H_z, the result is

$$H_z = \frac{+j}{(a' + ko^2 b' + ko^4 c')} \begin{bmatrix} k_2 \tilde{Jx}\{K_o K^2 + K_1 k_3^2 - K_1 K_o ko^2\} \\ -K_1 k_1 \tilde{Jy}\{k^2 - K_1 ko^2\} \end{bmatrix} \qquad (6.2.5)$$

and substituting in the values of $\tilde{Jx}$ and $\tilde{Jy}$ and writing the whole expression in terms of the cylindrical Fourier co-ordinates, (6.2.5) becomes

$$H_z = \frac{2\pi I \rho_o J_1(K\rho_o) K [\sin^2\xi \{K_o K^2 + K_1 k_3^2 - K_1 K_o ko^2\} + K_1 \cos^2\xi \{K^2 + k_3^2 - K_1 ko^2\}]}{[K^2 + k_3^2 - K_1 ko^2][K_1 K^2 \cos^2\xi + K_1 k_3^2 + K_o K^2 \sin^2\xi - K_1 K_o ko^2]} \qquad (6.2.6)$$

The result is clearly more complicated than the case of the D. C. magnetic field normal to the plane of the loop.

6.3 The Evaluation of the Impedance in the Uniaxial Medium

Applying the inverse Fourier transform to the expression of (6.2.6) and

then integrating the $\hat{z}$-directed magnetic field over the loop, one has the following integral representation for impedance.

$$Zin = \frac{j\omega\mu_o\rho_o}{(2\pi)^2}\int_0^{2\pi}\int_0^{\rho_o}\int_{-\infty}^{\infty}\int_0^{2\pi}\int_0^{\infty} \frac{J_1(K\rho_o)\,\rho\,K^2 e^{j[K\rho\cos(\xi-\phi)+k_3\delta]}\,J_1(K\rho_c)}{[K^2+k_3^2-K_1k_o^2][K_1K^2\cos^2\xi+K_oK^2\sin^2\xi+K_1k_3^2-K_1K_ok_o^2]} \cdot$$

$$\cdot\,[\sin^2\xi\{K_oK^2+K_1k_3^2-K_1K_ok_o^2\}+K_1\cos^2\xi\{K^2+k_3^2-K_1k_o^2\}]dKd\xi dk_3 d\rho d\phi \qquad (6.3.1)$$

As before, z has been set equal to δ.

The first integration will be performed on ϕ using the identity (2.6.9). The result is that

$$Zin = \frac{j\omega\mu_o\rho_o}{2\pi}\int_0^{\rho_o}\int_{-\infty}^{\infty}\int_0^{2\pi}\int_0^{\infty}\rho K^2 e^{jk_3\delta}\,J_1(K\rho_o)Jo(K\rho)\cdot$$

$$\cdot\,\frac{[\sin^2\xi\{K_oK^2+K_1k_3^2-K_1K_ok_o^2\}+K_1\cos^2\xi\{K^2+k_3^2-K_1k_o^2\}]dKd\xi dk_3 d\rho}{[K^2+k_3^2-K_1k_o^2][K_1K^2\cos^2\xi+K_oK^2\sin^2\xi+K_1k_3^2-K_1K_ok_o^2]} \qquad (6.3.2)$$

The next integration is performed on ρ using (3.2.5) which yields

$$Zin = \frac{j\omega\mu_o\rho_o^2}{2\pi}\int_{-\infty}^{\infty}\int_0^{2\pi}\int_0^{\infty} \frac{KJ_1^2(K\rho_o)e^{jk_3\delta}\,[\sin^2\xi\{K_oK^2+K_1k_3^2-K_1K_ok_o^2\}}{[K^2+k_3^2-K_1k_o^2]}\cdot$$

$$\cdot\,\frac{+K_1\cos^2\xi\{K^2+k_3^2-K_1k_o^2\}]dKd\xi dk_3}{[K_1K^2\cos^2\xi+K_oK^2\sin^2\xi+K_1k_3^2-K_1K_ok_o^2]} \qquad (6.3.3)$$

Next, the integral on k_3 will be performed by the method of contour integration

in the complex $\bar{k}_3$-plane. After extracting a factor K_1, the denominator of the integrand can be factored as follows

$$[k_3^2+(K^2-K_1 ko^2)] = (k_3+jm)(k_3-jm) \qquad (6.3.4)$$

where $$m = \sqrt{K^2-K_1 ko^2} \qquad (6.3.5)$$

Also $$[K_3^2+(K^2 \cos^2\xi + \frac{K_o}{K_1}K^2 \sin^2\xi - K_o ko^2)] = (k_3+jn)(k_3-jn) \qquad (6.3.6)$$

where $$n = \sqrt{K^2 \cos^2\xi + \frac{K_o}{K_1}K^2 \sin^2\xi - K_o ko^2} \qquad (6.3.7)$$

Thus,
$$Zin = \frac{j\omega\mu_o\rho_o^2}{2\pi K_1}\int_0^{2\pi}\int_0^{\infty} KJ_1^2(K\rho_o) \cdot$$
$$\cdot\int_{-\infty}^{\infty}\left[\frac{(K_1 \sin^2\xi\, k_3^2+K_o \sin^2\xi\, m^2)e^{jk_3\delta}}{(k_3+jm)(k_3-jm)(k_3+jn)(k_3-jn)} + \frac{K_1 \cos^2\xi\, e^{jk_3\delta}}{(k_3-jn)(k_3+jn)}\right] dk_3\, dK\, d\xi \qquad (6.3.8)$$

Notice that the term multiplied by $\cos^2\xi$ in the numerator of (6.3.3) has a factor which cancels part of the denominator. Notice also the apperance of m^2 in the first term of the numerator.

The contour of (6.3.8) is closed in the upper half plane and again slight losses are assumed to exist in the medium so that the poles, m and n do not lie on the real axis.

The first term of (6.3.8) may be broken into partial fractions and, thus, defining only the k_3 integral we have

$$I_{k_3} = \int_{-\infty}^{\infty} \frac{(K_1 k_3^2 \sin^2\xi + K_o m^2 \sin^2\xi) e^{jk_3\delta} dk_3}{(n^2-m^2)(k_3+jm)(k_3-jm)} \cdot$$

$$\cdot + \int_{-\infty}^{\infty} \frac{(k_3^2 K_1 \sin^2\xi + K_o m^2 \sin^2\xi) e^{jk_3\delta} dk_3}{(m^2-n^2)(k_3+jn)(k_3-jn)} \cdot$$

$$\cdot + \int_{-\infty}^{\infty} \frac{K_1 \cos^2\xi\, e^{jk_3\delta}}{(k_3+jn)(k_3-jn)} dk_3 \qquad (6.3.9)$$

Invoking Cauchy's integral formula, the result is

$$I_{k_3} = 2\pi j\left[\frac{\sin^2\xi\,(-K_1 m^2 + K_o m^2) e^{-m\delta}}{(n^2-m^2)2jm} + \frac{\sin^2\xi\,(K_o m^2 - K_1 n^2) e^{-m\delta}}{(m^2-n^2)2jm}\right.$$

$$\left. + \frac{K_1 \cos^2\xi\, e^{-n\delta}}{2jn}\right] \qquad (6.3.10)$$

Collecting terms we have

$$I_{k_3} = \pi K_1\left[\frac{\cos^2\xi\, e^{-n\delta}}{n} + \frac{\sin^2\xi\, e^{-m\delta}}{m}\right] \qquad (6.3.11)$$

It is clear now that m and n must be chosen to have positive real parts in order to insure convergence of the remaining integrals.

Thus, the impedance formula for the loop in the same plane as the D. C. magnetic field in an uniaxial medium is

$$Zin_{uniax.} = \frac{j\omega\mu_o\rho_o^2}{2} \int_0^{2\pi}\int_0^{\infty} K J_1^2(K\rho_o)\left[\frac{\cos^2\xi\, e^{-n\delta}}{n} + \frac{\sin^2\xi\, e^{-m\delta}}{m}\right] dK d\xi \qquad (6.3.12)$$

and setting $K\rho_o = x$, we have finally

$$Zin = \frac{j\omega\mu_o\rho_o}{2}\int_0^{2\pi}\int_0^{\infty}[xJ_1^2(x)][\frac{\cos^2\xi\, e^{-n'R}}{n'} + \frac{\sin^2\xi\, e^{-m'R}}{m'}]\, dx d\xi \quad (6.3.13)$$

where
$$n' = \sqrt{x^2\cos^2\xi + \frac{K_o}{K_1}x^2\sin^2\xi - K_o C_\lambda^2} \quad (6.3.14)$$

and
$$m' = \sqrt{x^2 - K_1 C_\lambda^2} \quad (6.3.15)$$

R and C_λ are defined as before by (3.2.9) and (4.1.15) respectively.

Since m' is not a function of ξ, integration of ξ is easily done for the second term of (6.3.13). The result is

$$Zin = \frac{j\omega\mu_o\rho_o\pi}{2}\int_0^{\infty}\frac{xJ_1^2(x)e^{-R\sqrt{x^2 - K_1C_\lambda^2}}}{\sqrt{x^2 - K_1C_\lambda^2}}\, dx$$

$$+\frac{j\omega\mu_o\rho_o}{2}\int_0^{2\pi}\int_0^{\infty}\frac{xJ_1^2(x)\cos^2\xi\, e^{-R\sqrt{x^2(\cos^2\xi + \frac{K_o}{K_1}\sin^2\xi) - K_oC_\lambda^2}}}{\sqrt{x^2(\cos^2\xi + \frac{K_o}{K_1}\sin^2\xi) - K_oC_\lambda^2}}\, dx d\xi \quad (6.3.16)$$

The first integral of this expression is equal to <u>half</u> of the impedance of the loop in an uniaxial medium with the magnetic field <u>normal</u> to the loop. See (5.3.6). A discussion of this result will be given later in the study.

CHAPTER 7 THE EXPERIMENTAL APPARATUS AND THE MEASUREMENT TECHNIQUE

7.1 Introduction

It is obviously desirable that the conditions that were assumed to exist in the theoretical derivation of the impedance be met as closely as possible in the experimental measurements. The plasma should be uniform and the electron temperature should be quite low. The plasma chamber should be large enough to accommodate a small loop, but for practical reasons, small enough to allow the construction of magnetic coils around the chamber for the production of the steady magnetic field, $\overline{B}o$.

In order that the properties of the medium be well known, the gas used in the chamber should be pure and free from contaminants. Some method for the experimental determination of the plasma parameters must be included as well.

One must also be able to vary the plasma parameters (X, Y, Z) throughout a reasonable range and with a certain amount of indepedance of each other. Finally, an accurate method of impedance measurement must be provided.

The following sections of this chapter describe in detail the apparatus that was used to achieve the goals outlined above, and the measurement techniques employed to determine the plasma parameters and the loop impedance.

7.2 The Brush Cathode Plasma

It was decided to construct a plasma chamber which employed brush cathodes and a brush anode, as described by Persson (1964). The brush cathode

method was chosen because the resulting plasma exhibits properties that are desirable for our purposes.

Persson (1964) gives a detailed description of the brush cathode plasma which will not be repeated here. However, a review of the important plasma properties follows.

The brush cathode plasma is a beam produced plasma that is highly uniform and exhibits low electron temperature. Helium has been used because it allows the plasma to fill the chamber completely at relatively low discharge voltages and produces a single electron when ionized. The plasma is steady-state in nature and recombination processes predominate. Relatively small tube currents are required to produce a plasma with a wide range of parameters (X, Y, Z). Furthermore, since most of the anode to cathode voltage drop occurs very near the cathode, the rest of the chamber is essentially field-free. Since the negative glow of the discharge can be made to fill the whole chamber beyond the cathodes, the plasma is very well behaved in that there are no striations or instabilities. The electron density of the beam is several orders of magnitude less than the plasma electron density so that the plasma is dominated by cool electrons. The negative glow is independant of the location and size of the anode. This permitted flexibility in the design of the chamber.

The double cathode geometry was used so that the intercathode separation was small compared to the reaching distance of the negative glow, thus minimizing the non-uniformities associated with electron beam attenuation in the

gas. The fact that low electron temperatures were obtained supports the contention that the plasma is field-free. The electron density is so high and the electron temperature so low that electron-ion collisions predominate, while the electron-molecule collision frequency is relatively low.

A description of the numerical values of parameters will be given later on.

7.3 Construction of the Brushes

The brush used by Persson consisted of an array of finely pointed tungsten wires fastened to a base plate. All the wires were electrically and mechanically connected at the base plate by a eutectic solder.

A simple discharge tube employing one cheaply constructed brush cathode was built to determine if the desirable properties listed by Persson could be achieved for the chamber size that was needed for our purposes. The cathode for the tube was made by dropping dime-store pins through a copper mesh (screen) and then soft soldering the pin heads to the mesh. The anode consisted of a copper ring, and two Langmuir probes were included in the chamber for plasma measurements.

This tube worked very well initially giving the desired uniform, low temperature plasma, and an appropriate electron density. However, due to the cheap construction, sputtering became a problem. It was clear that the brushes to be used had to be constructed of higher quality materials and built to last many hours without outgassing significantly or being affected by high tube currents.

Following Persson, the wires for the new brushes were made of tungsten, and were 25 mils in diameter and about 1.5 inches long. An etching apparatus was constructed to point 100 of the tungsten wires at a time. The 100 wires were mounted on a rotating wheel which dipped them, in sets of 10 wires at a time, in and out of a solution of KOH and water. The pins which were immersed in the solution completed a D. C. circuit resulting in the etching of the tungsten. Because of the rotation of the wheel, the tips of the wires were immersed longer than the base of the wires. This resulted in an even tapering of the wires from 25 mils at the base to less than 1 mil at the point. A 20 VDC source was used and the process of etching 100 pins took about 15 minutes.

Once a sufficient number of pins was etched, they were mounted in a jig of compressed carbon in which holes were drilled at a separation of 60 mils, centre to centre.

One hole was drilled for each pin and a total of 1669 pins were used for each cathode. A thin layer of nickel was electroplated onto a molybdenum base plate and the blunt tips of the pins. A copper paste was placed on the plate and the pins, mounted in the jig and seated on the plate, were heated to about 1100° C in a hydrogen furnace. When the assembly cooled off, the carbon jig was removed leaving the 1669 tungsten pins fastened to the base plate at 60 mils separation from each other.

The anode was constructed in the same manner using a smaller base plate and fewer pins. A brush anode provides better electrical contact with the nega-

tive glow and is assumed to have a larger effective area than a simple plate of copper.

7.4 The Vacuum System

Before the chamber is filled with pure helium, it is necessary to evacuate as much air as possible. The vacuum system that was used was capable of pumping the chamber down to a pressure of 4×10^{-5} mm of mercury. Since the pressures used in the experiment were of the order of 0.5 millimeters of mercury, this represents an initial volume ratio of contaminant (air) to gas (He) of 8×10^{-3}%. During the pump-down precedure, it was necessary to outgas the surface of the glass chamber by using a high voltage sparking coil. As soon as the pressure appeared to be stationary, the chamber was back-filled with He at about 1 mm and a discharge current run through the chamber. This resulted in the cleaning of the cathodes due to ion bombardment and was characterized by bright, sporadic flashes at the cathodes. When the cathodes were no longer unstable, the discharge polarity was reversed and the anode was cleaned in a similar manner. Then the pump down procedure was again initiated and the whole process repeated until a satisfactory low pressure was maintained. The duration of the whole process varied from hours to days, depending on the condition of the chamber and its electrodes.

A major consideration of the vacuum system was, of course, the leakage rate of the chamber. Only very slight leakage could be tolerated. As can be seen in Figure 1, the leakage rate over a period of an hour amounted to about

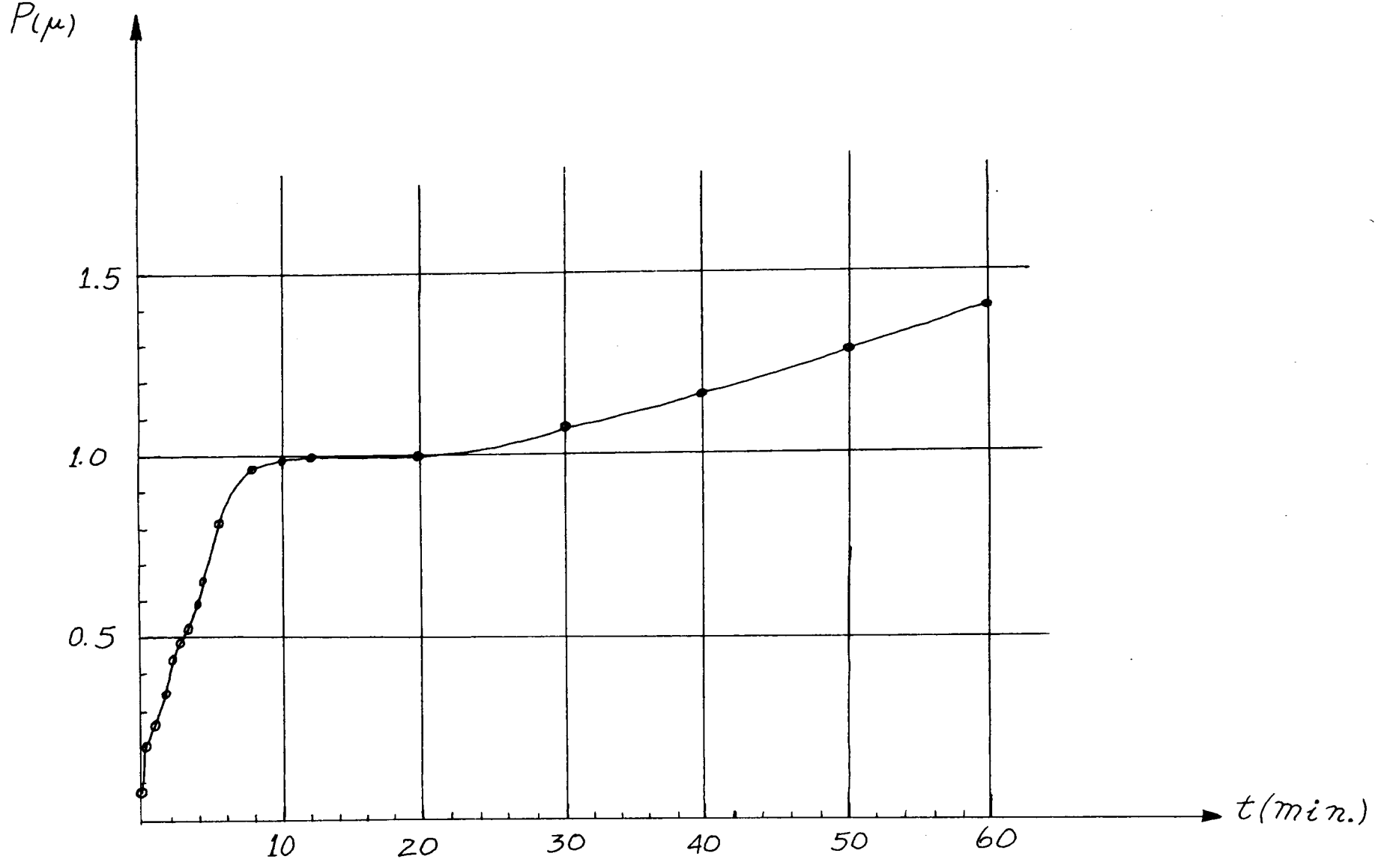

Figure 1 A Typical Leakage Curve

1.4μ which represents an introduction of 0.28% contaminant by volume.

7.5 The Glass Discharge Chamber

The glass discharge chamber was constructed of a cylindrical tube of glass with a cathode mounted at each end of the tube and the anode at the mid-point along the axis of the tube as shown in Figure 2. The tube was 3 1/2 inches in diameter and approximately 15 inches long. The electrodes were inserted into the tube and supported by metal tabs which were sprung against the inner walls of the chamber. The electrical connection from each base plate was passed through a uranium glass seal to the outside of the chamber. The inter-cathode spacing was approximately 12 inches and the negative glow of the plasma was easily made to fill the whole chamber in between the tips of the pointed wires of the electrodes.

7.6 The D.C. Magnetic Field Coils

In order to produce a steady magnetic field inside and along the axis of the cylindrical discharge chamber, two identical coils were constructed. Each coil fitted quite closely around the glass chamber and they were mounted as close together as was permitted by the glasswork which supported the anode and the small loop. Special consideration had to be given to heat dissipation in the coils because they carried currents of the order of 22A, and the heat losses in the coils were of the order of 500 watts. Each coil was air-cooled by a forced air fan.

Figure 3 shows the value of the plasma parameter Y at 1 G Hz produced by

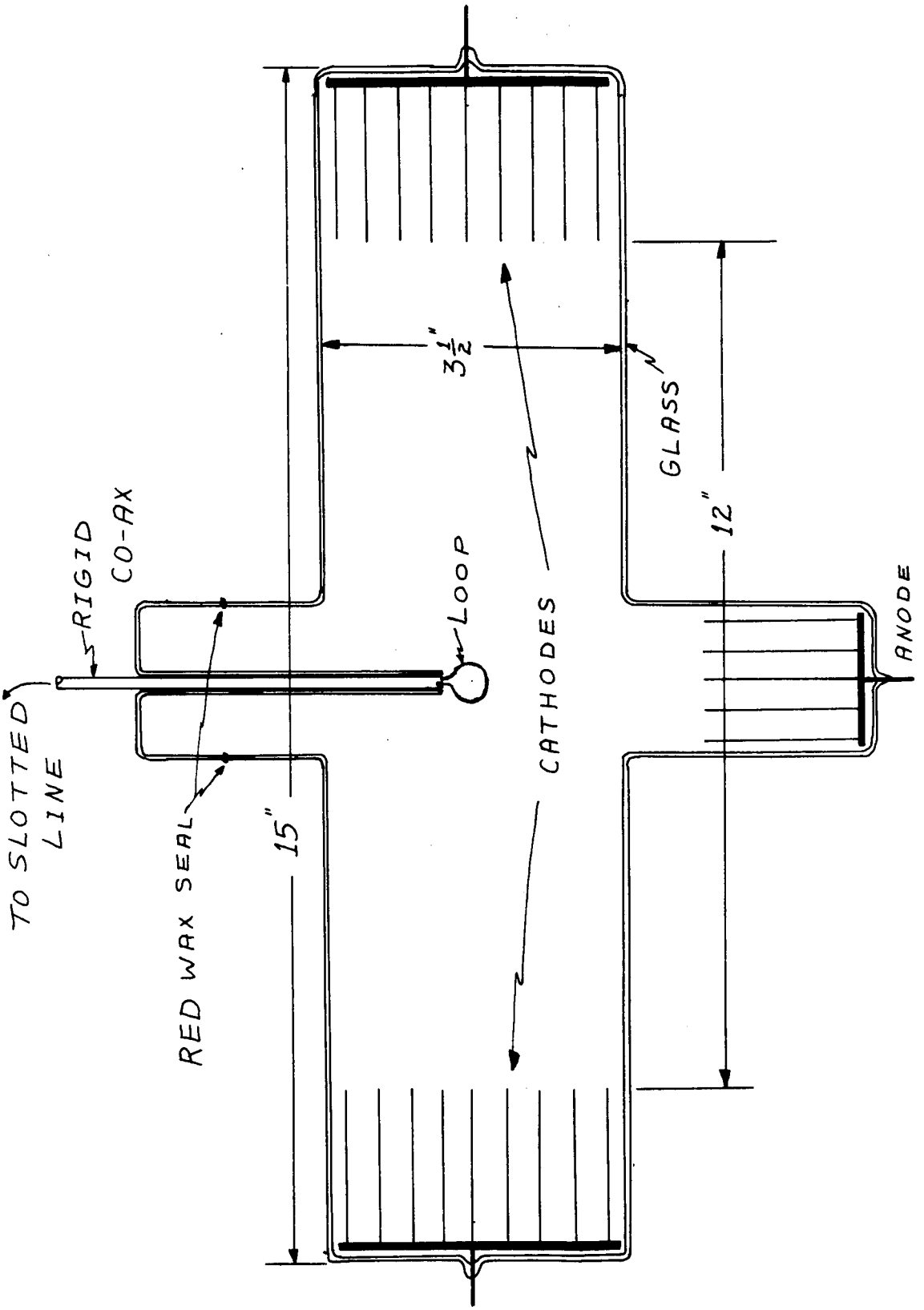

Figure 2 Glass Discharge Tube with Loop and Brush Electrodes

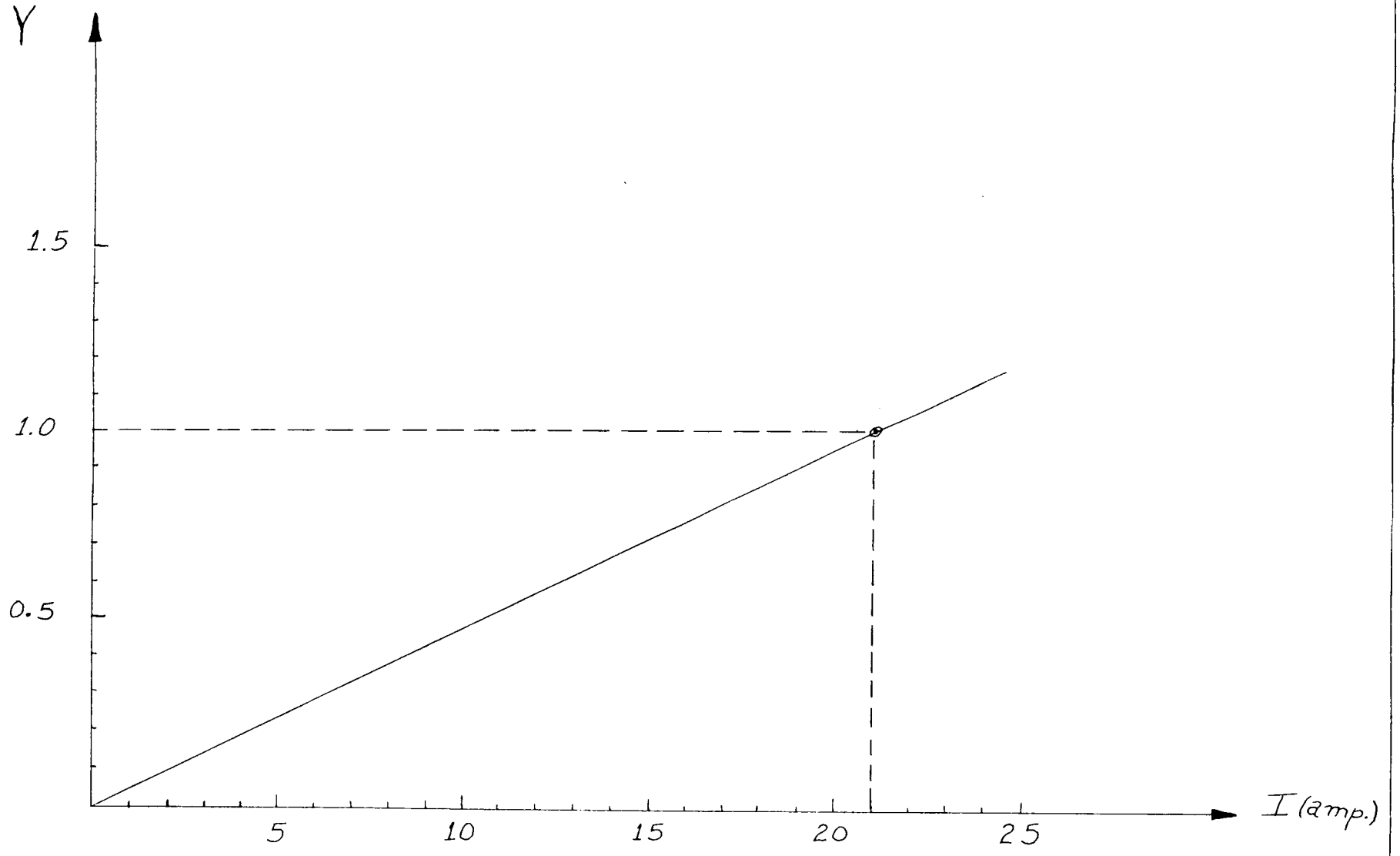

Figure 3 Calibration Curve of Y versus Coil Current at 1 KMHz

the coils at the location of the small loop as a function of coil current. The magnetic field was measured by means of a Hall probe.

The power supply for the coils consisted of a full wave rectifier and a bank of R-C filters. The current was varied by changing the A. C. input to the rectifier by means of a Variac transformer.

Throughout the experiment the value of the plasma parameter Y was determined from the D. C. coil current by means of the calibration curve already shown.

7. 7 The Small Loop

The small loop used in this experiment was constructed by forming the inner conductor of a rigid 50 ohm coaxial line into a loop which was then spot-welded to the outer metal sheath of the coaxial line.

The loop dimensions were as follows. The loop radius, ρ_o, was

$$\rho_o = 0.5585 \text{ cm} \qquad (7.7.1)$$

and the wire diameter δ, was

$$\delta = 0.0458 \text{ cm} \qquad (7.7.2)$$

These dimensions were determined by the use of a calibrated microscope.

These dimensions led to a value of the ratio R, given by (3. 2. 9) of

$$R = \frac{\delta}{\rho_o} = 0.0820 \qquad (7.7.3)$$

Since it was important to insure that the plasma did not diffuse to the metal sheath of the rigid coaxial line, it was enclosed in a glass tube as shown in

collapse the ion sheath which surrounds it. In this region, the effective area of the probe is unknown because of the ion sheath. The current to the probe is essentially due to electrons and the slope of the line A B yields the electron temperature.

The slope m is

$$m = \frac{eV_{PA}}{kT_e} \qquad (7.8.1)$$

so a very steep slope corresponds to a low electron temperature. T_e is the magnitude of the electron charge and k is Boltzman's gas constant.

As the probe is made more positive with respect to the anode, the ion sheath surrounding the probe collapses at C and the effective area of the probe is equal to its physical area. The probe current at point C is

$$I = JA \qquad (7.8.2)$$

where J is the current density and A the physical area of the probe, which is known. But J is proportional to Ne $\bar{v}$, where N is the electron density, and $\bar{v}$ the thermal velocity of the electron. The thermal velocity is easily calculated from the electron temperature already determined, thus, only N is unknown and can be calculated.

Efforts were made to design and build a logarithmic amplifier which would facilitate the display of the probe characteristics on an oscilloscope. However, the range of measurable probe current was over 5 decades and the design problems became too time consuming and the idea was dropped.

The probe that was used in the experiment was the loop itself. It was

isolated from a D. C. point of view from the r. f. equipment by means of inside and outside D. C. blocks in the coaxial line. The result was that the only D. C. path from the loop to the anode was through the plasma, as was desired. A much smaller probe had been used earlier but Persson (1964) cautions that a very small probe yields non-reproducable measurements. The loop area was very nearly 1 cm^2, and the Langmuir probe characteristics were indeed reproducable. The loop was cleaned by ion bombardment at frequent intervals during the series of measurements. Kostelnicek (1964) points out that the better the probe and anode are cleaned, the sharper the break in the Langmuir curve. This is important in the accurate determination of the slope and the "break" current of the curve, (at ion sheath collapse).

A very sensitive ammeter was used to measure the probe current. The range of the ammeter was from 10^{-6} ma to 10 ma. With the pressures and discharge currents used in the experiments, a probe to anode voltage range from -30 VDC to +30 VDC was adequate to cover the range of interest.

During the impedance measurements, the loop was maintained at a potential such that the ion sheath was collapsed.

7. 9 The Collision Frequency and the Plasma Parameter Z

Methods for determining the plasma parameters X and Y have already been outlined. It remains to establish a means of calculating the collision frequency. The total collision frequency is the sum of the electron-ion collision frequency and the electron-molecule collision frequency (Balmain, 1963). According to

Persson (1964), the electron-ion collisions predominate in the brush cathode plasma.

Balmain (1963) gives the following relations for electron-ion and electron-molecule collision frequency.

$$\nu_{ei} = \frac{3.62\times10^{6} N_i}{T_e^{3/2}} \ln\left[\frac{3.3\times10^{6} T_e^{3/2}}{N_i}\right] \qquad (7.9.1)$$

and

$$\nu_{em} = \frac{4}{3}\bar{v} p_c p \qquad (7.9.2)$$

where N_i is the ion density (which is equal to the electron density), T_e is electron temperature in degrees Kelvin, $\bar{v}$ is the thermal average velocity of the electron, P_c is the probability of electron-molecule collision (P_c = 19 for He) and p is the pressure of He in mmHg.

Both electron-ion and electron molecule collision frequencies were calculated by means of the previous formulae and in most cases $\nu_{ei} \gg \nu_{em}$, except at high electron temperatures where ν_{ei} was quite small.

7.10 The r.f. System and the Measurement of Impedance

The measurement of impedance was accomplished by straight forward slotted line techniques. As will be discussed in the next section, a frequency range from 500 M Hz to 1050 M Hz was selected for the measurements. A great deal of care was taken in the construction of the coaxial feed to the small loop beyond the slotted line. This was necessary because of the nature of the impedance being measured. Since the loop is very small in terms of the wave-

length, the loop impedance was almost purely reactive, especially in the free space case where no plasma existed.

A reference point was established by immersing the whole loop in a bath of mercury.

A 1200 M Hz low pass filter was used in the frequency range from 1050 M Hz down to 750 M Hz, and a 800 M Hz filter was used below 750 M Hz.

The frequency was monitored by means of a resonant cavity and the wavelength was measured by means of the slotted line as a check each time the frequency was changed. A crystal detector was used in the slotted line and measurements were taken at as low a power input as possible without losing the signal in noise.

Because the reference point of impedance was the shorted loop itself, the null shift and the standing wave ratio could be plotted on a Smith Chart giving the loop impedance directly.

7.11 The Range of Plasma Parameters Used

The three basic parameters that could be controlled in this experimental measurement were r.f. frequency, electron density and D.C. magnetic field. Very little control was possible over the collision frequency.

At first it was hoped that the electron density could be controlled with a fair amount of accuracy by changing only the discharge current. This was true to a certain degree, but it must be remembered that if the discharge current is increased, the electron temperature would usually increase too. Thus, there was not a linear relation between discharge current and electron density. One

was usually able, however, to obtain an electron density within a factor of 1 to 5 of the value that was desired. This was accomplished by running a visual Langmuir probe test and adjusting the discharge current until the desired "break" current was obtained, all the time assuming that the electron temperature would range between 200° C to 1200° C. The unknown electron temperature was the variable that contributed to the difficulty of achieving the exact electron density desired.

A more serious problem arose when there was a non-zero D. C. magnetic field present. The larger the magnitude of the D. C. magnetic field, the higher the electron temperature. Thus, even if a desired electron density had been obtained in the absence of the magnetic field, it would change when the magnetic field was added. So, although a desired value of B_o was easily set by dialing the correct value of coil current, it was difficult to obtain the correct electron density.

A value of B_o could have been set, (fixing plasma parameter Y) and then the tube current changed, thus, changing X. However, this would have meant that a new set of Langmuir probe characteristics would have had to be determined for each and every combination of X and Y, which would have been very time consuming.

To alleviate the situation, the following method was used to change the plasma parameters X and Y.

First, a desired value of Y was set by setting a current value in the mag-

netic coils, and fixing the r.f. signal frequency at 1050 M Hz. Then, the discharge current was set to give a desired "break" current in the Langmuir characteristic. Once the Langmuir characteristics had been accurately determined, the exact value of X, Y, and Z were known.

From that point on changes in X, Y, and Z were accomplished by lowering the r.f. signal frequency 50 M Hz at a time and measuring the impedance at each of the frequencies down to 500 M Hz. Since X is inversely proportional to the square of the frequency, an increase in X up to a factor of 4.41 was accomplished by lowering the frequency in steps. Likewise, an increase in Y up to a factor of 2.1 was possible.

One disadvantage of this method, aside from having to re-tune the r.f. circuit each time the frequency was changed, was that the value of Z also changed. But since control over Z was difficult, if not impossible, this method was considered to be as good as any, considering that only one Langmuir characteristic had to be determined for a set of twelve different combinations of X, Y, and Z.

The number twelve, of course, is the number of 50 M Hz steps that exist between and including 1050 M Hz and 500 M Hz.

The numerical range of the plasma parameters achieved was $0 \leq X \leq 15.65$, $0 \leq Y \leq 2.0$, $0.0047 \leq Z \leq 0.18$. These were not obtained simultaneously, but represent the maximums and minimums achieved amongst all the measured parameters.

CHAPTER 8 THE NUMERICAL INTEGRATION OF THE THEORETICAL EXPRESSIONS

The derived expressions for the impedance of the loop are in integral form. There are three such expressions. The first is the integral representation for the first order correction to the quasi-static result when $\overline{B}_o$ is normal to the loop, and is given by equation (4.1.16). The second integral is the representation of the loop impedance in a uniaxial medium when $\overline{B}_o$ is normal to the loop as given by equation (5.3.6). The third integral is the representation of the impedance of the loop in an uniaxial medium in which the magnetic field, $\overline{B}_o$, is parallel to the plane of the loop. This is equation (6.3.16) which consists of a single and a double integral.

It is, of course, desirable to study the numerical results given by these integral representations. Thus, programs were written to evaluate the integrals numerically using a high-speed digital computer (University of Illinois IBM 7094).

There is a marked resemblance, as might be expected, in the three integrals. They all involve Bessel Functions of the first kind of order one, as well as exponential functions. They all involve integrals from zero to infinity as well, which posed the problem of accuracy and convergence in the numberical evaluation. For this reason an attempt was made to find equivalent expressions in the form of definite integrals. This attempt was successful in the case of equation (4.1.16), the first order correction term to the quasi-static impedance.

(4.1.16) is repeated here.

$$Zin_{corr.} = \frac{-j\omega\mu_o\rho_o C\lambda^2 K_1 K_o \pi}{K_1 - K_o} \int_0^\infty \frac{J_1^2(x)}{x^2}\left[e^{-Rx} - \frac{e^{-\beta Rx}}{\beta}\right] dx \quad (8.1.1)$$

Bateman (Vol. no. 1, p. 183, 1954) gives the following formula.

$$I(p) = \int_0^\infty \frac{e^{-pt} J_1^2(t)dt}{t^2} = \frac{1}{2\pi}\int_0^\pi (1+\cos\phi)\left[\sqrt{p^2+2(1-\cos\phi)} - p\right] d\phi \quad (8.1.2)$$

Thus,
$$Zin_{corr} = \frac{-j\omega\mu_o\rho_o C\lambda^2 K_1 K_o \pi}{K_1 - K_o}\left[I(R) - \frac{1}{\beta} I(\beta R)\right] \quad (8.1.3)$$

After setting
$$\theta = \phi/2 \quad (8.1.4)$$

and defining
$$\psi(R) = \int_0^{\pi/2} \cos^2\theta \sqrt{R^2 + 4\sin^2\theta}\, d\theta \quad (8.1.5)$$

(8.1.3) becomes

$$Zin_{corr.} = \frac{-j\omega\mu_o\rho_o C\lambda^2 K_1 K_o^2}{K_1 - K_o}\left[\psi(R) - \frac{1}{\beta}\psi(\beta R)\right] \quad (8.1.6)$$

This is the definite integral expression that was used for the numerical evaluation of Zin_{corr}.

Equation (5.3.6) was programmed as it stands and equation (6.3.16) was programmed to evaluate only the double integral, because the single integral is equal to one half of the integral given by (5.3.6), as will be discussed later. The program technique used was COMPLEX FORTRAN which gave the results in complex form directly. The numerical method used was Gauss-Legendre quadrature.

It should be noted, as mentioned before, that if R were set equal to zero,

each integral would diverge. The fact that R is a small number is cause for special care in the evaluation of the indefinite integrals.

Thus, equation (5.3.6) was evaluated by integrating numerically over intervals of five, each interval being divided into at least fifteen segments with a specified desired accuracy of 1 part in 10^4 for both the real and imaginary part of the integral. This routine was repeated, (0 to 5, 5 to 10, 10 to 15, etc.) until the numerical contributions of the last interval contributed less than 1 part in 10^4 to the total integral. This resulted invariably in the upper limit of the integral being 75.0. The upper limit was independant of the plasma parameters used.

The evaluation of (8.1.6) to give $Zin_{corr.}$ was accomplished by integrating from 0 to $\pi/2$ using at least fifteen divisions, and requiring an accuracy of 1 part in 10^4 for both the real and imaginary part of the integral.

The double integral of equation (6.3.16) was programmed to integrate from 0 to π in 10 divisions and from 0 to 30 in 96 divisions. It was found that when K_1 was set equal to K_o, in which case (6.3.16) and (5.3.6) are identical, that the numerical results of the double integral routine agreed with the results of the numerical integration of (5.3.6) within less than 0.1%. Thus, the upper limit of 30 on the indefinite integral was deemed satisfactory.

The programs were designed to accept plasma parameters X, Y, and Z as well as ω, ρ_o, and δ as input data and each program yielded the impedance result, normalized to 50 ohms.

The complete calculated results, presented later in this study, consumed about five hours of computer time. Equation (8.1.6) took 0.8 sec/run; (5.3.6) took 10 sec/run and the double integral of (6.3.16) took 30 sec/run, a run being one set of input parameters, (ω, ρ_o, δ, X, Y, Z).

CHAPTER 9 A DISCUSSION OF THE DERIVED THEORETICAL FORMULAE

9.1 The First Order Correction Term, $\bar{B}_o$ Normal to the Loop

Equation (4.1.16) for the first order correction term to the quasi-static impedance is repeated here for convenience.

$$Zin_{corr.} = \frac{-j\omega\mu_o\rho_o C\lambda^2 K_1 K_o \pi}{K_1 - K_o} \int_0^\infty \frac{J_1^2(x)}{x^2} \left[e^{-Rx} - \frac{e^{-\beta Rx}}{\beta}\right] dx \quad (9.1.1)$$

where
$$\beta^2 = K_1/K_o \quad (9.1.2)$$

The following observations are pertinent:

(i) $Zin_{corr.}$ is propertional to $C\lambda^2$, a very small number.

(ii) If there are any losses ($Z \neq 0$), K_1 and K_o are complex which results in a contribution to the real part of $Zin_{corr.}$. (Values of $Z=0.01$ were common in the experimental plasma). These slight losses contribute only a very small real part.

(iii) By examining (9.1.2) one sees that it is possible for β^2 to be negative, for some values of X and Y, even if Z is set nearly equal to zero. This would cause β to be almost pure imaginary and thus, would contribute to the real part of $Zin_{corr.}$.

Assuming for the moment that the losses in the medium are zero, the region in which β^2 is negative is shown in Figure 6b. This region is described by $X < 1$, $Y < 1$, $Y^2 > 1-X$ and by $X > 1$, $Y > 1$ and is referred to by Bal-

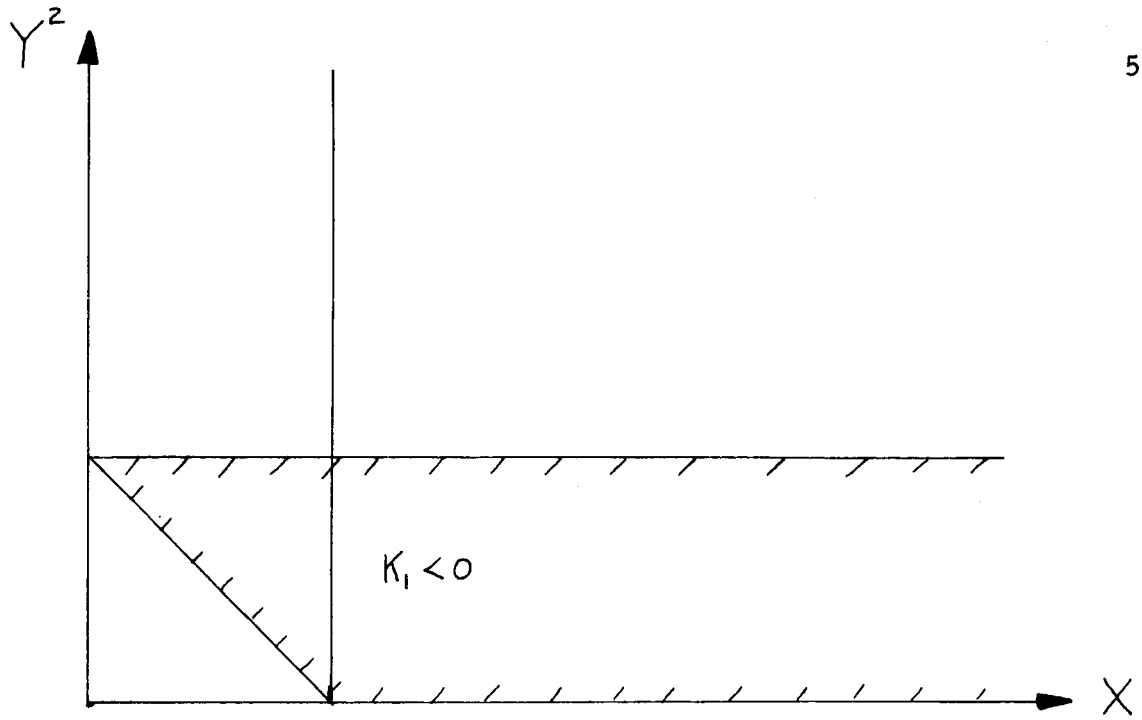

Figure 6 (a) The (X, Y^2) Plane, Behavior of K_1

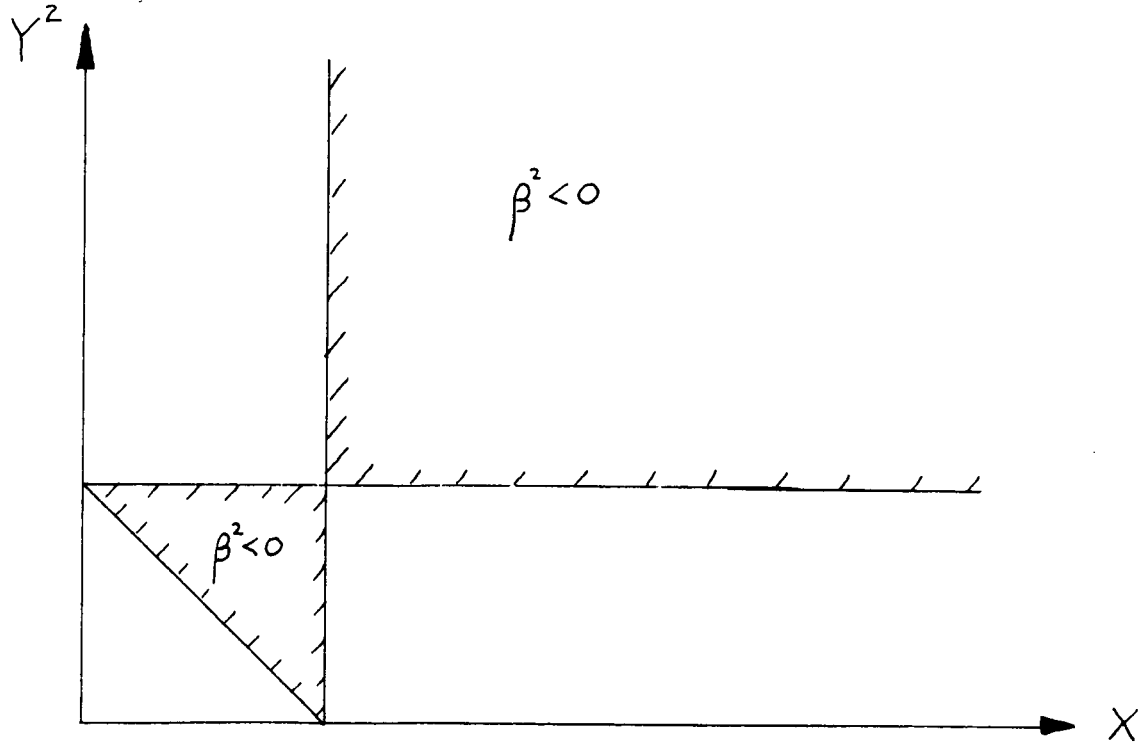

Figure 6 (b) The (X, Y^2) Plane, Behavior of K_1/K_o

main (1963) as the hyperbolic region, because the source-free wave equation is hyperbolic for those combinations of plasma parameters X and Y. Thus, we expect a contribution to the real part of $Zin_{corr.}$ in the region (hyperbolic) where β^2 is negative over and above the contribution due to slight losses in the medium ($Z \neq 0$).

(iv) Assuming slight losses which implies

$$U \ll 1 \qquad (9.1.3)$$

then
$$\beta^2 \simeq \frac{1-Y^2-X}{(1-Y^2)(1-X)} \qquad (9.1.4)$$

It can be seen from (9.1.4) that as $Y^2 \longrightarrow 1$ in the hyperbolic region, $\beta^2 \longrightarrow -\infty$ for finite non-zero X. This is the point at which we would expect the largest contribution to the real part of the loop impedance.

(v) As will be seen in the numerical results, the largest contribution to the real part of the total impedance occurs when $Y \simeq 1$.

(vi) Note also in (9.1.4) that when $Y < 1$ and X is very large, (not in the hyperbolic region), that $\beta^2 \longrightarrow \frac{1}{1-Y^2}$ and thus, there is a significant contribution to the imaginary part of $Zin_{corr.}$.

When $K_1 = K_o = 1$, $Zin_{corr.} = 0$, and the loop impedance is just the free space impedance predicted by the quasi-static theory.

9.2 The Loop Impedance in a Uniaxial Medium; $\overline{B}_o$ Normal to the Loop

Equation (5.3.6) for the loop impedance is repeated here for convenience.

$$Zin_{uniax} = j\omega\mu_o\rho_o\pi\int_0^{\infty}\frac{xJ_1^2(x)e^{-R\sqrt{x^2-K_1C_\lambda^2}}}{\sqrt{x^2-K_1C_\lambda^2}}\,dx \qquad (9.2.1)$$

The following observations are pertinent.

(i) As $C_\lambda \rightarrow 0$, $Zin_{uniax} \rightarrow Zin_{free\ space}$ for finite K_1.

(ii) Unless slight losses are assumed to exist, K_1 is pure real and there exists some value of x such that $x^2 = K_1C_\lambda^2$ (9.2.2) The assumption of slight losses ($Z \neq 0$) assures that the integrand of (9.2.1) is always finite and produces a contribution to the real part of Zin_{uniax}.

(iii) In the regions where K_1 is large and negative, the only contribution to the real part of Zin_{uniax} is due to the slight losses.

(iv) When K_1 is positive, (Figure 6a), there will be a contribution to the real part of Zin_{uniax} and this contribution will increase as K_1 increases.

(v) The greater the deviation of K_1 from unity, the greater the deviation of Zin_{uniax} from the free space impedance.

(vi) For $X > 1$ the general behavior of the uniaxial impedance is the same as the behavior of the quasi-static impedance with the first order correction term.

(vii) The factor K_o does not appear in this uniaxial impedance expression because, as was pointed out earlier, the $\hat{z}$-component of the $\overline{E}$ field is zero.

(viii) When $K_1 = 1$, i.e. $X = Y = 0$, then $Zin_{uniax} = Zin_{free\ space}$.

9.3 A Note on the Comparison of the Quasi-Static Impedance and the Uniaxial Impedance Results

As noted before, the first order correction term to the quasi-static impedance derives its characteristic from the behavior of β

where
$$\beta^2 = K_1/K_o \approx \frac{1-Y^2-X}{(1-Y^2)(1-X)} \tag{9.3.1}$$

when
$$0 < Z \ll 1.0 \tag{9.3.2}$$

The uniaxial impedance formula derives its characteristics from the behavior of K_1 where

$$K_1 \approx \frac{1-Y^2-X}{(1-Y^2)} \tag{9.3.4}$$

It is seen that these factors are very similar for small X, but each factor contributes the opposite type of behavior for $X \lessgtr 1$. For example, when $X < 1$, and $Y^2 > 1-X$ the first order correction term has a real part due to the negative value of β^2. But when $X < 1$ and $Y^2 > 1-X$, the uniaxial impedance has no real part, except that part due to slight losses ($Z \neq 0$). However, for $X > 1$ a contribution to the real part of both expressions occurs for $Y > 1$ and does not for $Y < 1$.

9.4 The Loop Impedance in an Uniaxial Medium; $\overline{B}_o$ Parallel to the Loop

Equation (6.3.16) is repeated here for convenience.

$$Zin_{uniax} = \frac{j\omega\mu_o\rho_o\pi}{2}\int_0^\infty \frac{xJ_1^2(x)e^{-R\sqrt{x^2-K_1C_\lambda^2}}}{\sqrt{x^2-K_1C_\lambda^2}}\,dx$$

$$+\frac{j\omega\mu_o\rho_o}{2}\int_0^{2\pi}\int_0^\infty \frac{x\cos^2\xi\, J_1^2(x)e^{-R\sqrt{x^2(\cos^2\xi+\frac{K_o}{K_1}\sin^2\xi)-K_oC_\lambda^2}}}{\sqrt{x^2(\cos^2\xi+\frac{K_o}{K_1}\sin^2\xi)-K_oC_\lambda^2}}\,dx\,d\xi \qquad (9.4.1)$$

The following observations are pertinent.

(i) The first integral of (9.4.1) is equal to 1/2 the impedance of the loop in an uniaxial medium where the magnetic field is normal to the loop, as can be seen from (5.3.6).

(ii) When Y=0, $K_1=K_o$ and the double integral simplifies to a single integral which is equal to the first integral of (9.4.1). Thus, as is certainly expected, both uniaxial results are equal when Y=0.

(iii) When X=Y=0, $K_o=K_1=1$ and a free space impedance formula results, as expected. This result has a very small real part due to C_λ^2 but is essentially the free space result.

(iv) In the double integral there is a contribution to the real part of the impedance when K_o is positive but this is small because C_λ^2 is small.

(v) The factor K_o/K_1 appears under the root sign which contributes to the real part of the impedance when the plasma parameters fall in the hyperbolic region as outlined before.

(vi) Setting $Z \neq 0$ (slight losses) contributes to the real part of the impedance.

(vii) In general, the impedance of a loop in a uniaxial medium in which the magnetic field, $\overline{B}_o$, is parallel to the loop, is a much more complicated function of the plasma parameters than for the case where $\overline{B}_o$ is normal to the loop. We would, therefore, intuitively expect the plasma to affect the loop impedance in a more complicated fashion in this orientation as compared to the first orientation.

(viii) The larger the deviation of K_o and K_1 and $\frac{K_o}{K_1}$ from unity, the larger the loop impedance should deviate from the free space impedance.

CHAPTER 10 THE NUMERICAL RESULTS OF THE EVALUATION OF THE THEORETICAL FORMULAE

10.1 Introduction

In the experimental measurement program, the r.f. frequency was changed in order to effect a change of plasma parameters. This was done for practical reasons as was explained earlier.

Thus, the parameters X, Y, and Z changed simultaneously.

It is desirable to study the theoretical behavior of the loop impedance under more controlled conditions, where only one plasma parameter (electron density, magnetic field, $\overline{B}_o$, or collision frequency) is varied while the others are kept constant, as well as the r.f. frequency, ω. For this reason a complete set of computer calculations was performed in which the r.f. frequency was set at 1 G Hz and the loop impedance as a function of X was calculated for a fixed Y and Z.

A value of Z=0.01 was chosen throughout because it was of the same order as the values of Z attained throughout the measurement program.

Eleven different values of X and eleven different values of Y were used in the computation. They are

$$X = (0,\ 0.5,\ 0.75,\ 0.9,\ 1.0,\ 1.1,\ 2.0,\ 5.0,\ 10.0,\ 40.0,\ 100.0) \quad (10.1.1)$$

and

$$Y = (0,\ 0.707,\ 0.9,\ 0.95,\ 0.999,\ 1.0,\ 1.01,\ 2.0,\ 5.0,\ 10.0,\ 20.0) \quad (10.1.2)$$

The results of these calculations are shown on the Smith Charts of this chapter.

10.2 Results When $\overline{B}_o$ Is Normal to the Loop

Figures 7 to 17 inclusive show the numerical results of the computation of the loop impedance. The quasi-static result (free space) plus the first order correction term is plotted as well as the result calculated for the uniaxial medium for the sake of comparison. They are labelled Q.S. and U. respectively. The impedance marked F.S. occurs when X=0.

Note that for $Y \lesssim .95$ there is a negligable real part to either impedance. Further more, in both cases, the theoretical loop impedance is essentially that of free space unless X is very large. As X increases, the impedance locus sweeps along the edge of the Smith Chart and this sweep is invariably greater in the case of X=100 in the "quasi-static plus first order correction term" impedance than for the uniaxial impedance.

For $0.999 \lesssim Y \lesssim 1.01$ a real part to the loop impedance appears in both cases. This real part appears at $Y < 1$ because $Z \neq 0$. This real part is largest in the uniaxial impedance and only moderate values of X (say X=5) are required to yield a significant real part. On the other hand, X must be greater than at least 40 before any significant real part is seen in the "quasi-static plus first order correction term" case. Also in the latter case, of $X < 10$, the impedance is essentially that of free space.

For $2.0 \lesssim Y \lesssim 20$ the uniaxial formula predicts essentially free space un-

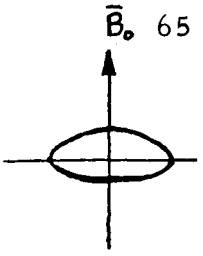

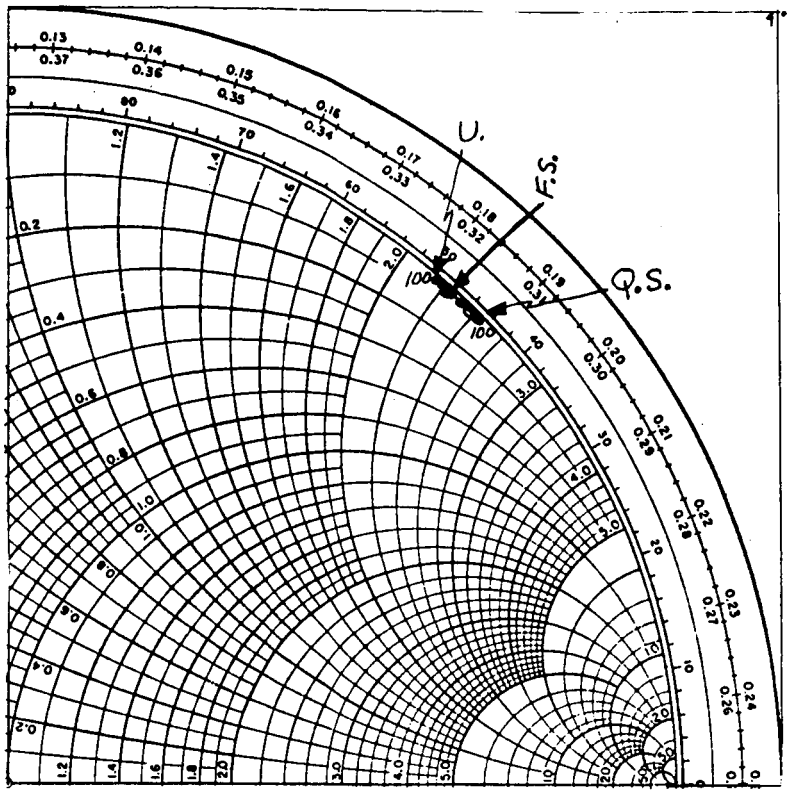

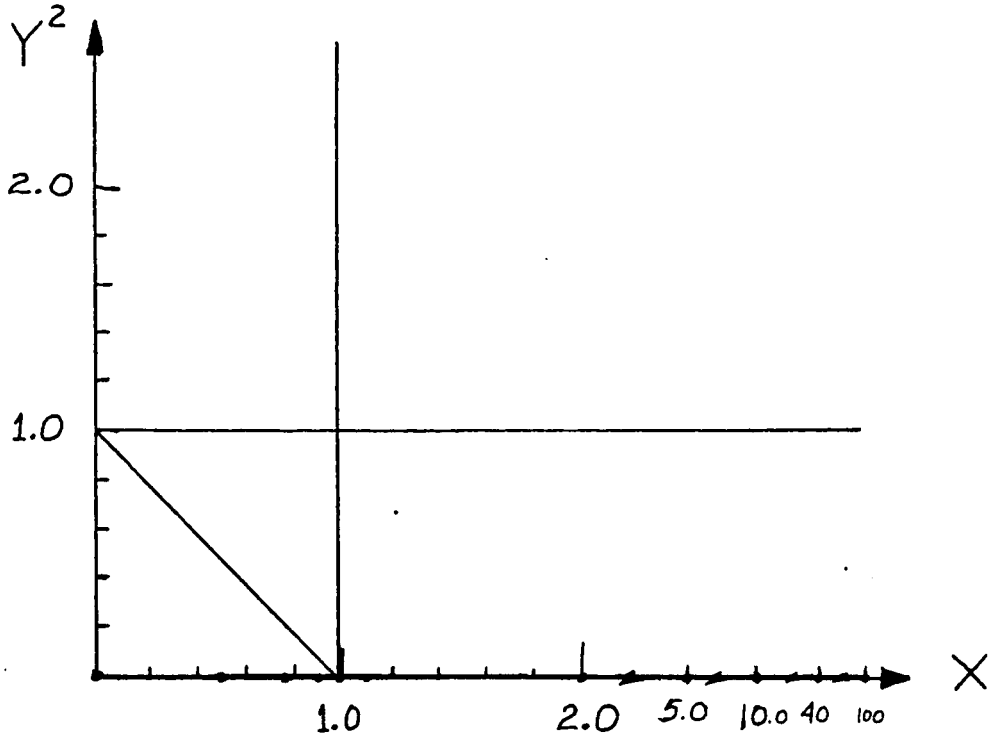

Figure 7 Calculated Loop Impedance; $\bar{B}_o$ Normal to Loop

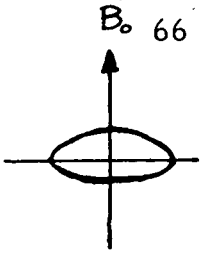

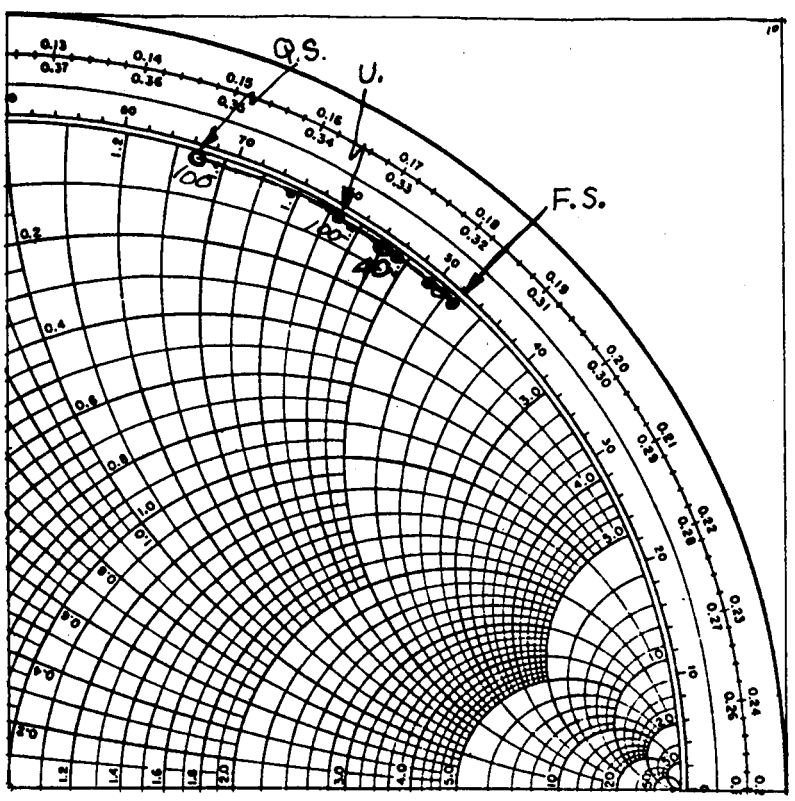

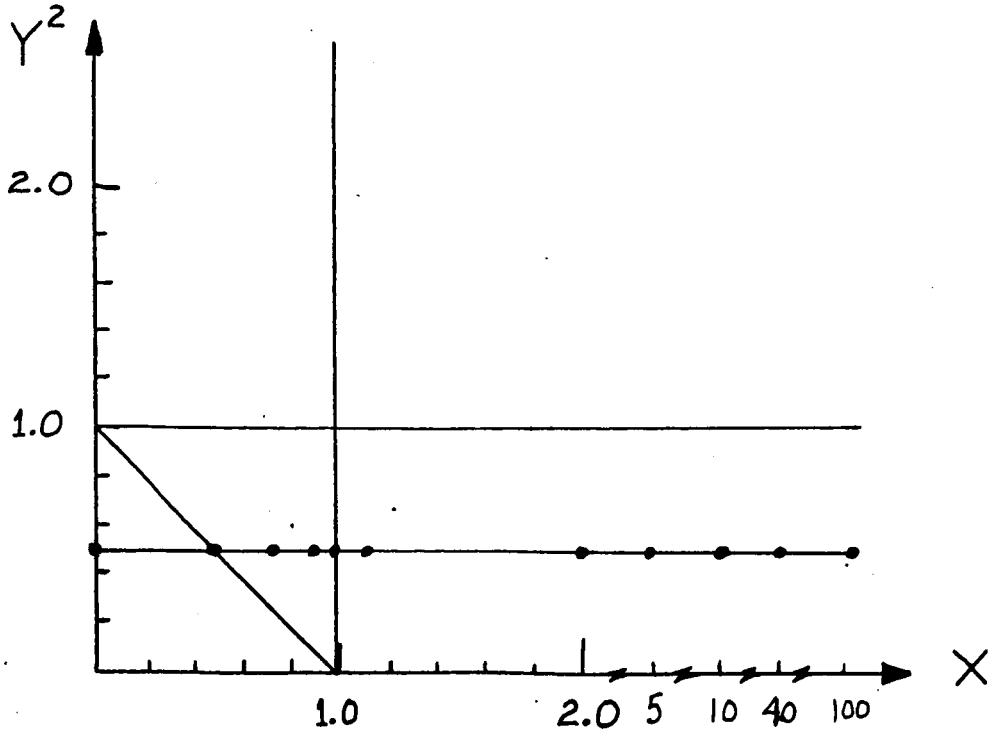

Figure 8 Calculated Loop Impedance; $\bar{B}_o$ Normal to Loop

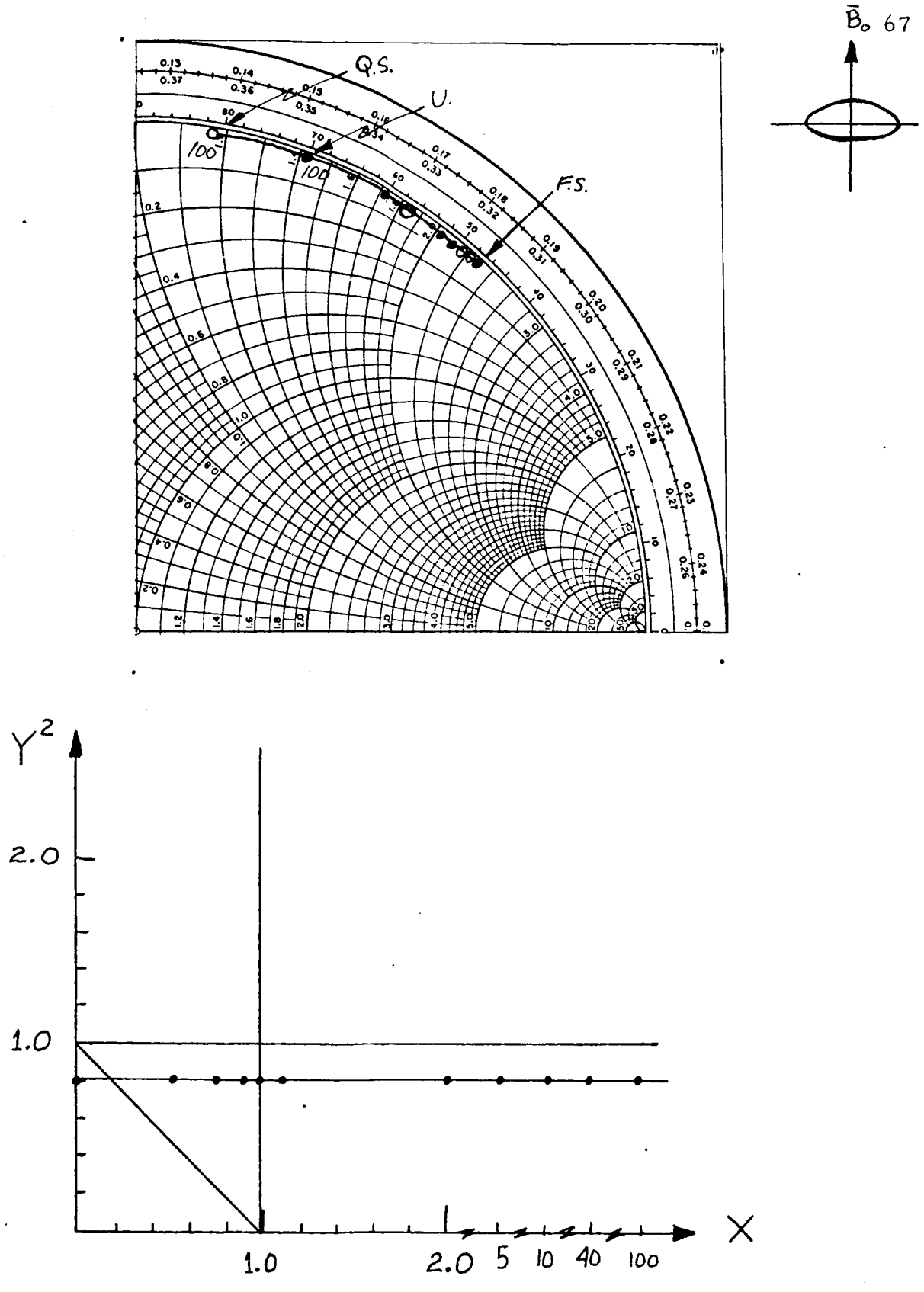

Figure 9 Calculated Loop Impedance; $\bar{B}_o$ Normal to Loop

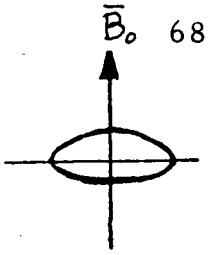

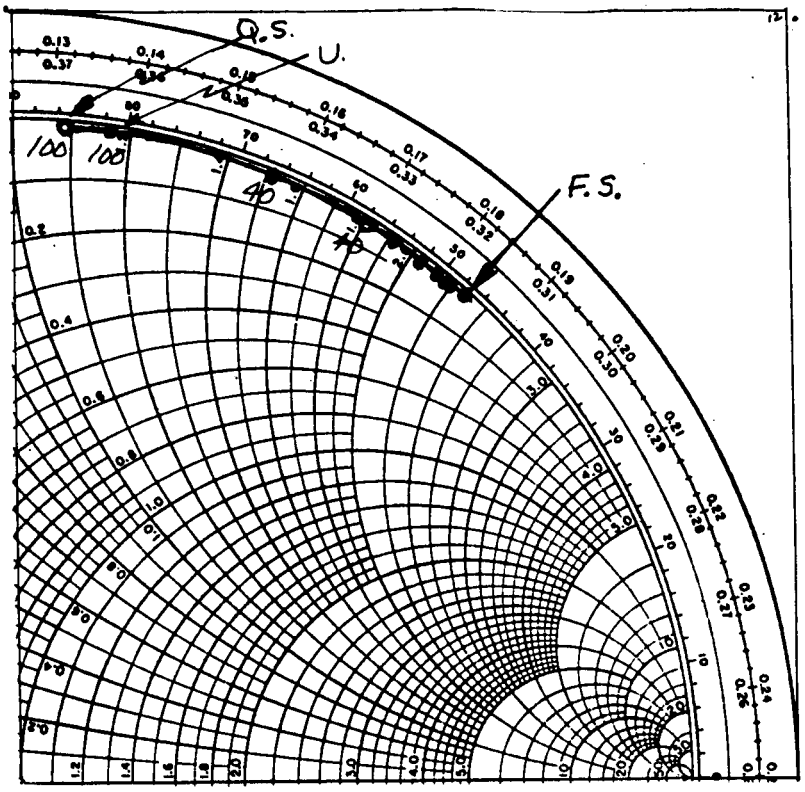

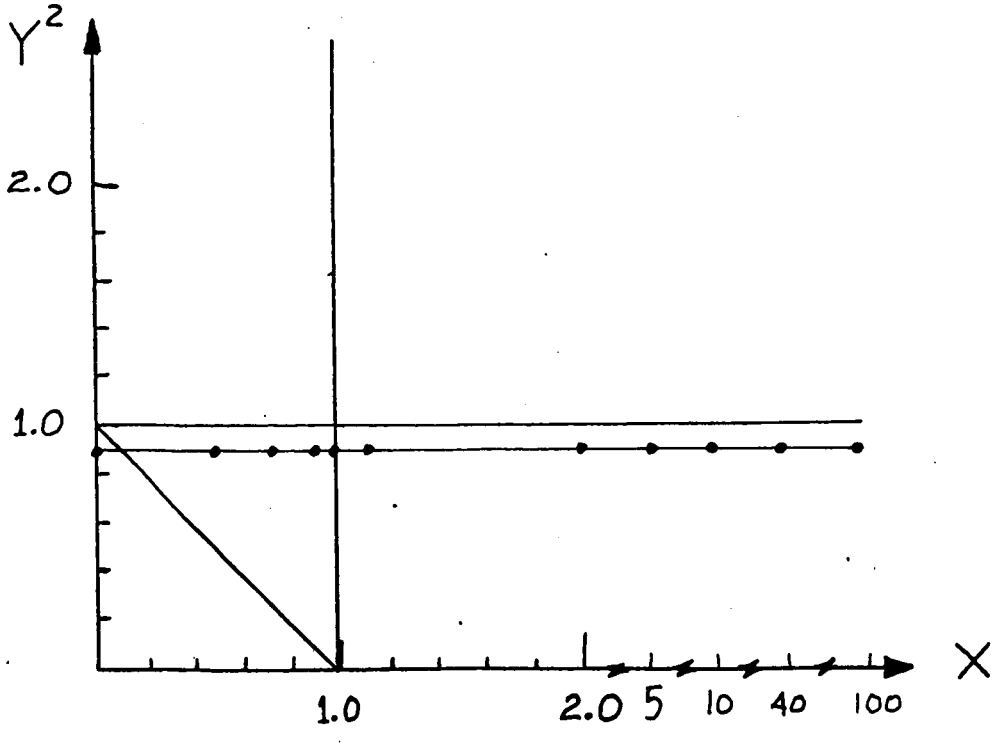

Figure 10 Calculated Loop Impedance; $\bar{B}_o$ Normal to Loop

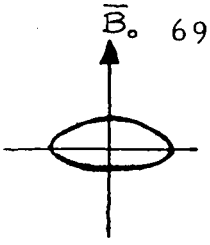

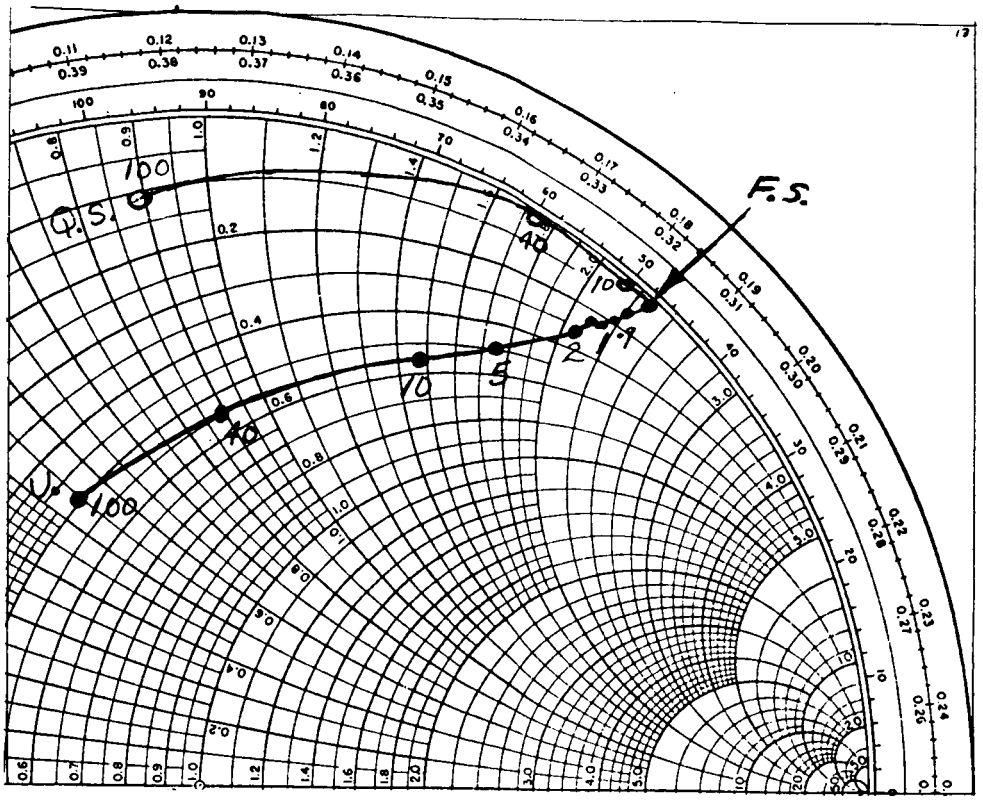

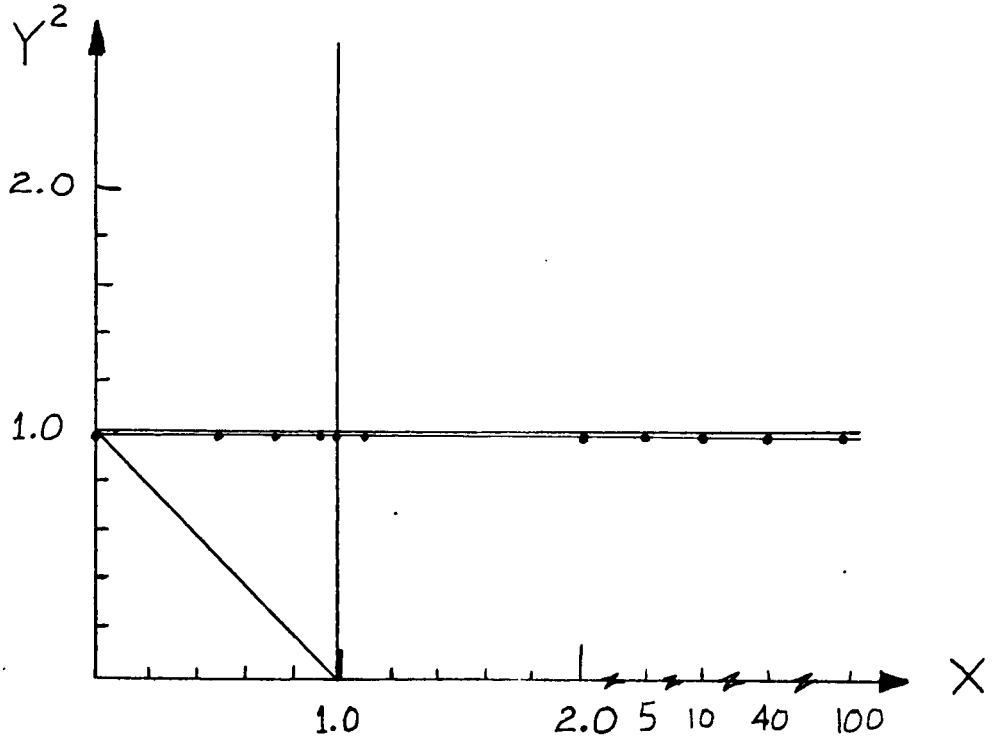

Figure 11 Calculated Loop Impedance; $\bar{B}_o$ Normal to Loop

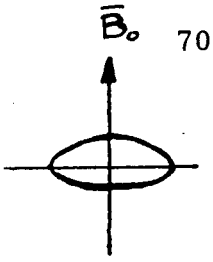

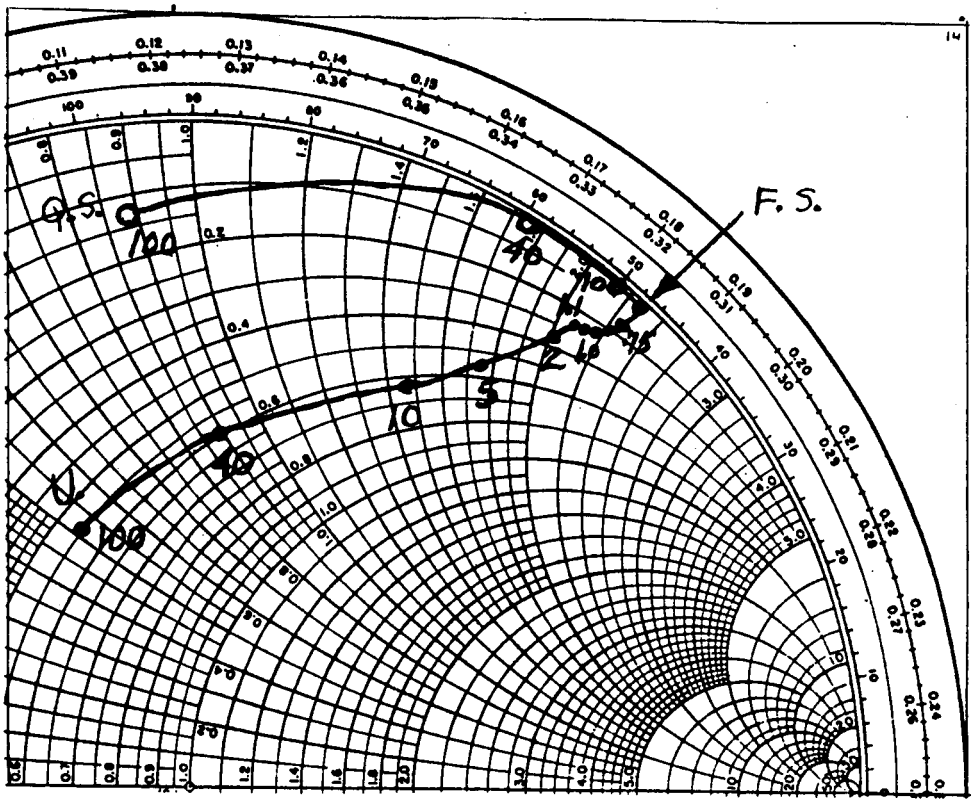

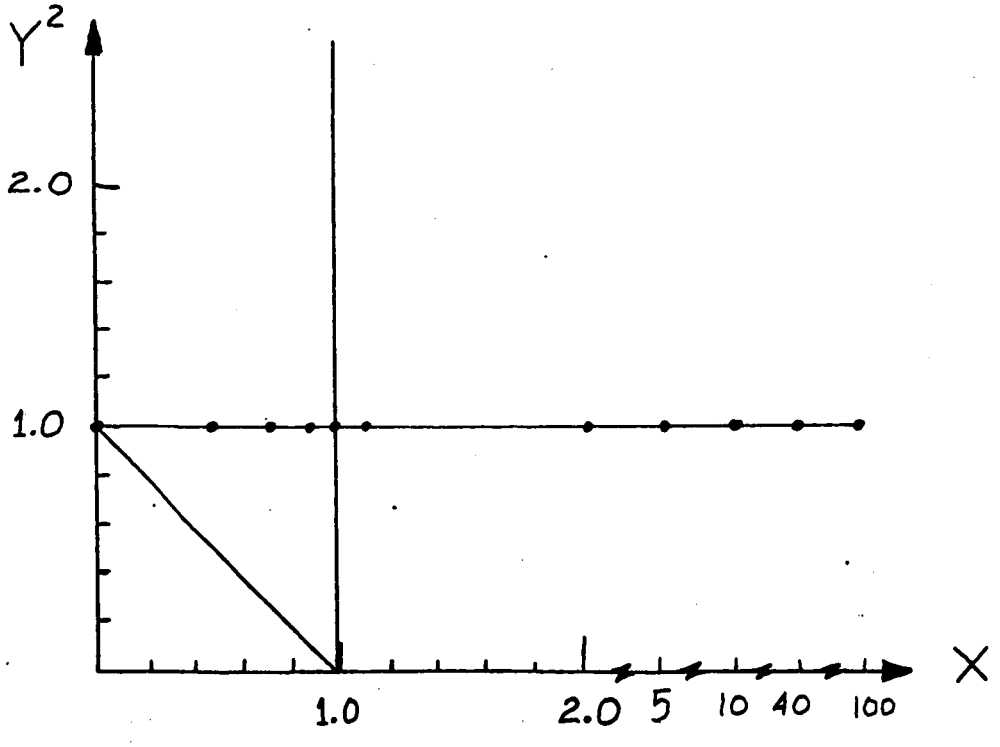

Figure 12 Calculated Loop Impedance; $\bar{B}_o$ Normal to Loop

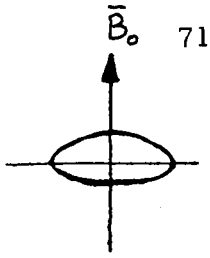

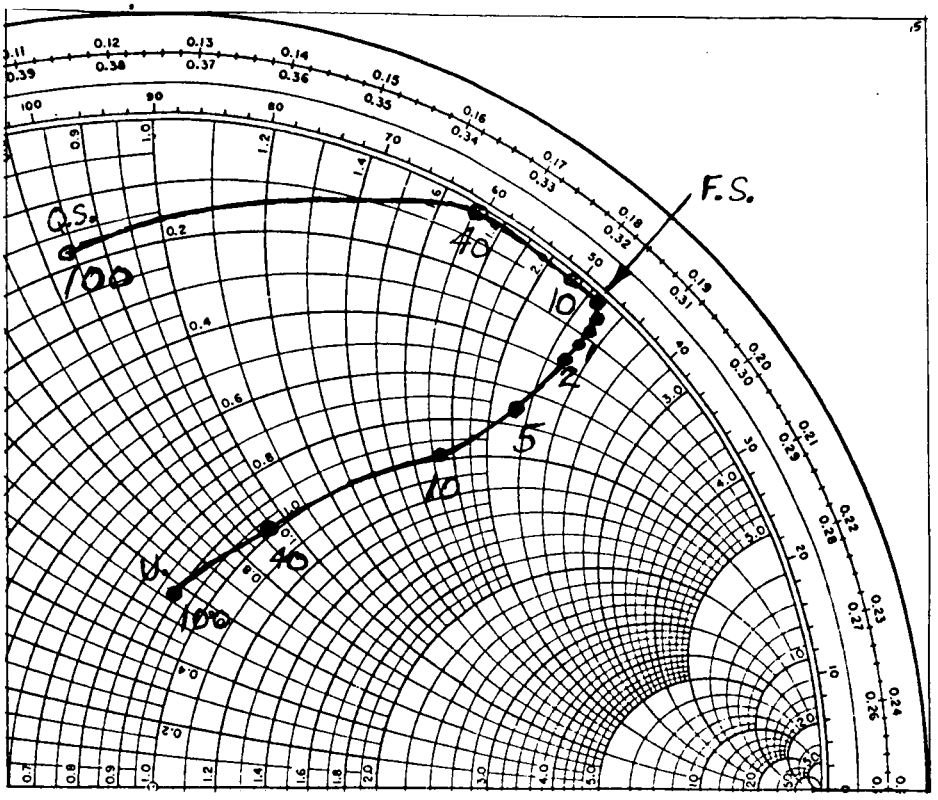

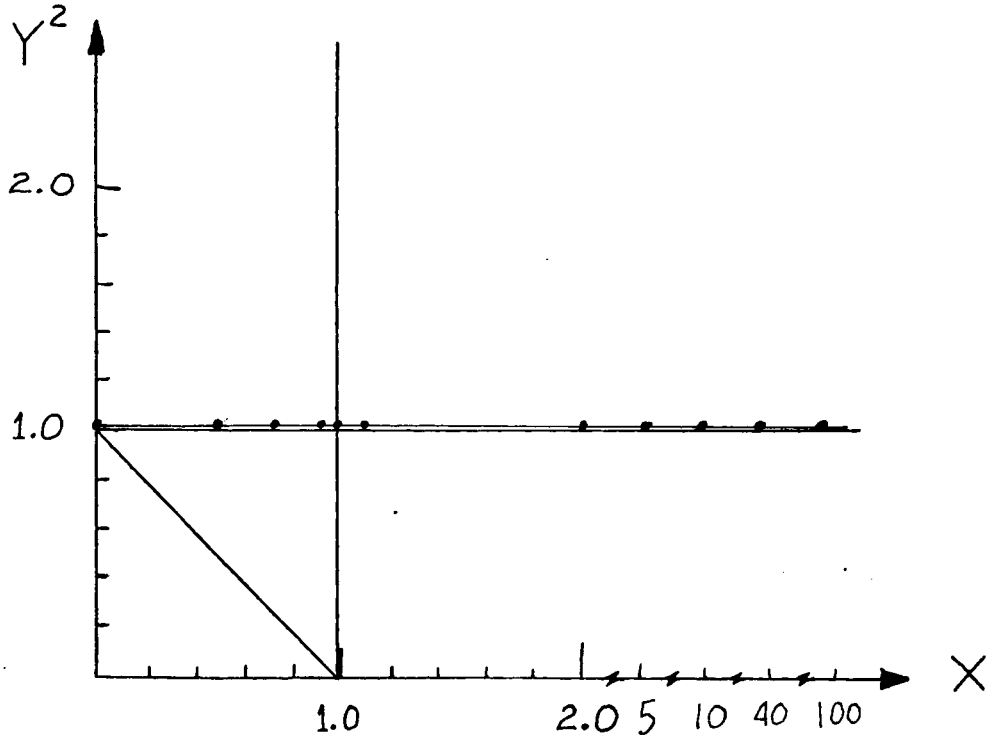

Figure 13 Calculated Loop Impedance; $\bar{B}_o$ Normal to Loop

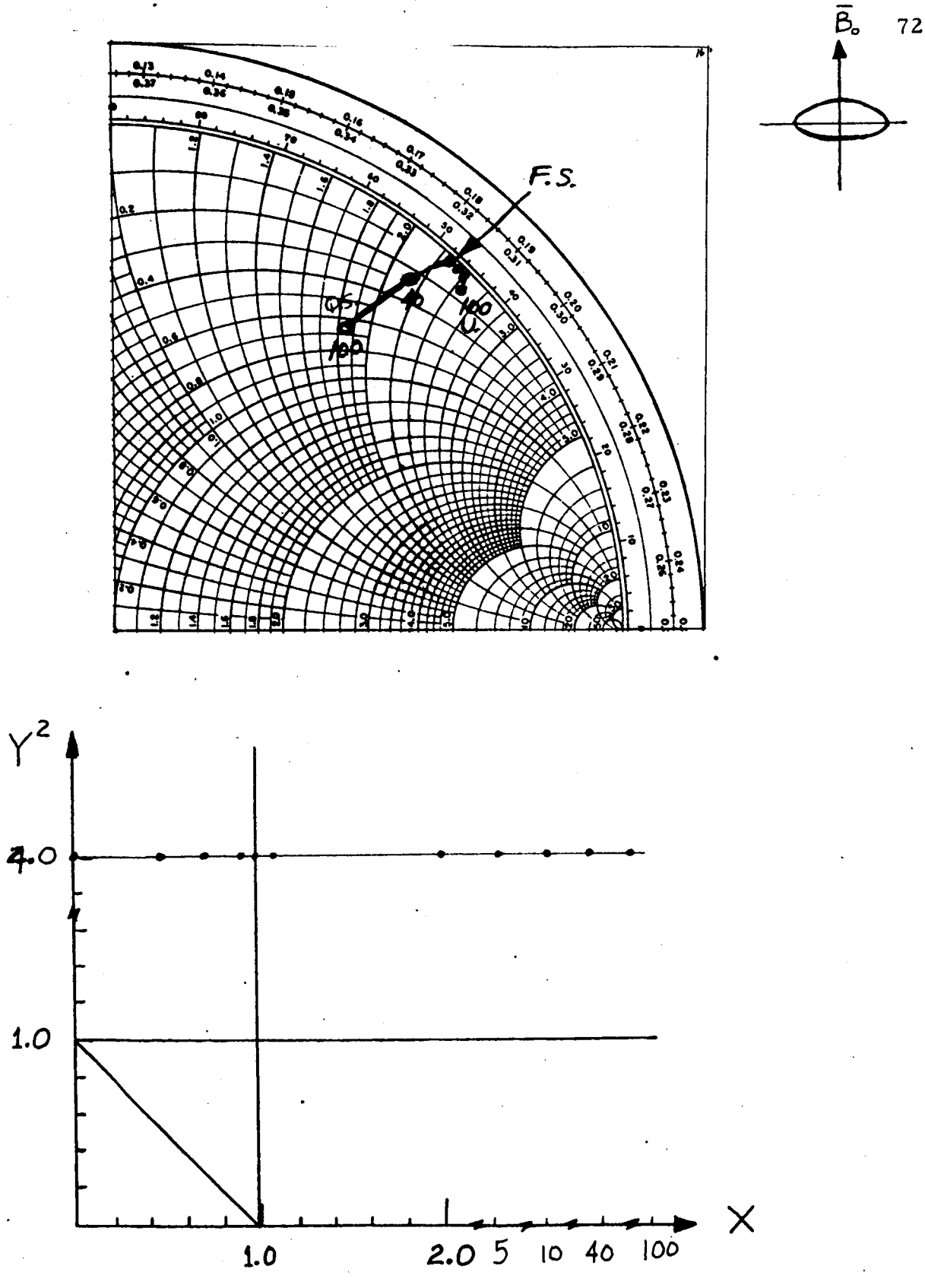

Figure 14 Calculated Loop Impedance; $\bar{B}_o$ Normal to Loop

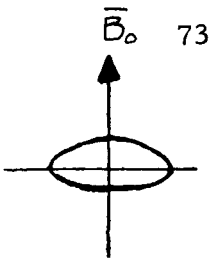

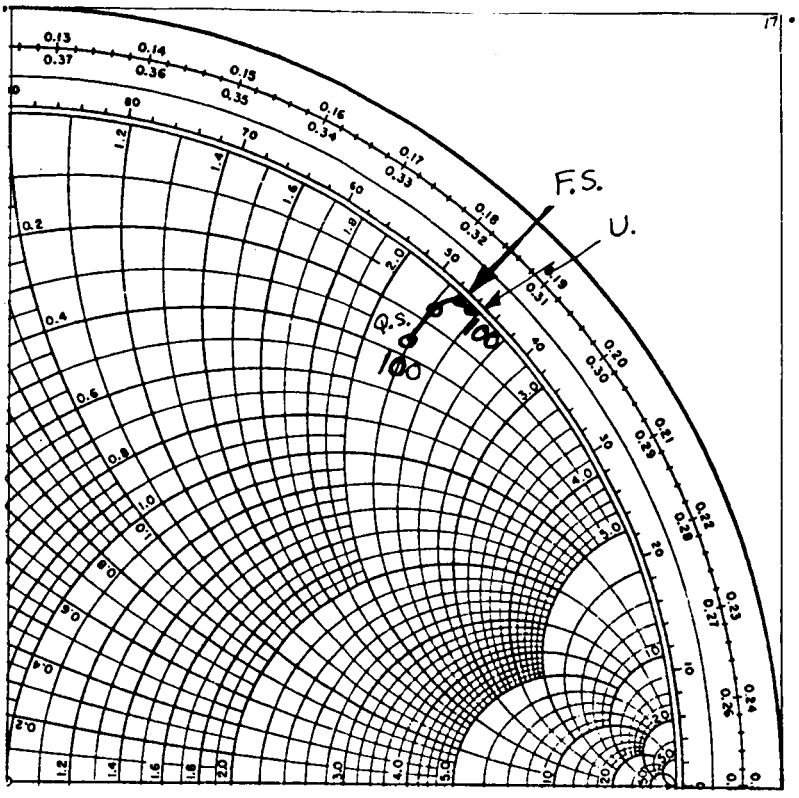

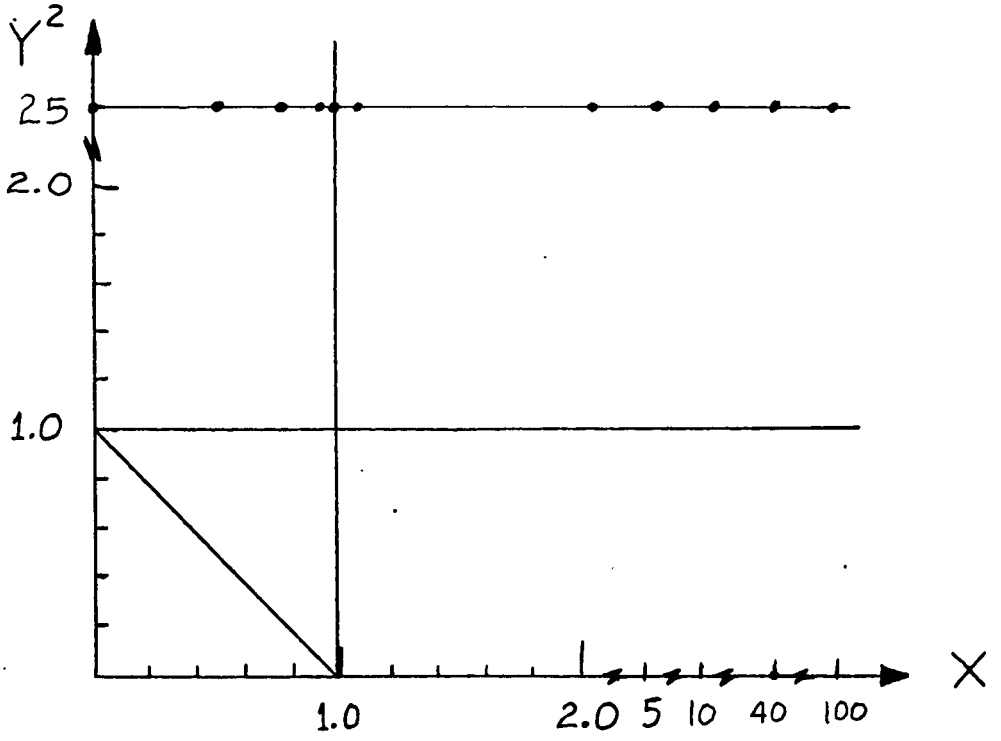

Figure 15 Calculated Loop Impedance: $\bar{B}_o$ Normal to Loop

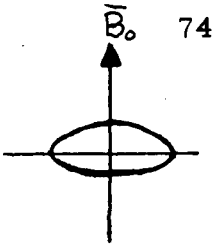

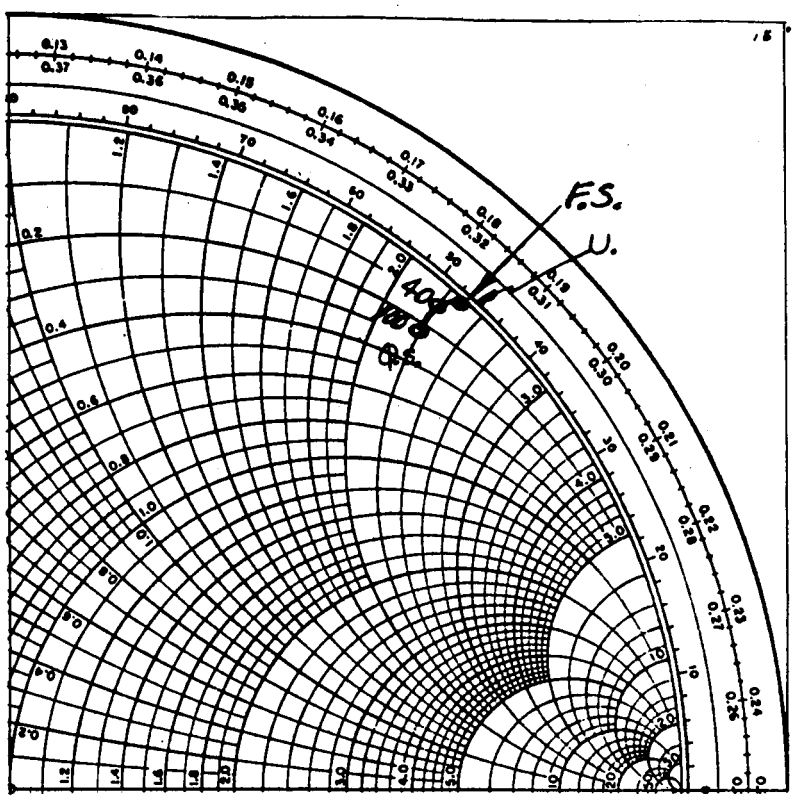

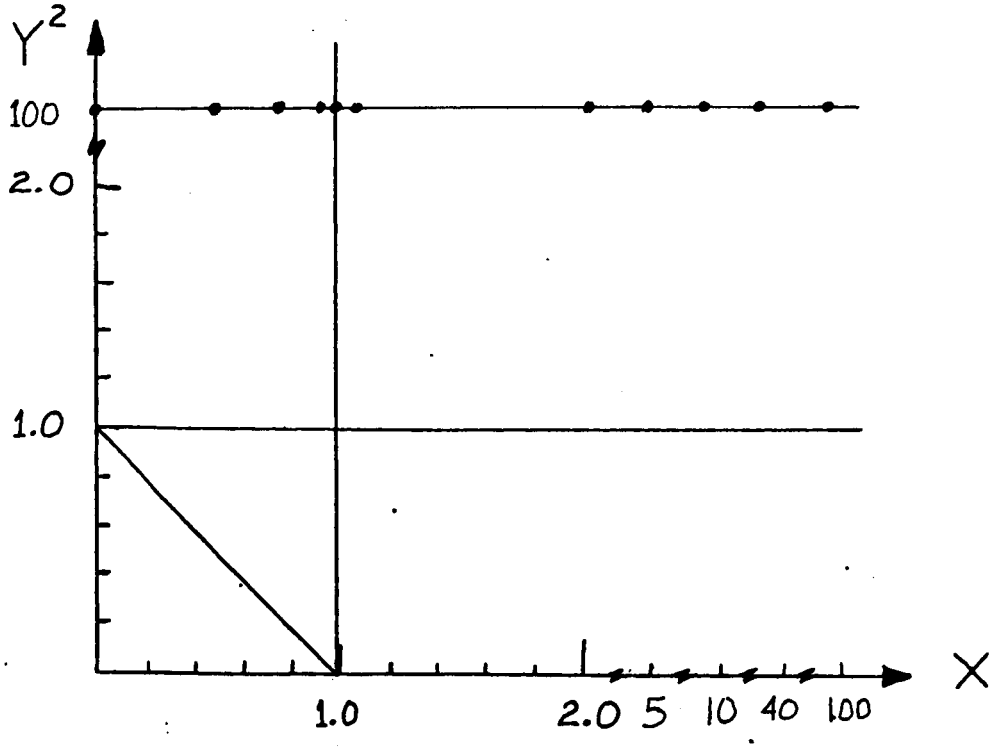

Figure 16 Calculated Loop Impedance; $\bar{B}_o$ Normal to Loop

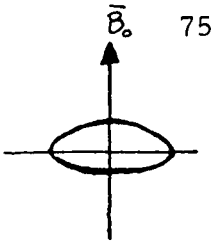

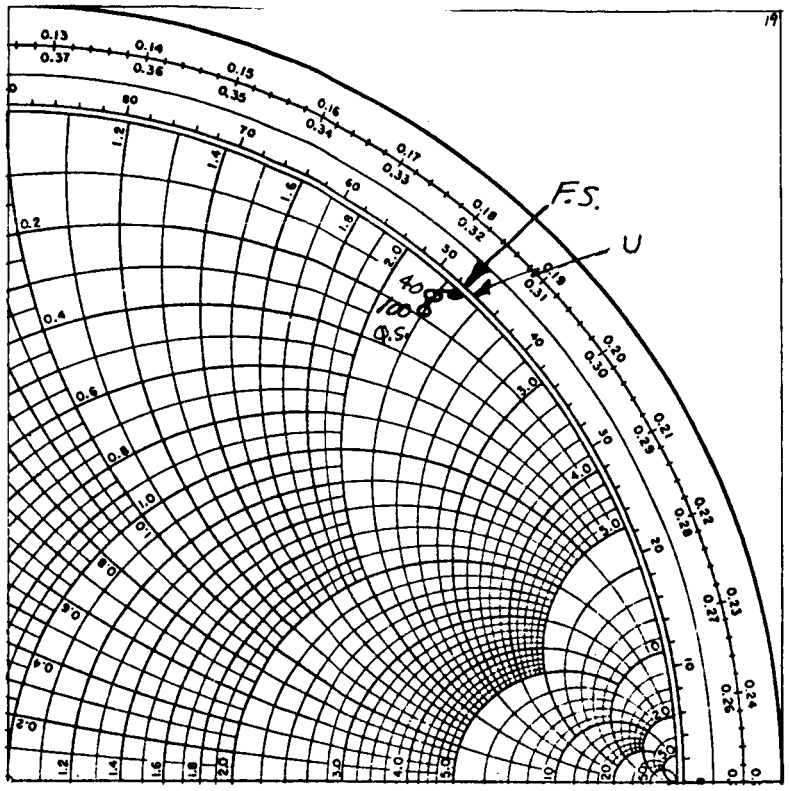

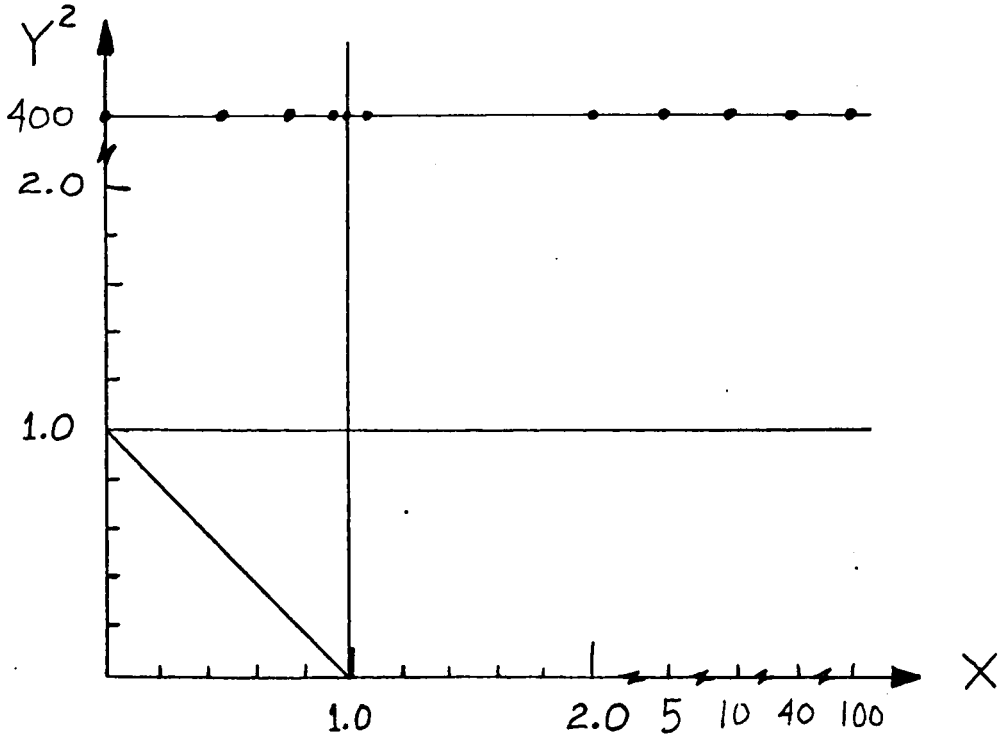

Figure 17 Calculated Loop Impedance; $\bar{B}_o$ Normal to Loop

less X is very large. This is because the factor K_1 is essentially equal to one, unless X is very large, and the term $K_1 C_\lambda^2$ is small and contributes little change from free space. The case of the "quasi-static plus first order correction term" is different, however, because for large Y, $\beta^2 \rightarrow -\frac{1}{X}$ thus contributing a real part to the loop impedance which varies as X varies. For both formulae X must be larger than 10 to cause any significant change from the free space value of loop impedance.

10.3 Results When $\overline{B}_o$ Is Parallel to the Loop

Figures 18 to 28 inclusive show the numerical results for this case. As was anticipated in Chapter 9, the loop impedance in this case exhibits a more complex plasma parameter dependance. The impedance is essentially reactive unless the plasma parameters fall inside the aforementioned hyperbolic region of the (X, Y^2) plane. However, relatively small values of X are required to cause a significant change from the free space value of impedance.

For $Y \leq 0.95$ the impedance locus consists of a loop which returns to the pure reactive edge of the Smith Chart when $X \geq 1$, except when Y=0.95 and X=100, in which case there is a small real part to the impedance, due to the factors $K_1 C_\lambda^2$ and $K_o C_\lambda^2$.

For $0.999 \leq Y \leq 1.01$ this loop becomes closed very tightly for $X \leq 1$ and then, for $X > 1$, the real part of the impedance increases with X to an relatively constant value when $X \geq 10$.

For $Y \geq 2.0$ the impedance locus becomes more complicated and exhibits

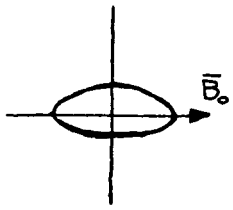

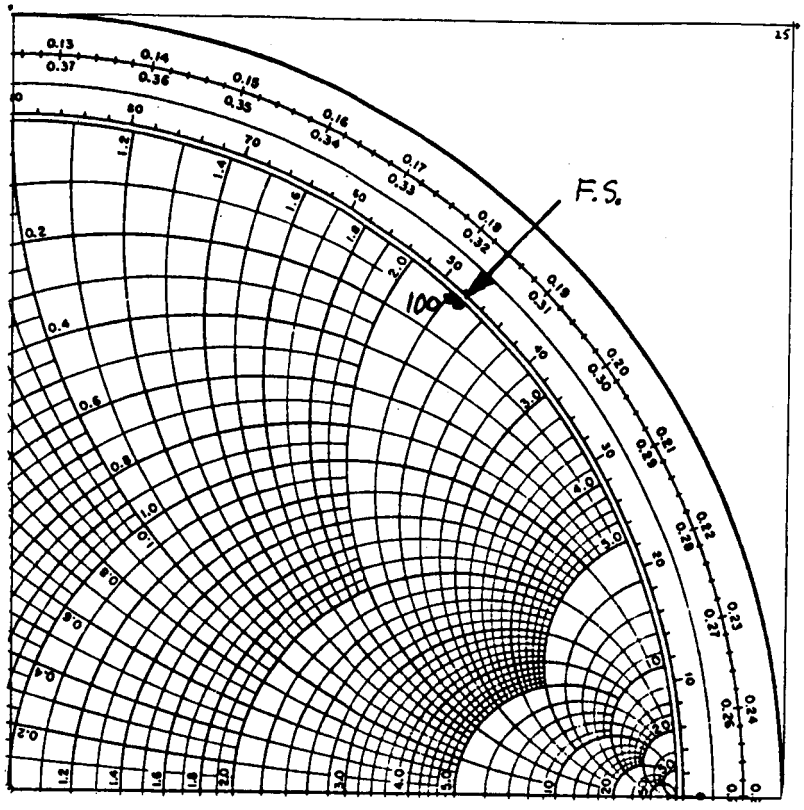

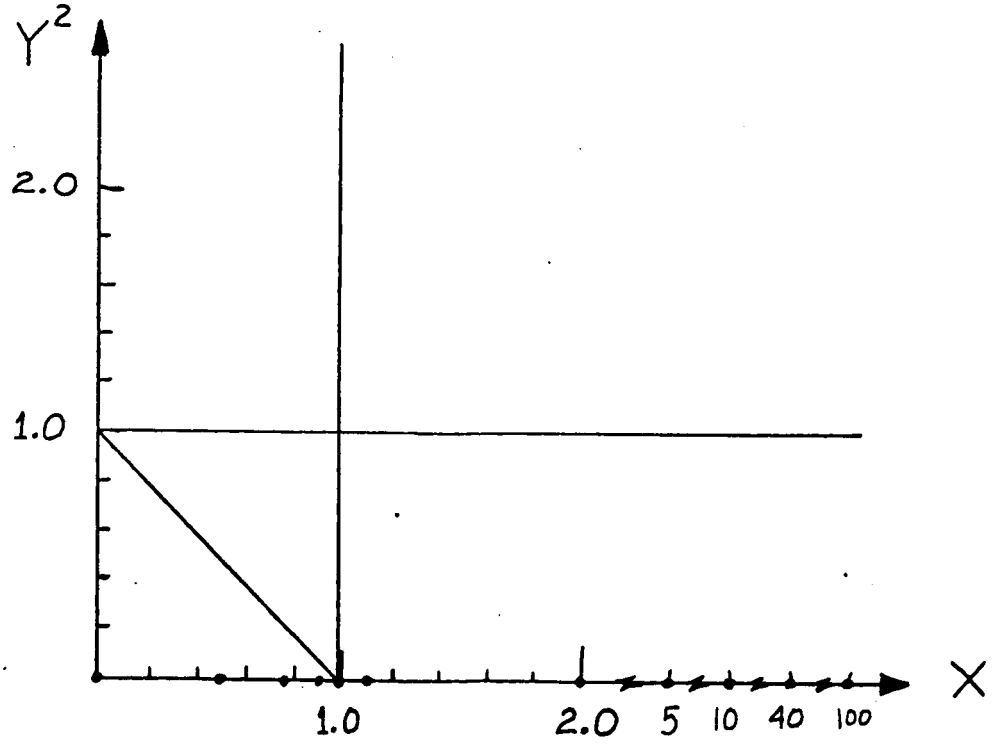

Figure 18 Calculated Loop Impedance; $\bar{B}_o$ Parallel to Loop

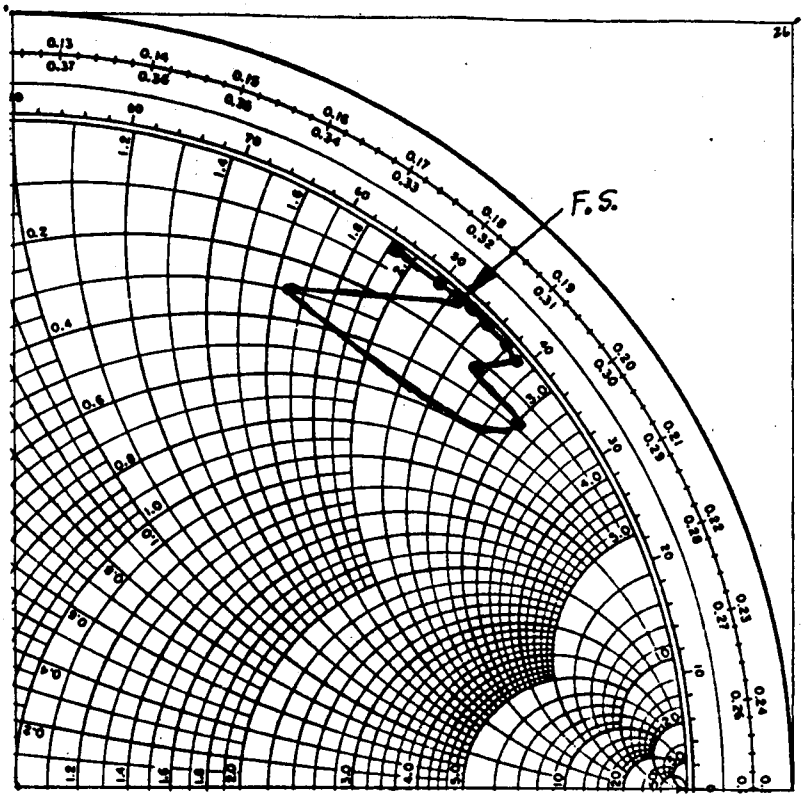

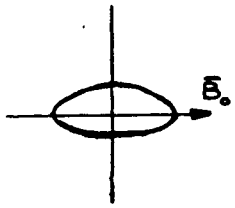

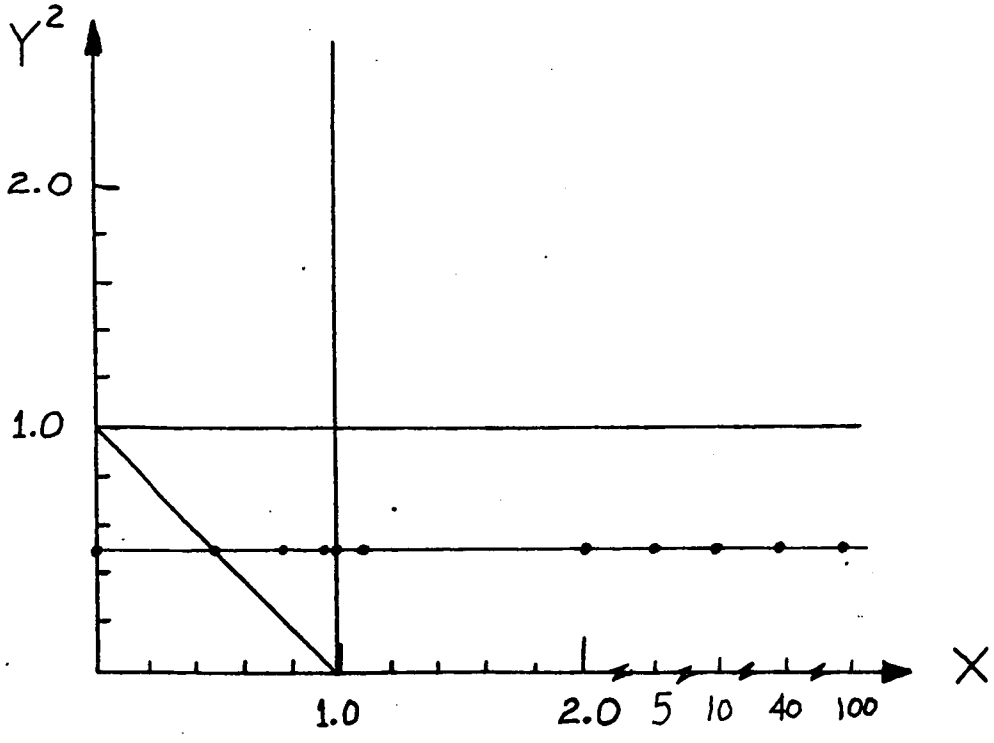

Figure 19 Calculated Loop Impedance; $\bar{B}_o$ Parallel to Loop

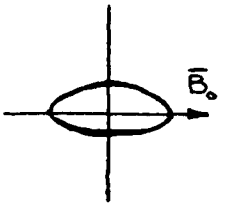

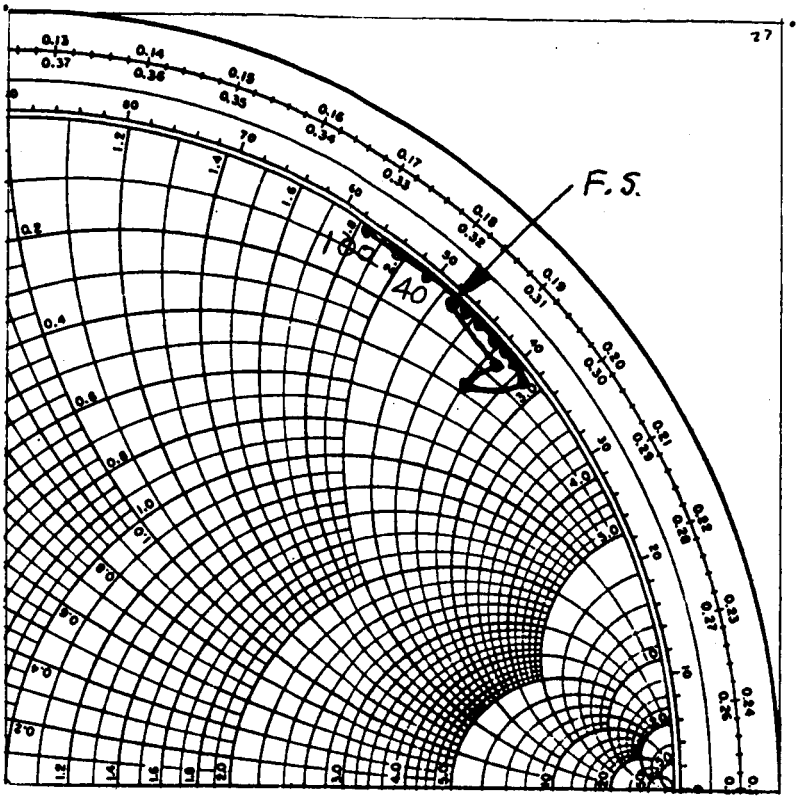

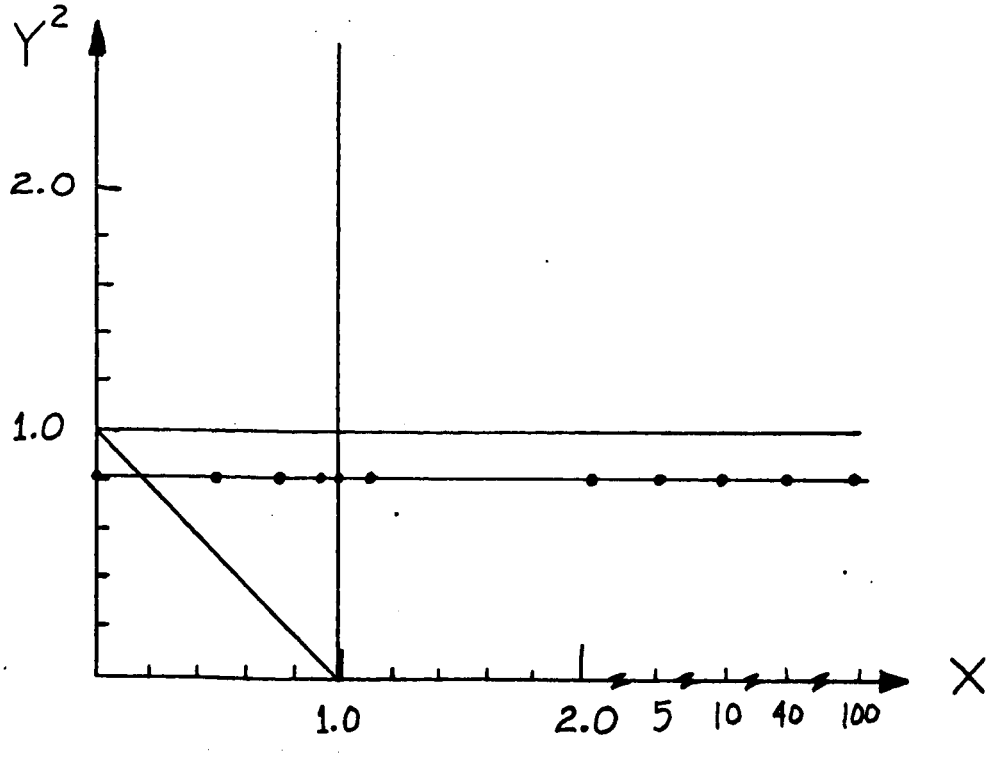

Figure 20 Calculated Loop Impedance; $\bar{B}_o$ Parallel to Loop

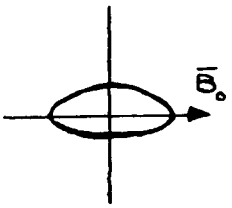

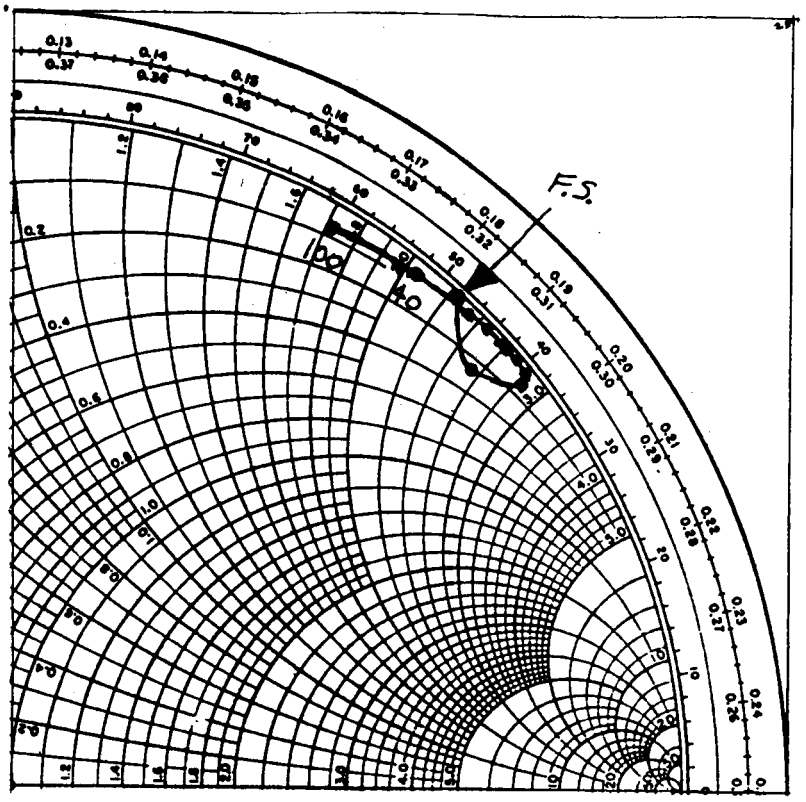

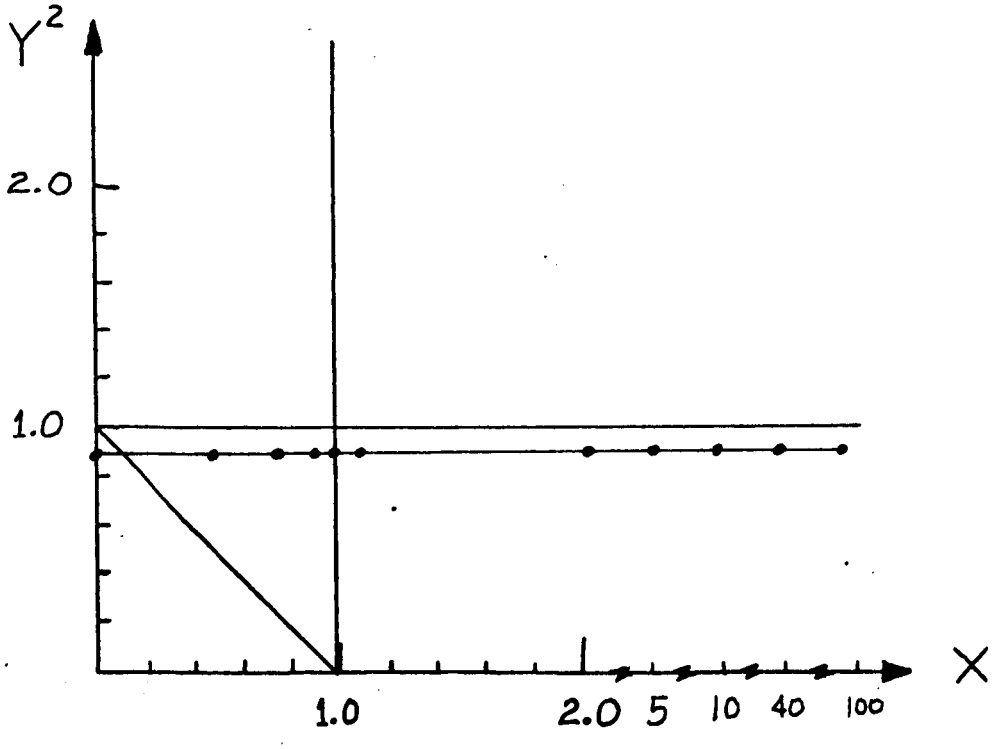

Figure 21 Calculated Loop Impedance; $\bar{B}_o$ Parallel to Loop

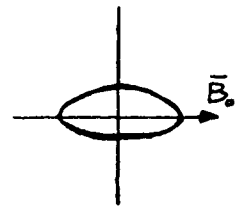

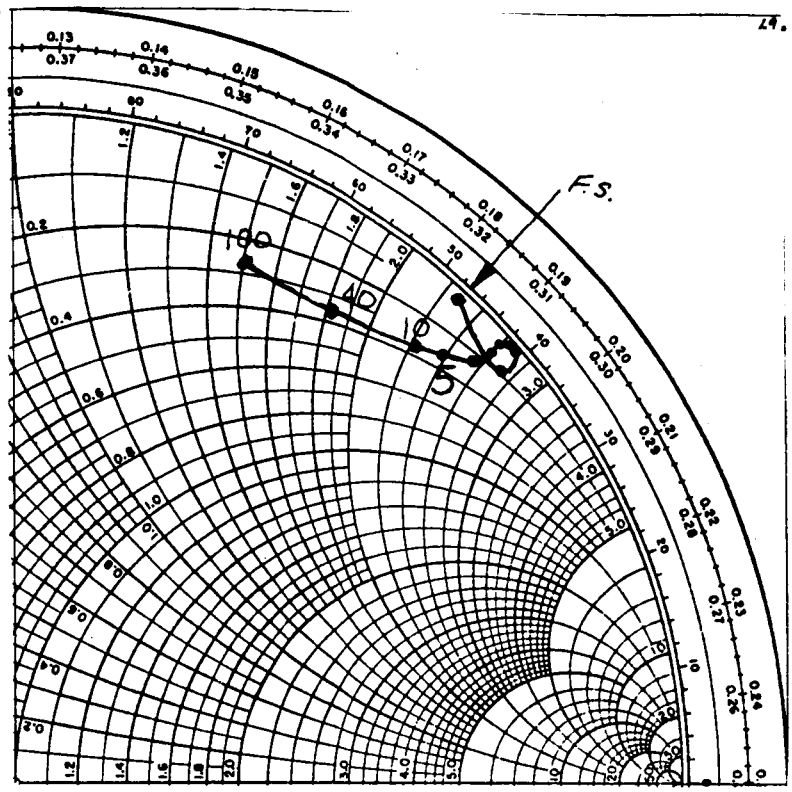

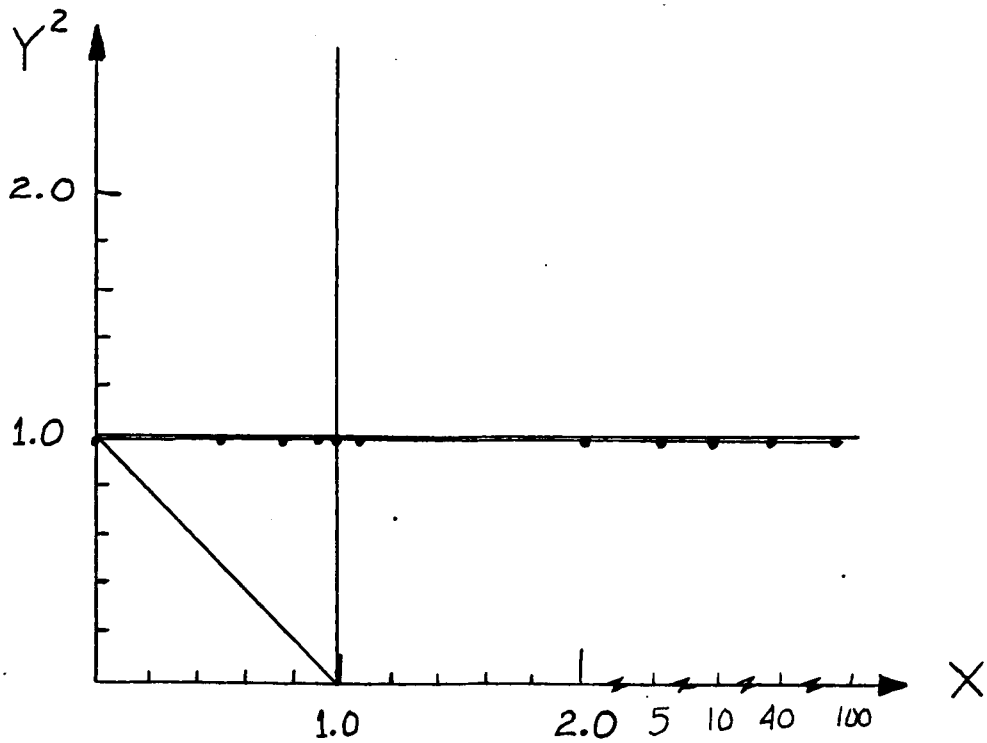

Figure 22 Calculated Loop Impedance; $\bar{B}_o$ Parallel to Loop

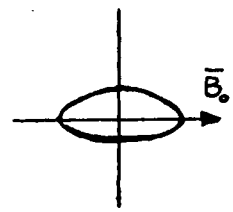

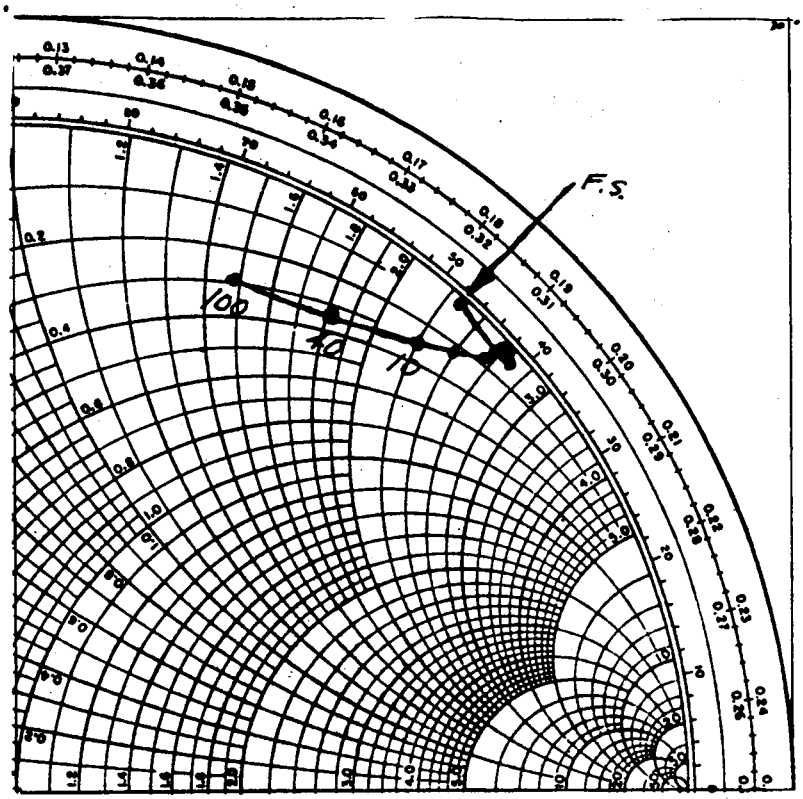

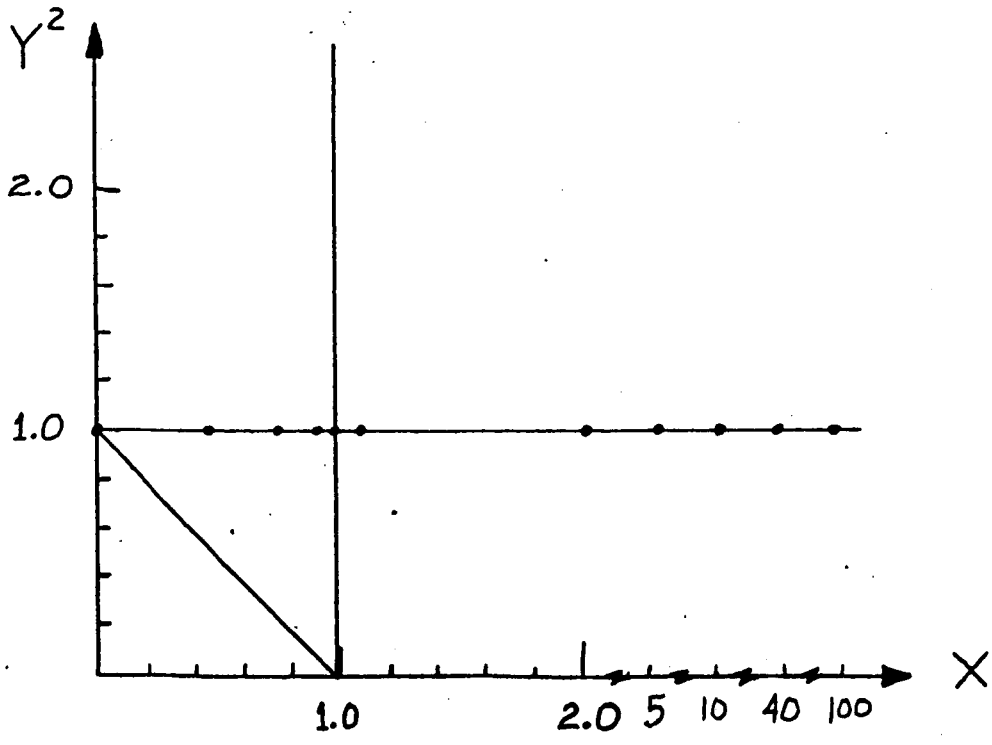

Figure 23 Calculated Loop Impedance; $\bar{B}_o$ Parallel to Loop

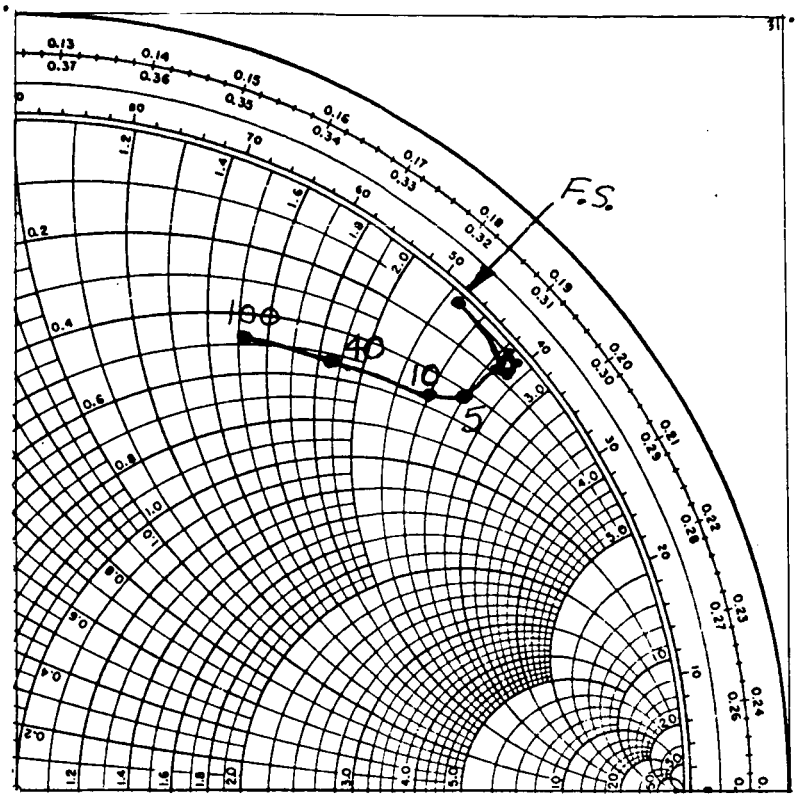

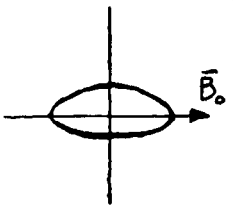

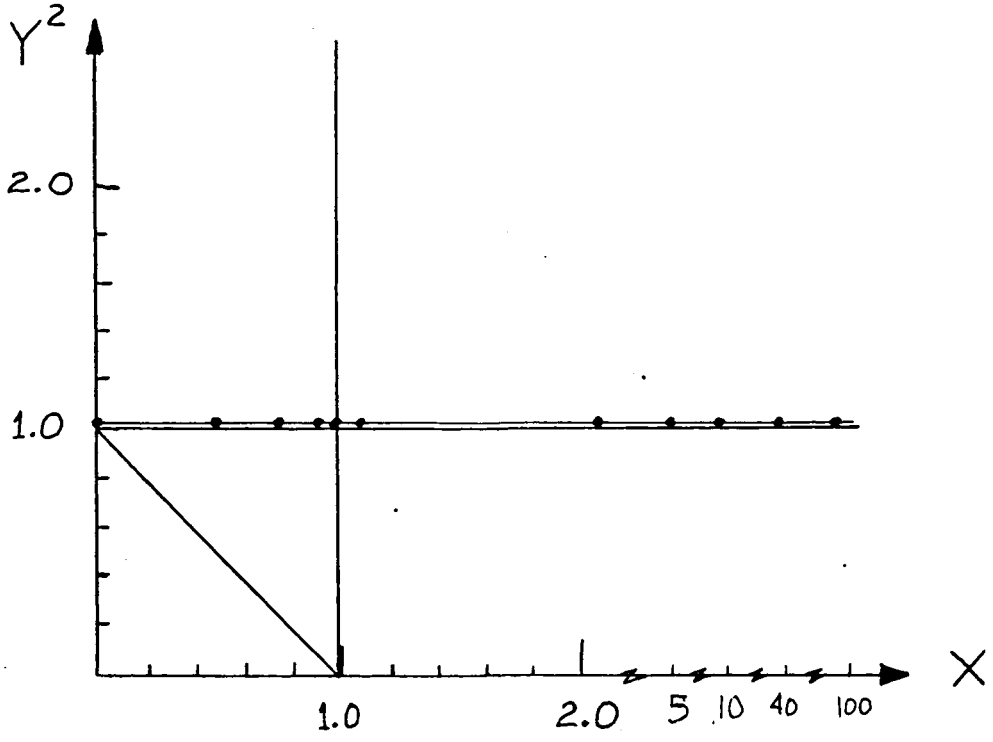

Figure 24 Calculated Loop Impedance; $\bar{B}_o$ Parallel to Loop

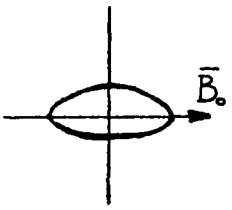

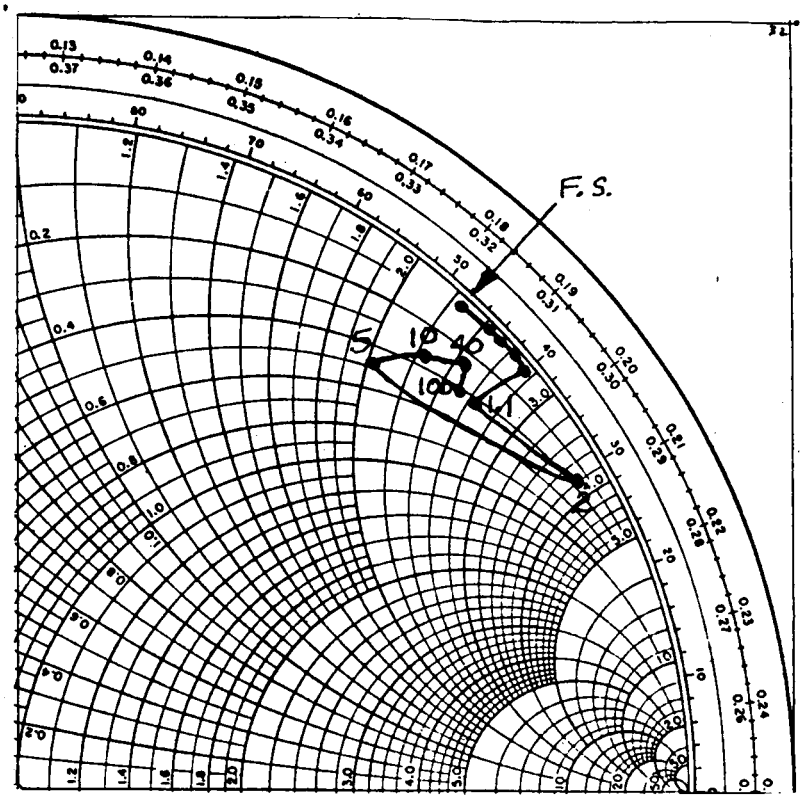

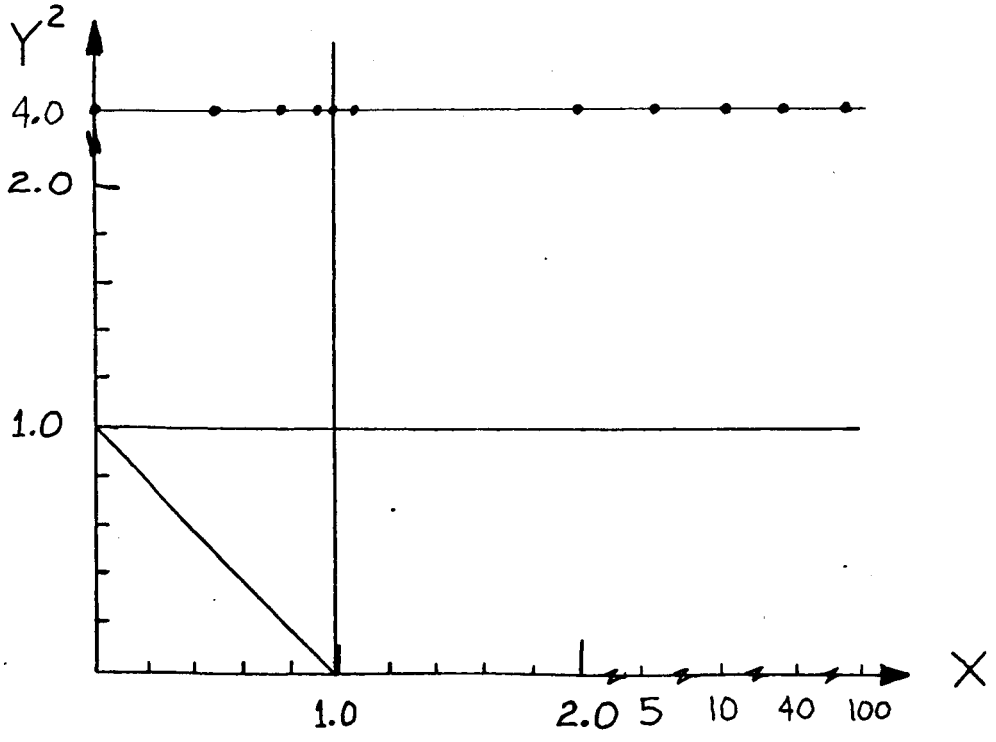

Figure 25 Calculated Loop Impedance; $\bar{B}_o$ Parallel to Loop

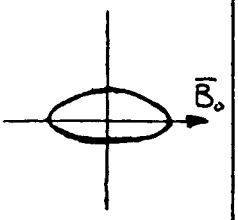

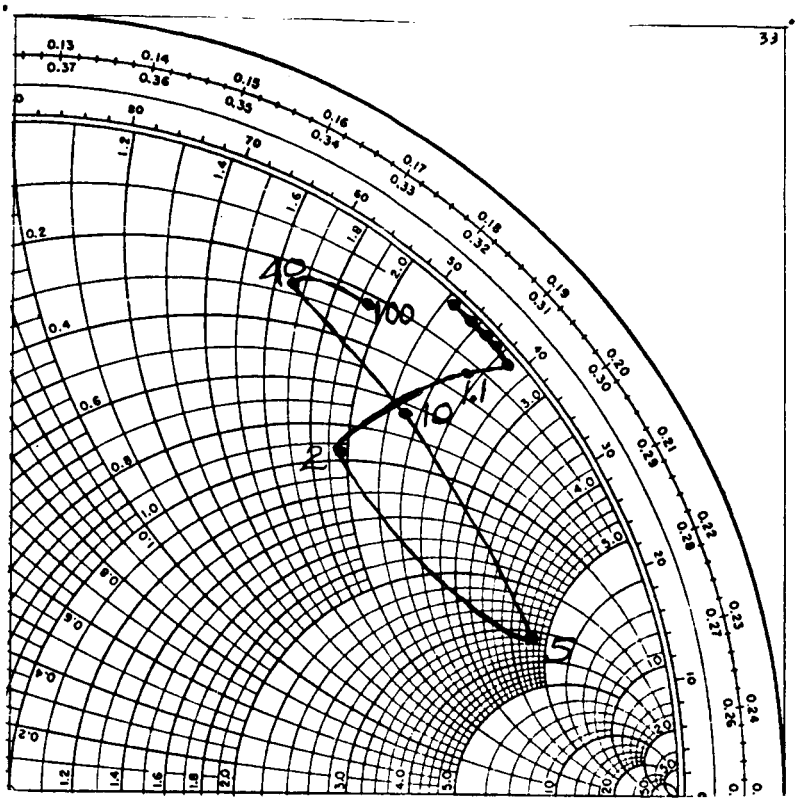

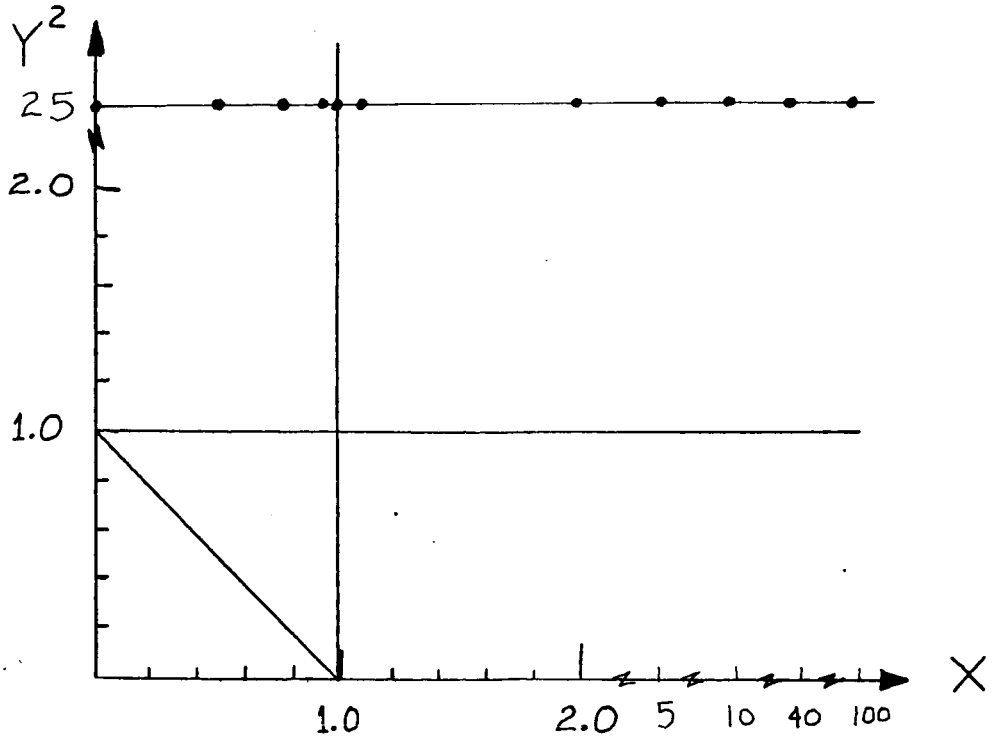

Figure 26 Calculated Loop Impedance; $\bar{B}_o$ Parallel to Loop

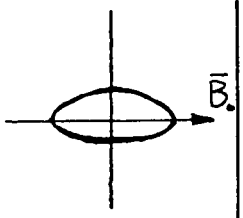

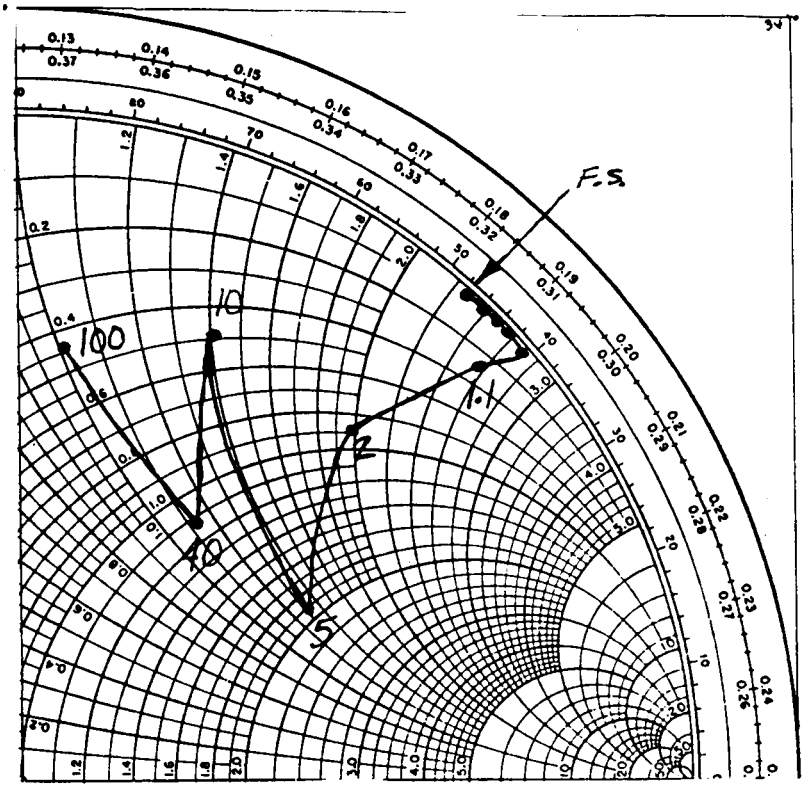

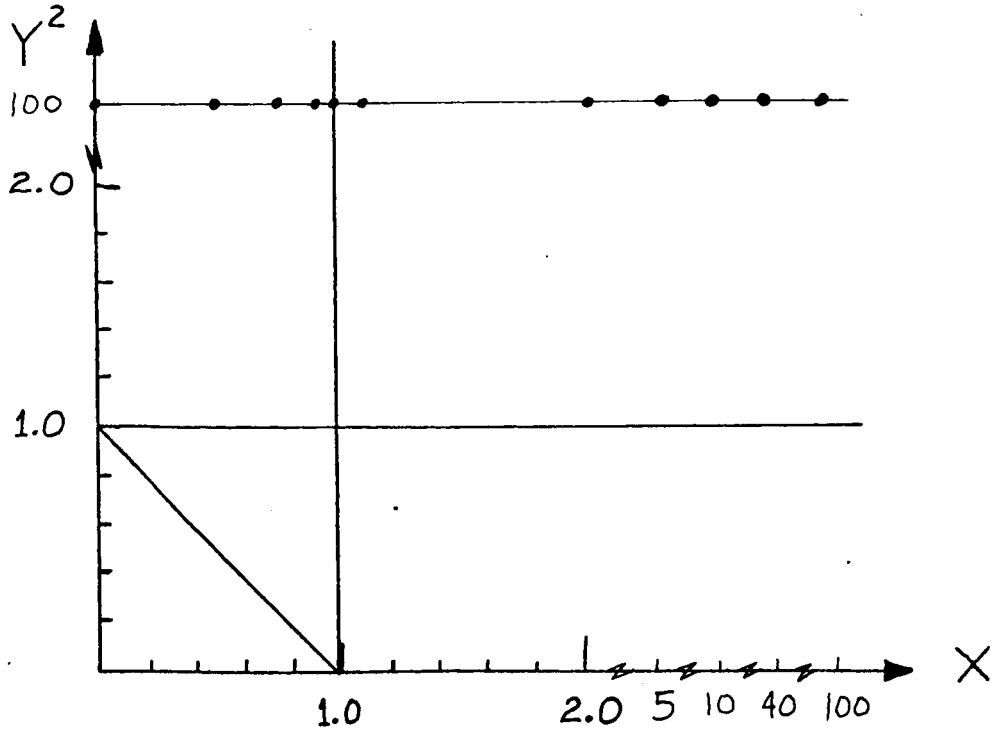

Figure 27 Calculated Loop Impedance; $\bar{B}_o$ Parallel to Loop

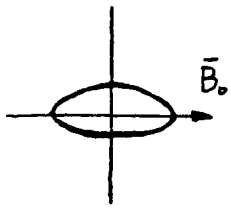

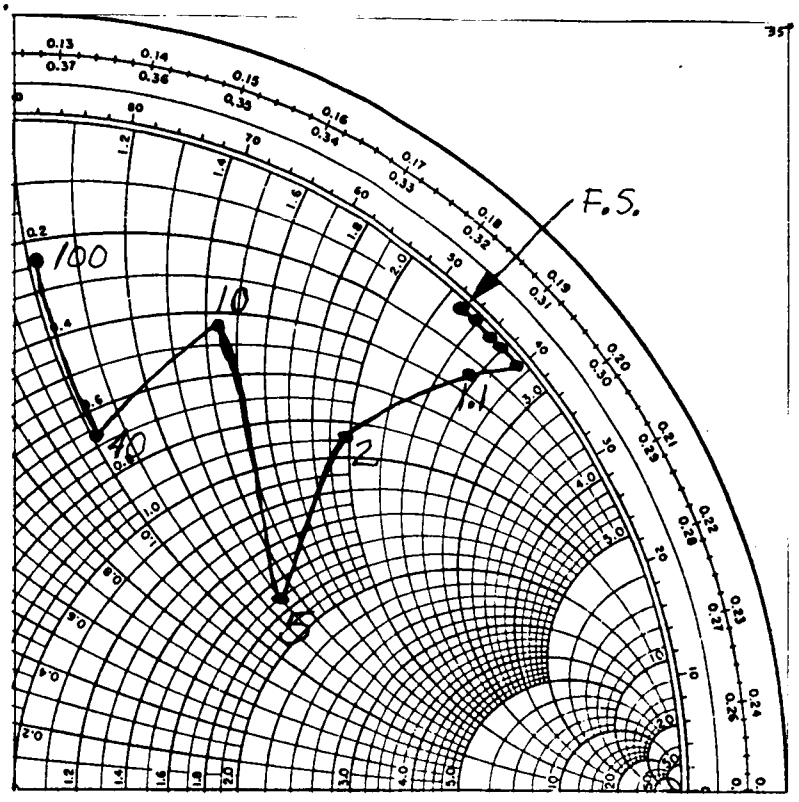

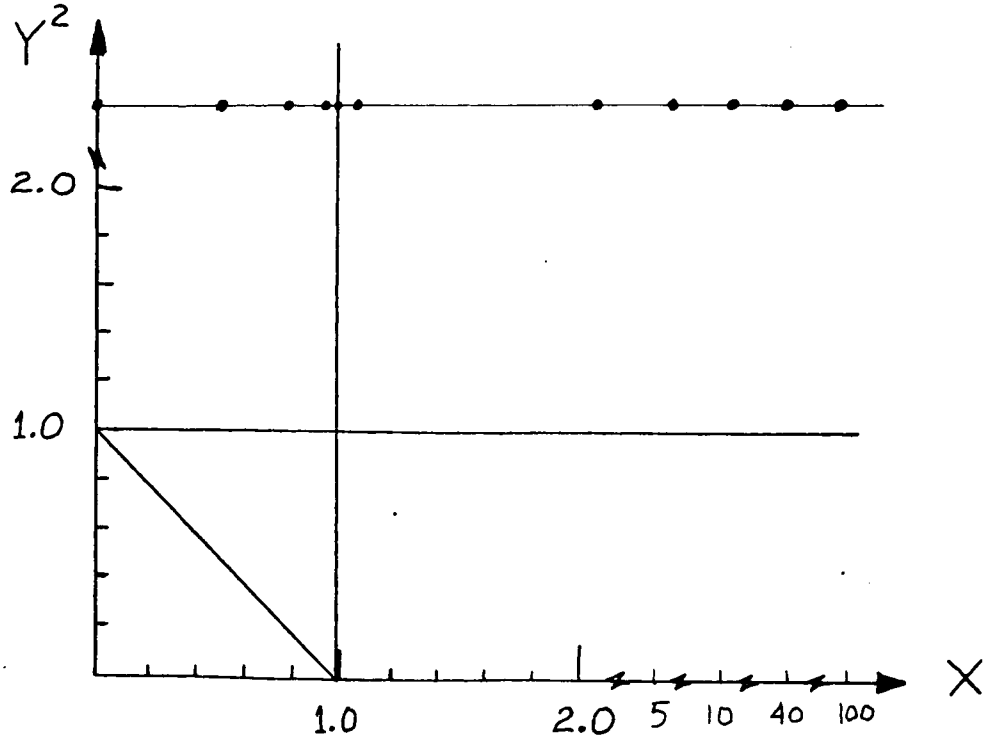

Figure 28 Calculated Loop Impedance; $\bar{B}_o$ Parallel to Loop

the largest real part at X=5. The behavior of the impedance locus in indeed unusual in this region of the (X, Y^2) plane. This is because the impedance is a function of K_o, K_1, and $\frac{K_o}{K_1}$ combined.

10.4 Summary

Keeping in mind the range of plasma, parameters attainable in the measurement program ($0 \leq X \leq 15$, $0 \leq Y \leq 2.0$) and remembering that these ranges were not attainable simultaneously, one can anticipate the following results of the measurement program.

First, for $\overline{B}_o$ normal to the loop, the measured impedance should be essentially the free space impedance, except when $Y \simeq 1$.

In the case of $\overline{B}_o$ parallel to the loop, one would expect to encounter unusual impedance loci when the plasma parameters fall in the hyperbolic region and much smoother behavior and smaller real part to the impedance when outside the hyperbolic region.

CHAPTER 11 THE RESULTS OF THE EXPERIMENTAL MEASUREMENT OF THE LOOP IMPEDANCE

11.1 $\overline{B}_o$ Normal to the Loop

Figures 29 to 36 inclusive show the measured impedance of the loop in the plasma when $\overline{B}_o$ was normal to the loop and under various combinations of ω, X, Y, and Z. It should be remembered that the r.f. frequency was changed from 1050 M Hz to 500 M H in 50 M Hz steps in order to vary X and Y. The theoretical impedance, as calculated by the computer for the same values of ω, ρ_o, δ, X, Y, and Z, is shown for purposes of comparison. The measured curve is labelled MEAS.

As was anticipated in the discussion of the theoretical formulae and their numerical results in Chapters 9 and 10 the measured impedance was essentially that of free space, except when $Y \simeq 1$. All of the null-shifts measured on the slotted line fell within 10% of the predicted theoretical null-shifts. The measured real part of the impedance was usually higher than predicted by the theory, which might be expected due to the relatively high standing wave ratio. It is assumed that some r.f. heating of the plasma occurred. Every effort was used to keep the input r.f. signal to a minimum without losing the nulls in noise.

Figure 31 exhibits increasing real part below 900 M Hz, in which case X is increasing to the largest value achieved in the measurement program. It is

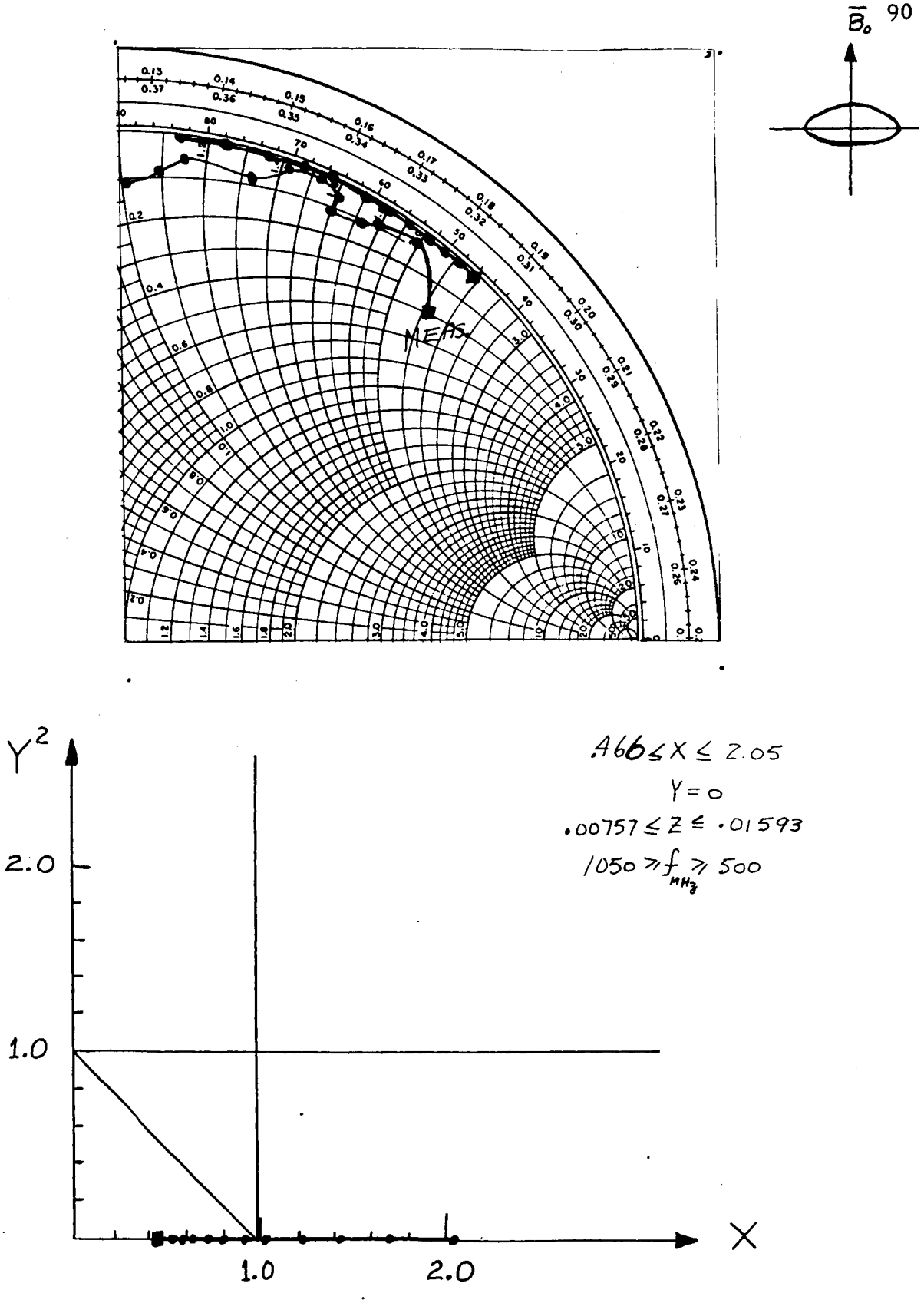

Figure 29 Measured Results Compared to Theory;
$\bar{B}_o$ Normal to the Loop, No. 1

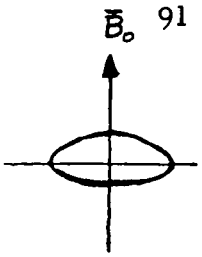

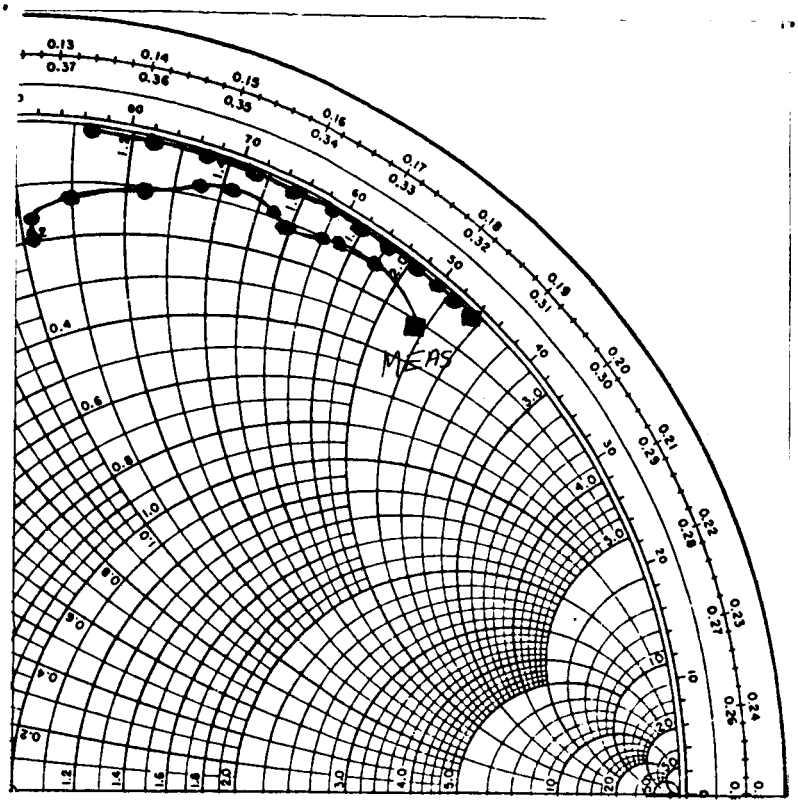

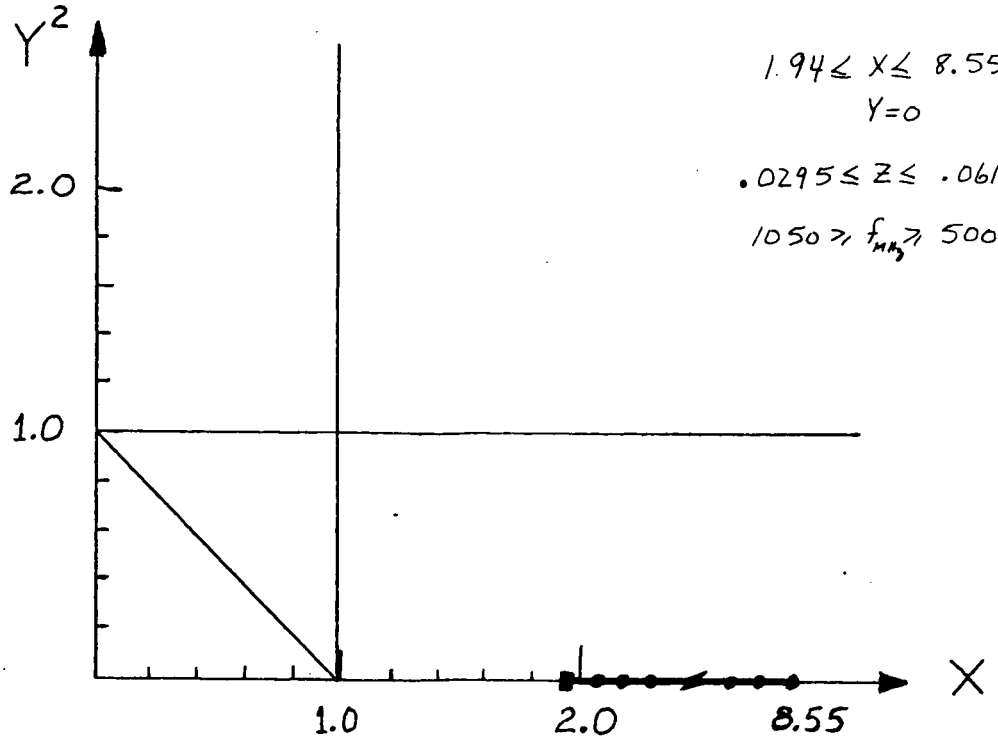

Figure 30 Measured Results Compared to Theory;

$\bar{B}_o$ Normal to the Loop, No. 2

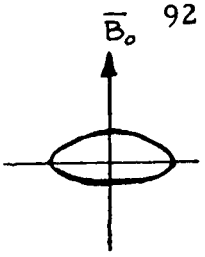

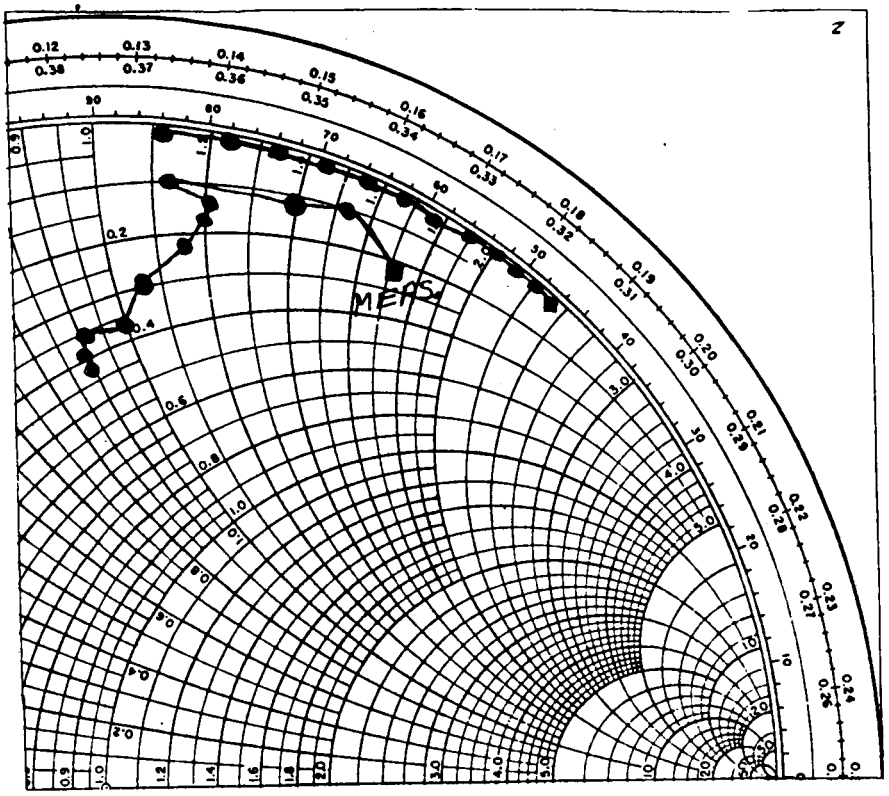

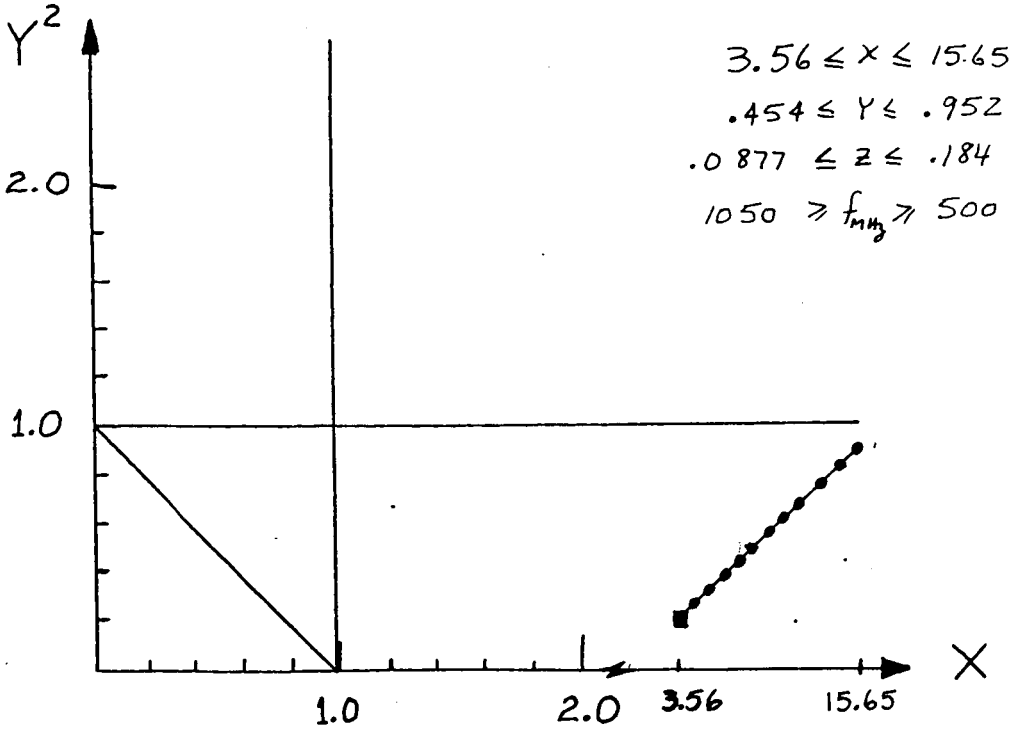

$3.56 \leq X \leq 15.65$

$.454 \leq Y \leq .952$

$.0877 \leq Z \leq .184$

$1050 \gg f_{MHz} \gg 500$

Figure 31 Measured Results Compared to Theory;

$\bar{B}_o$ Normal to the Loop, No. 3

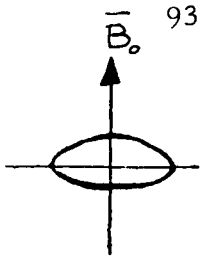

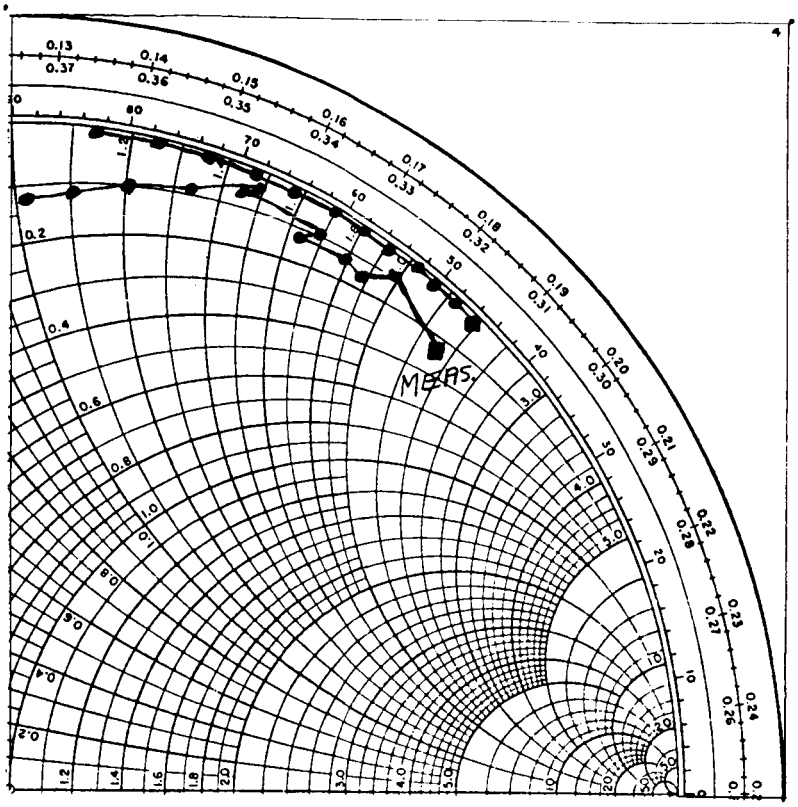

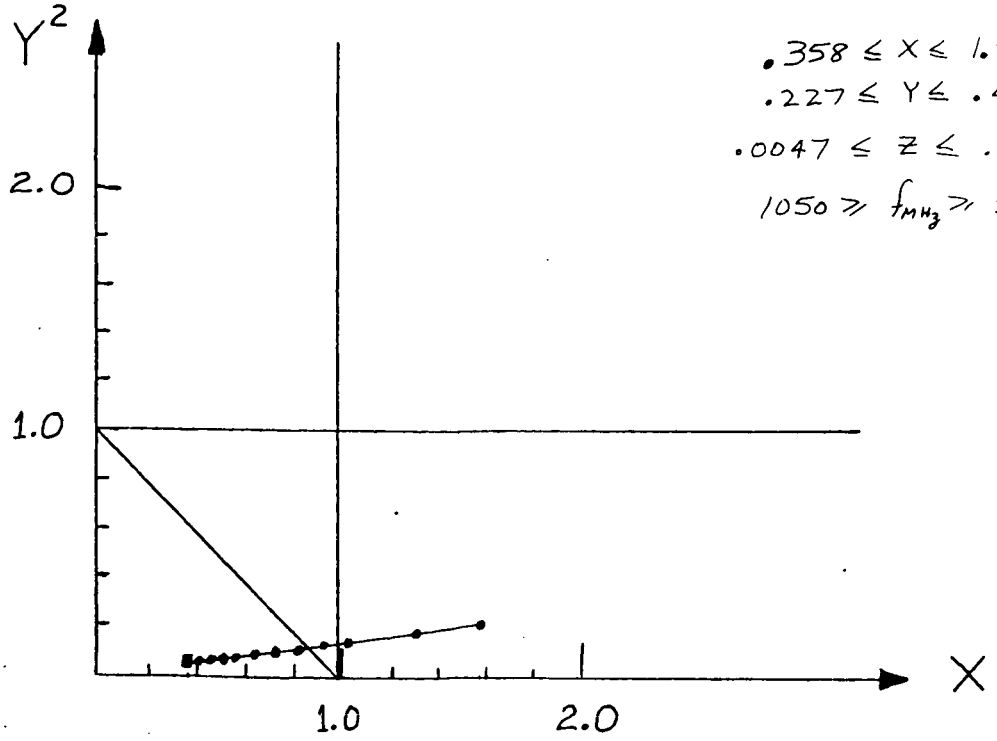

$.358 \leq X \leq 1.575$

$.227 \leq Y \leq .476$

$.0047 \leq Z \leq .0098$

$1050 \geq f_{MHz} \geq 500$

Figure 32 Measured Results Compared to Theory;

$\bar{B}_o$ Normal to the Loop, No. 4

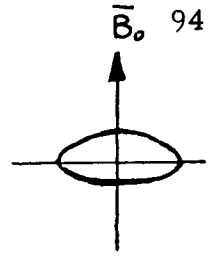

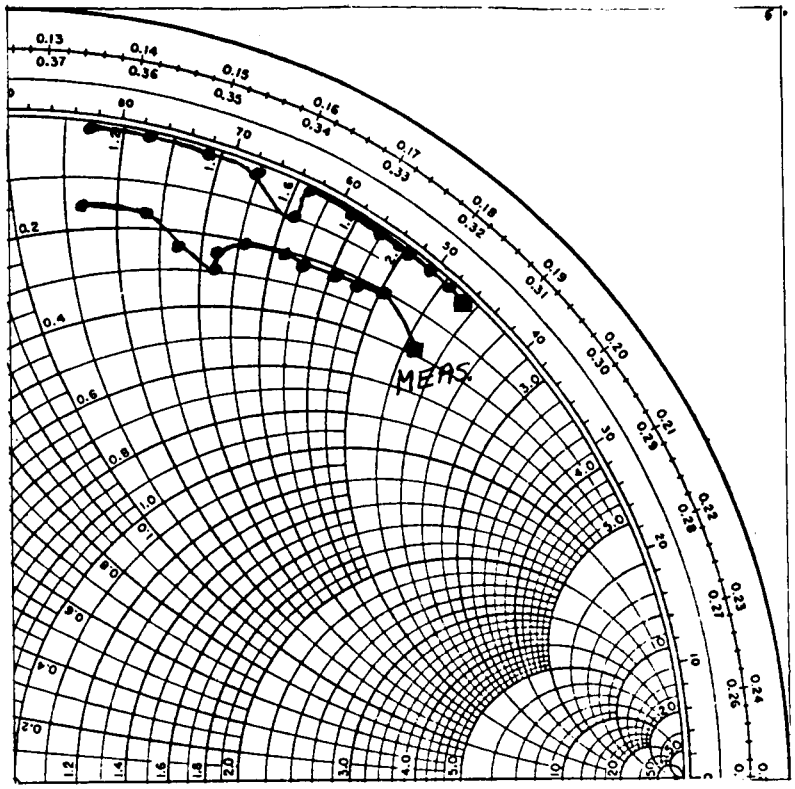

$.825 \leq X \leq 3.63$
$.680 \leq Y \leq 1.43$
$.0070 \leq Z \leq 0.014$
$1050 \geq f_{MHz} \geq 500$

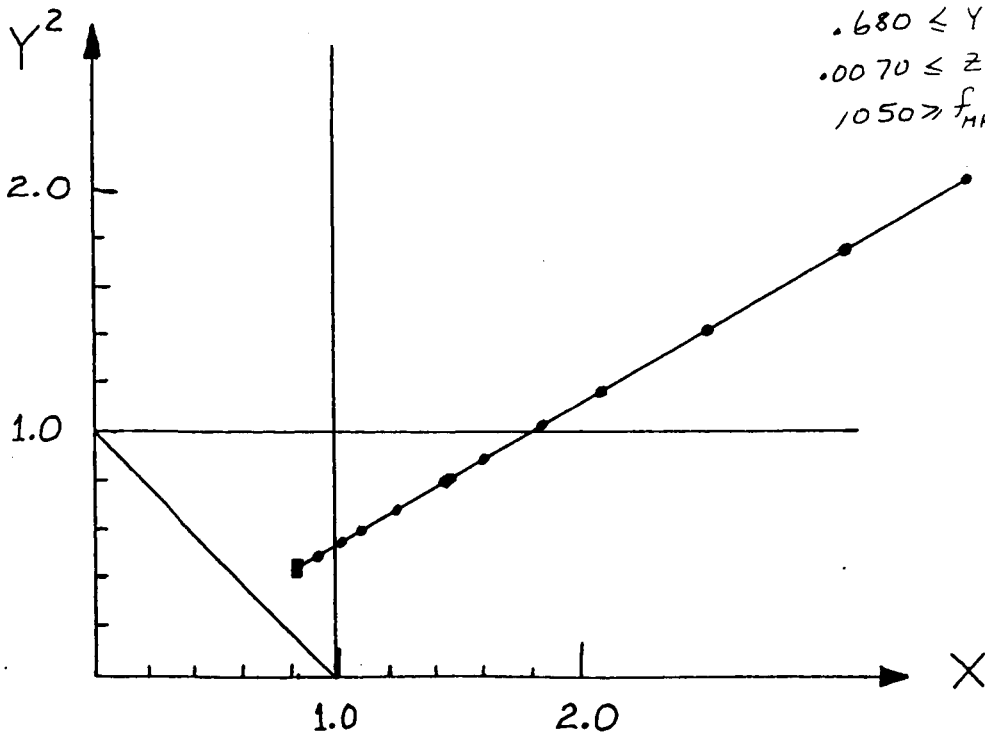

Figure 33 Measured Results Compared to Theory;
$\bar{B}_o$ Normal to the Loop, No. 5

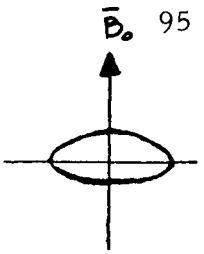

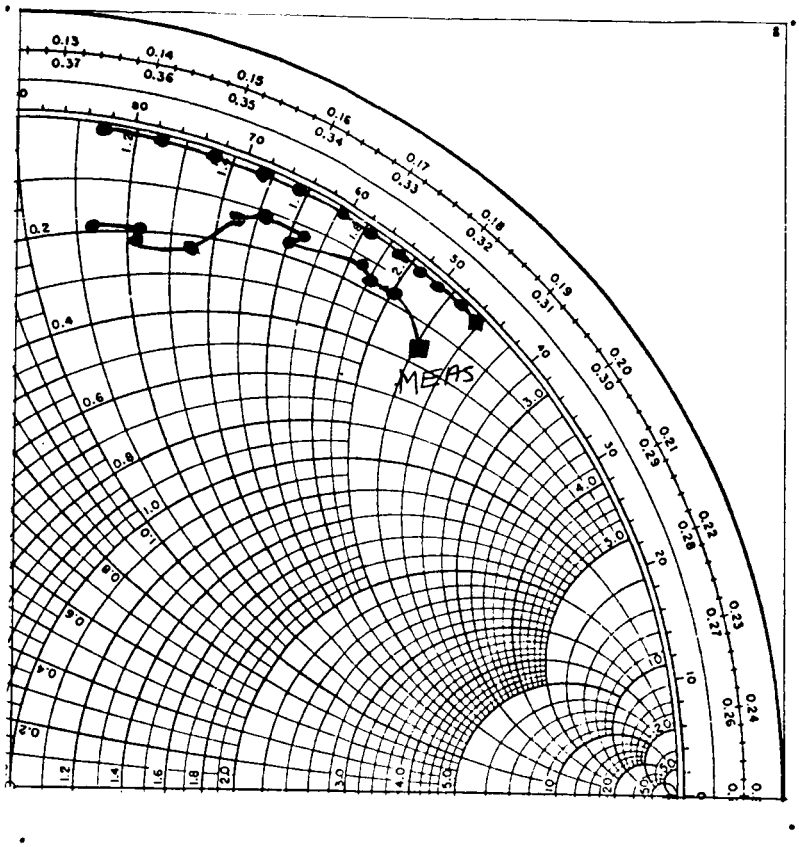

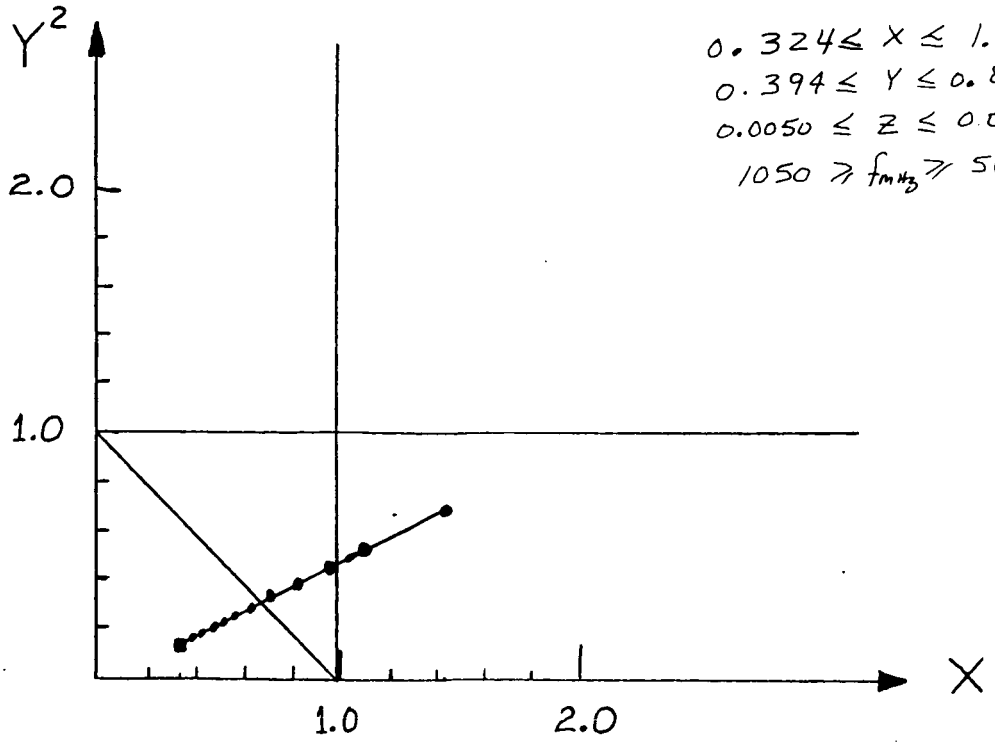

$0.324 \leq X \leq 1.42$
$0.394 \leq Y \leq 0.828$
$0.0050 \leq Z \leq 0.0105$
$1050 \geq f_{mHz} \geq 500$

Figure 34 Measured Results Compared to Theory;
$\bar{B}_o$ Normal to the Loop, No. 6

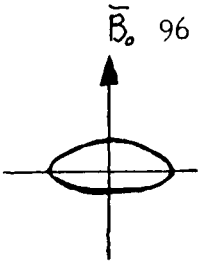

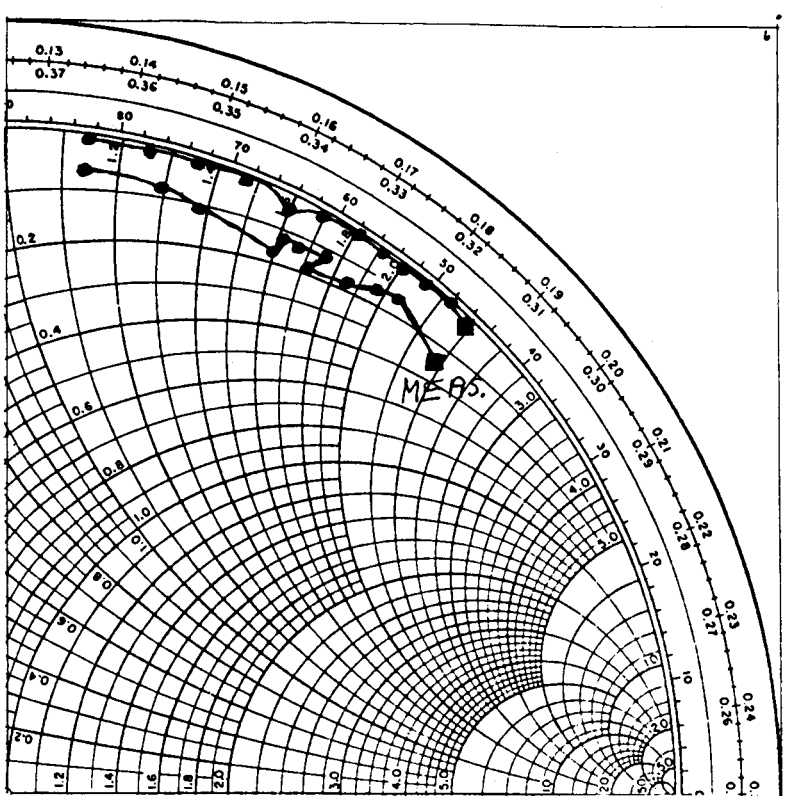

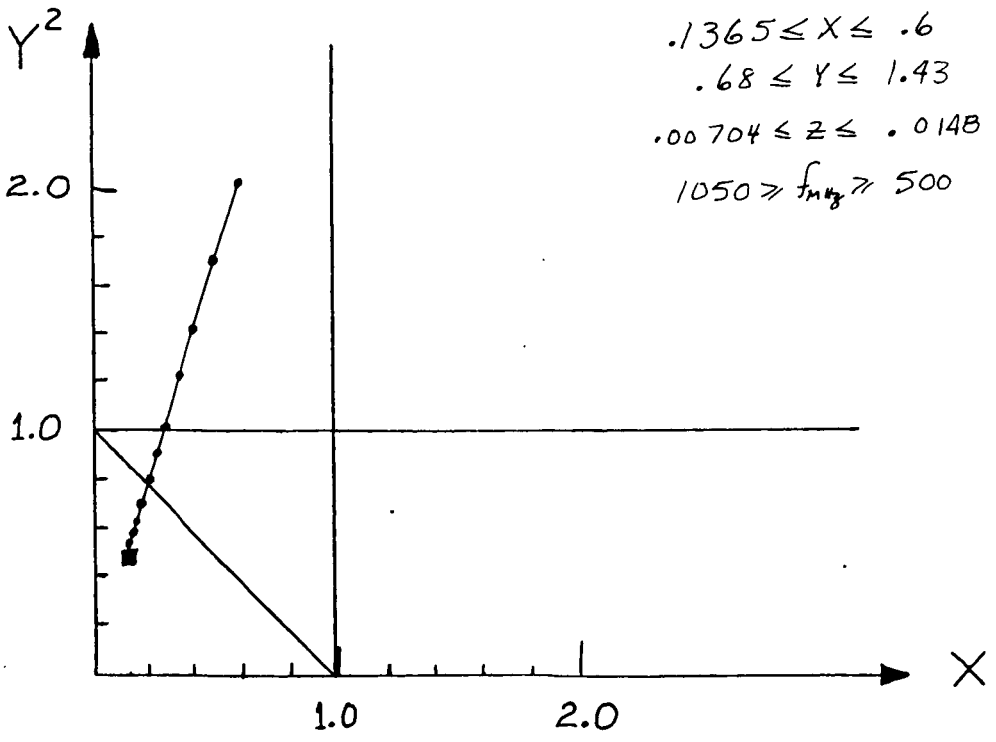

$.1365 \leq X \leq .6$

$.68 \leq Y \leq 1.43$

$.00704 \leq Z \leq .0148$

$1050 \geq f_{MHz} \geq 500$

Figure 35 Measured Results Compared to Theory; $\bar{B}_o$ Normal to the Loop, No. 7

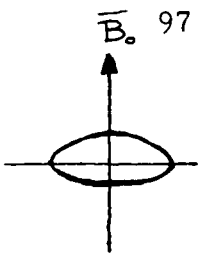

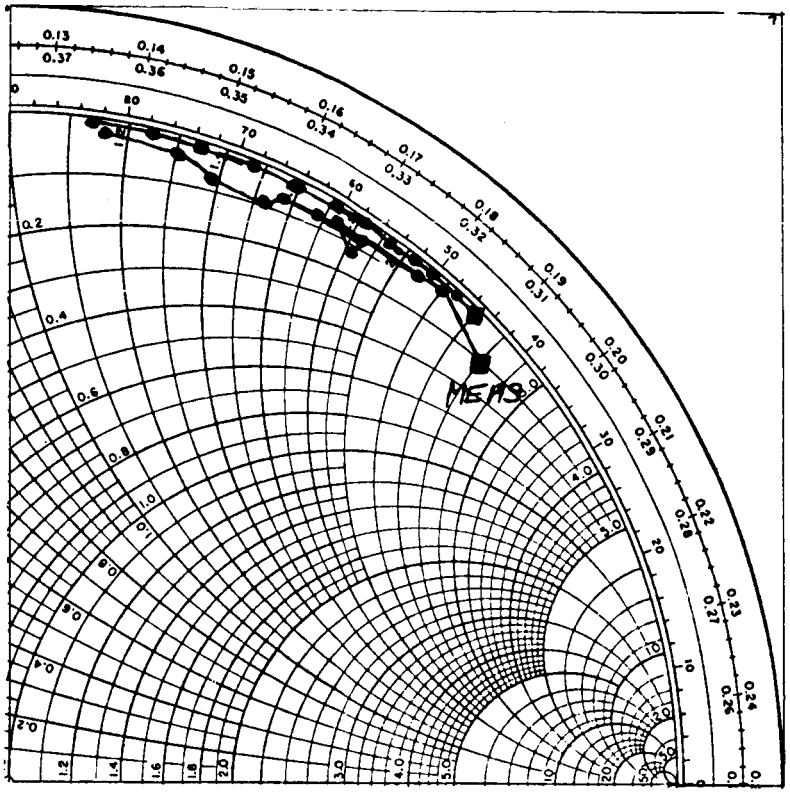

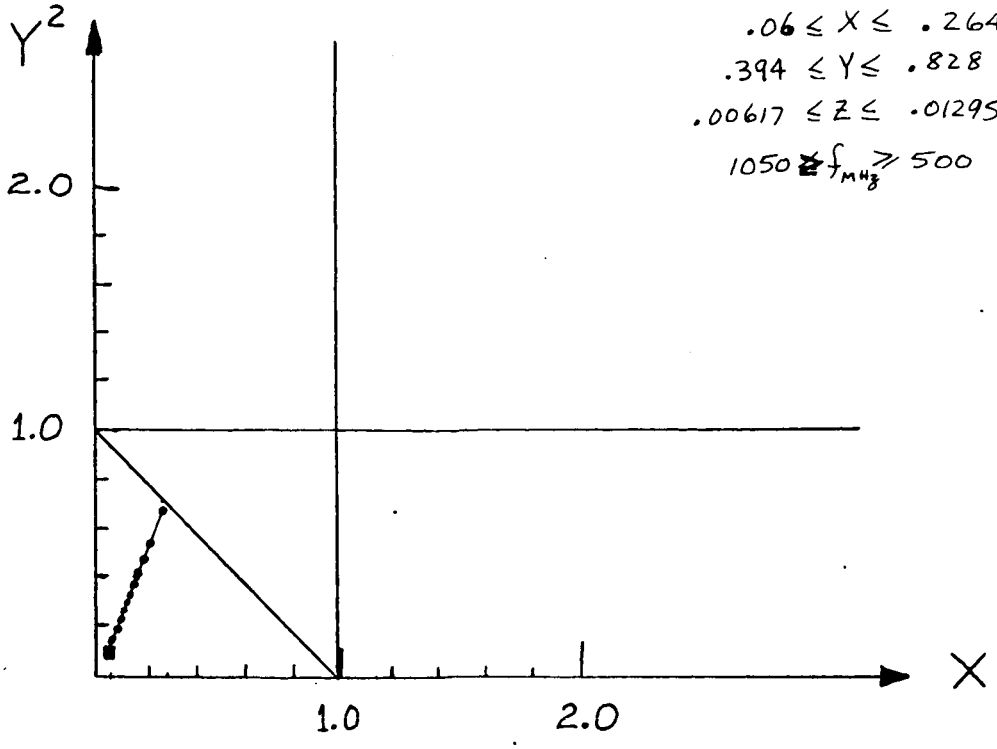

$.06 \leq X \leq .2640$

$.394 \leq Y \leq .828$

$.00617 \leq Z \leq .01295$

$1050 \geq f_{MHz} \geq 500$

Figure 36 Measured Results Compared to Theory;

$\bar{B}_o$ Normal to the Loop, No. 8

exhibiting the kind of behavior one would expect if X were large and Y were greater than 1. At 500 M Hz, Y=0.95. This is the only case for this orientation in which the measurements show any significant deviation from the theory.

In Figure 33 and Figure 35 the theory predicts an increase in the real part of the impedance as Y passes through Y=1. It appears that this increase has been detected in Figure 33 which was marked by a drop in VSWR from over 12 to about 8 at $Y \simeq 1$.

This is not the case in Figure 35 where the predicted real part is negligibly small and there was no noticeable drop in VSWR at $Y \simeq 1$.

The remaining Figures show an excellent agreement with the theory, which predicts free space impedance and negligible dependance on the plasma parameters. It is felt that the qualitative and quantitative behavior of the measured impedance agrees well with the theory for this orientation.

11.2 $\overline{B}_o$ Parallel to the Loop

Figures 37 to 41 inclusive show the measured loop impedance when $\overline{B}_o$ was parallel to the loop and under various combinations of ω, X, Y, and Z. A brief glance at the Smith Charts shows that the quantitative behavior of the measured impedance for this orientation does not agree as well with the theory as it did for the first orientation. However, note that when the theory predicted a smooth impedance locus, as in Figure 37, and Figure 41, the measured impedance loci were indeed smooth and the general shape of the theoretical loci was reproduced in the measurements. On the other hand, when unusual

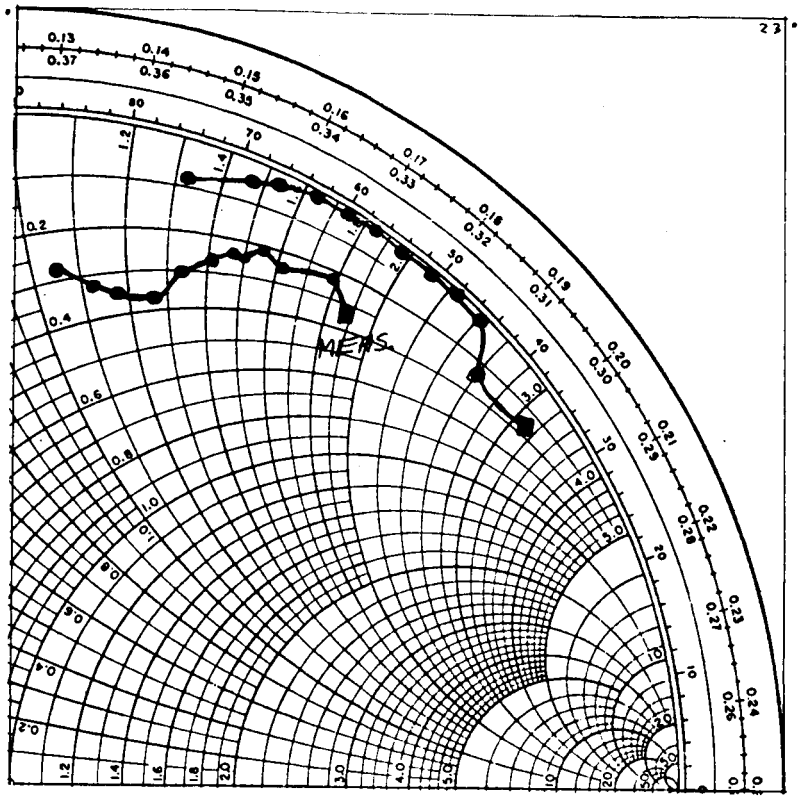

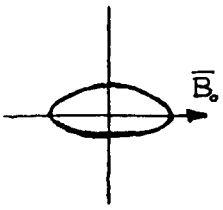

$.877 \leq X \leq 3.86$

$.544 \leq Y \leq 1.162$

$.00664 \leq Z \leq .01392$

$1050 \geq f_{MHz} \geq 500$

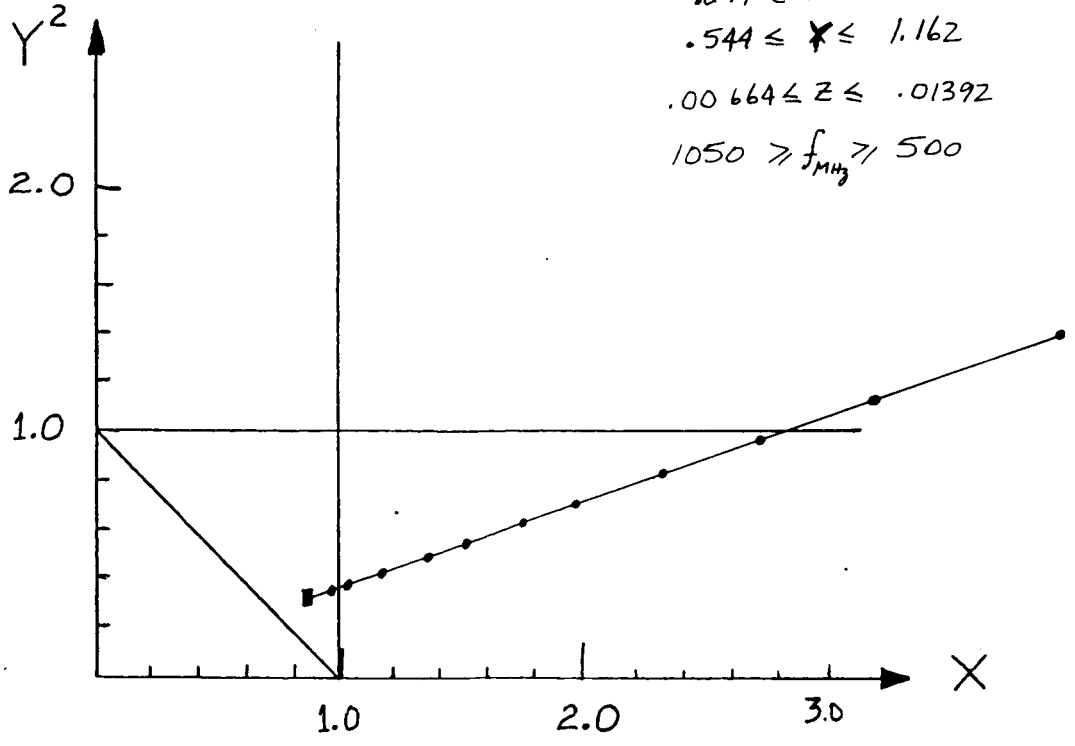

Figure 37 Measured Results Compared to Theory;
$\bar{B}_o$ Parallel to the Loop, No. 1

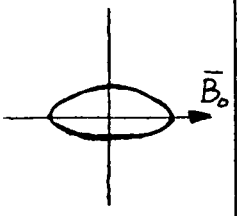

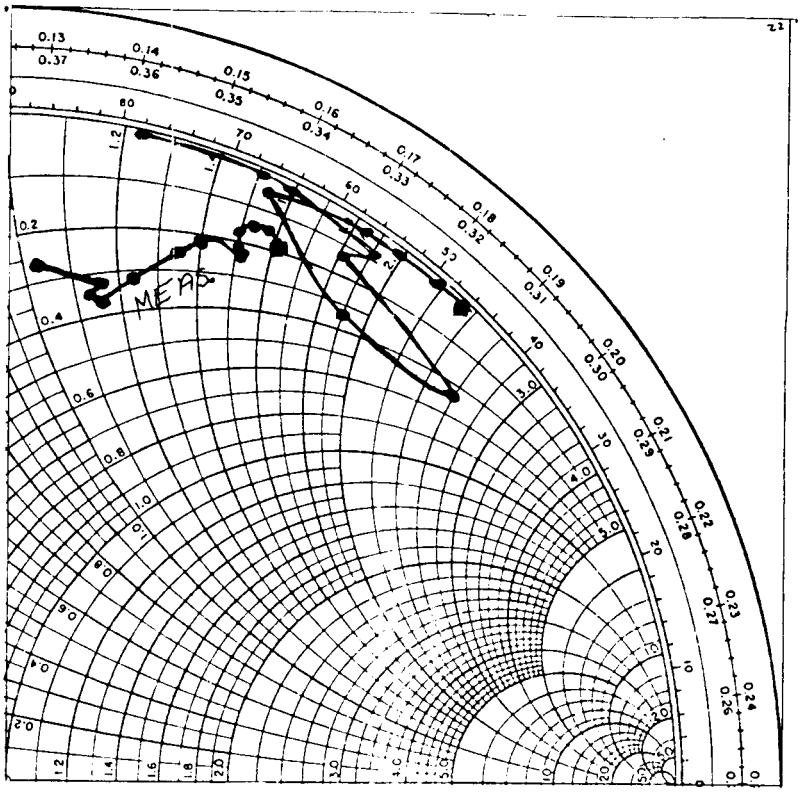

$.309 \leq X \leq 1.37$
$.571 \leq Y \leq 1.195$
$.0046 \leq Z \leq .00966$
$1050 \geq f_{MHz} \geq 500$

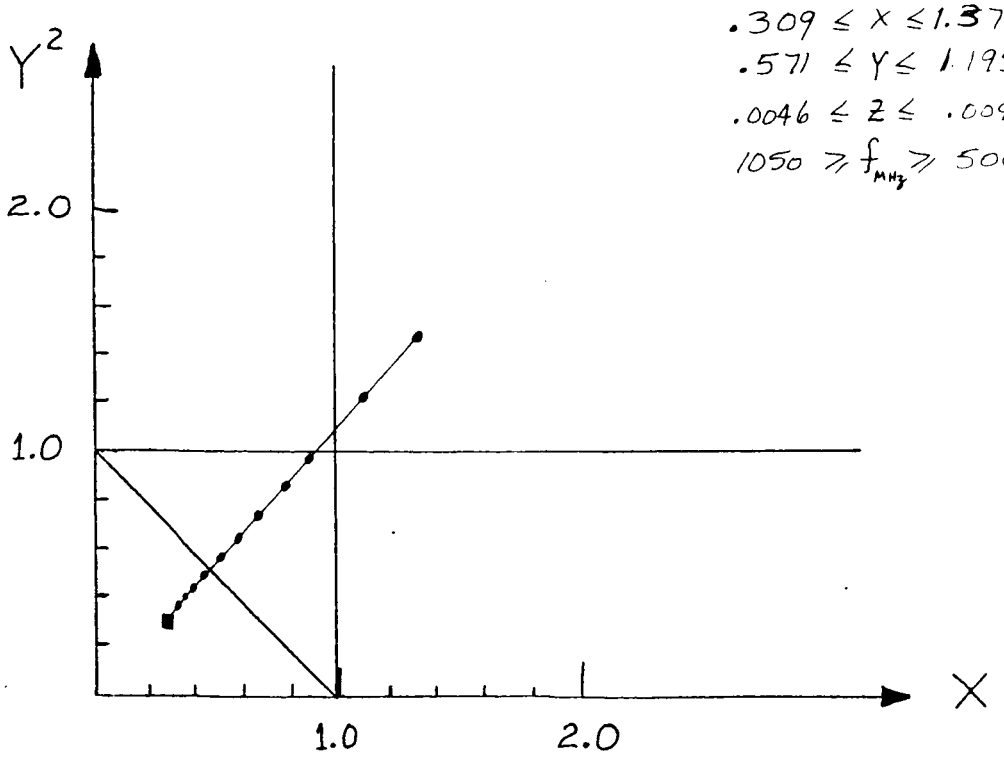

Figure 38 Measured Results Compared to Theory;
$\bar{B}_o$ Parallel to the Loop, No. 2

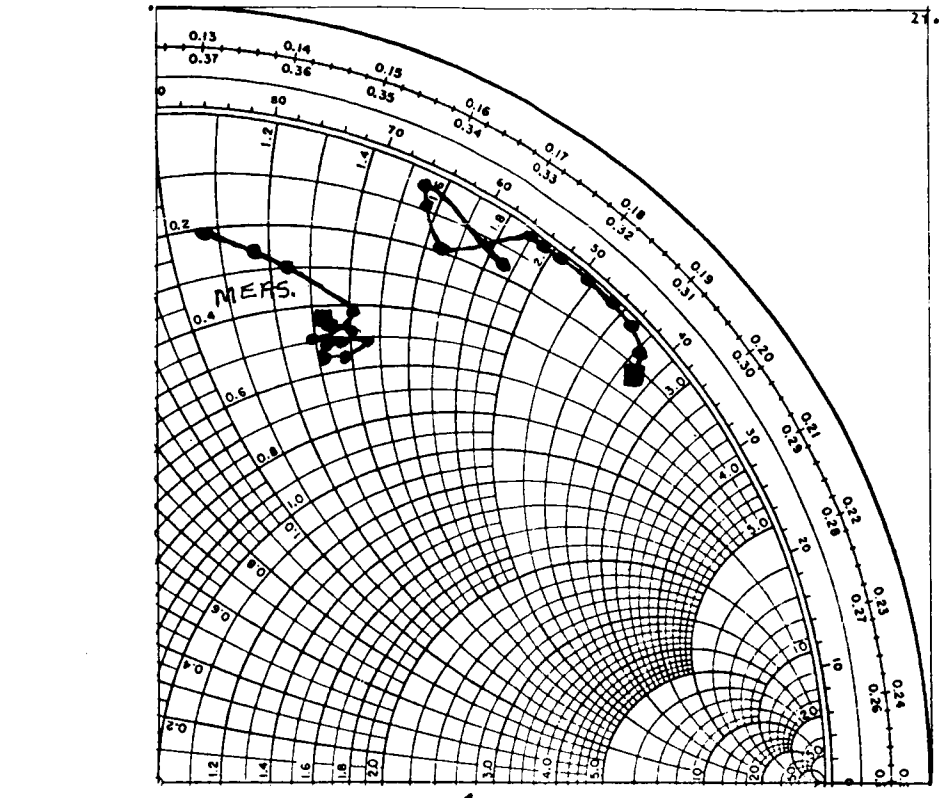

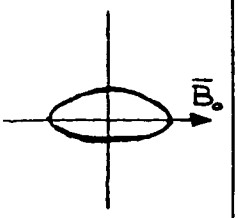

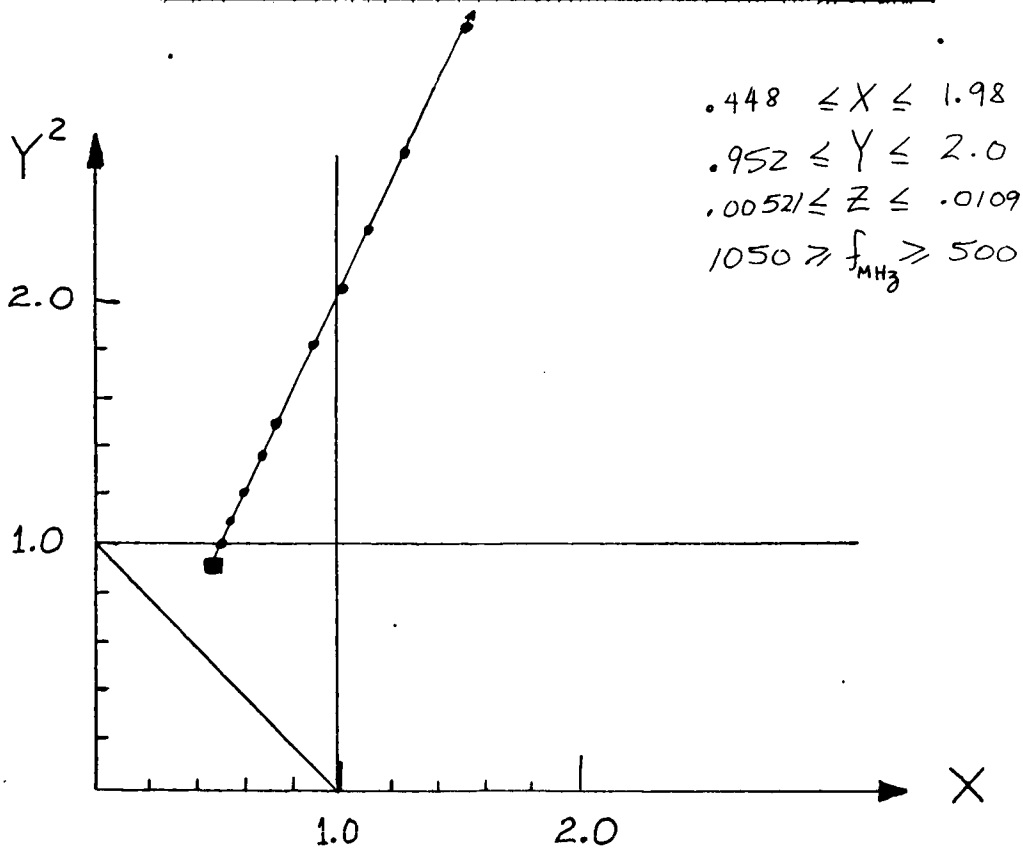

$.448 \leq X \leq 1.98$

$.952 \leq Y \leq 2.0$

$.00521 \leq Z \leq .0109$

$1050 \geq f_{MHz} \geq 500$

Figure 39 Measured Results Compared to Theory;

$\bar{B}_o$ Parallel to the Loop, No. 3

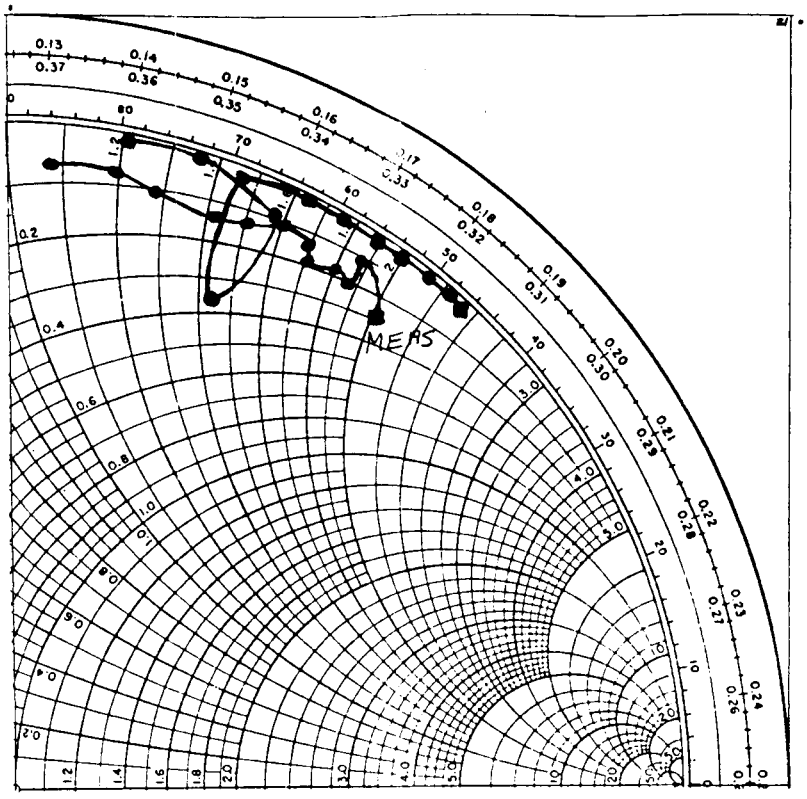

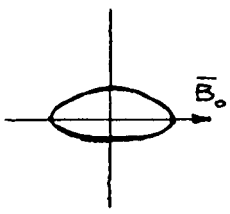

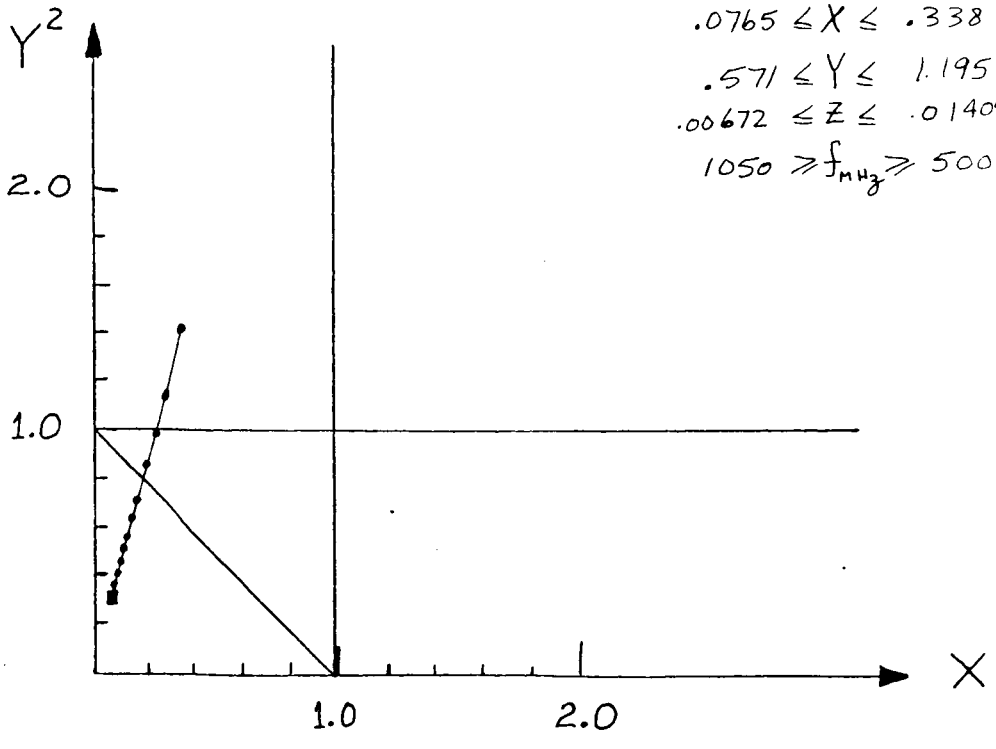

$.0765 \leq X \leq .338$

$.571 \leq Y \leq 1.195$

$.00672 \leq Z \leq .01409$

$1050 \geq f_{MHz} \geq 500$

Figure 40 Measured Results Compared to Theory;

$\bar{B}_o$ Parallel to the Loop, No. 4

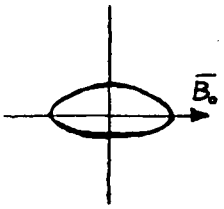

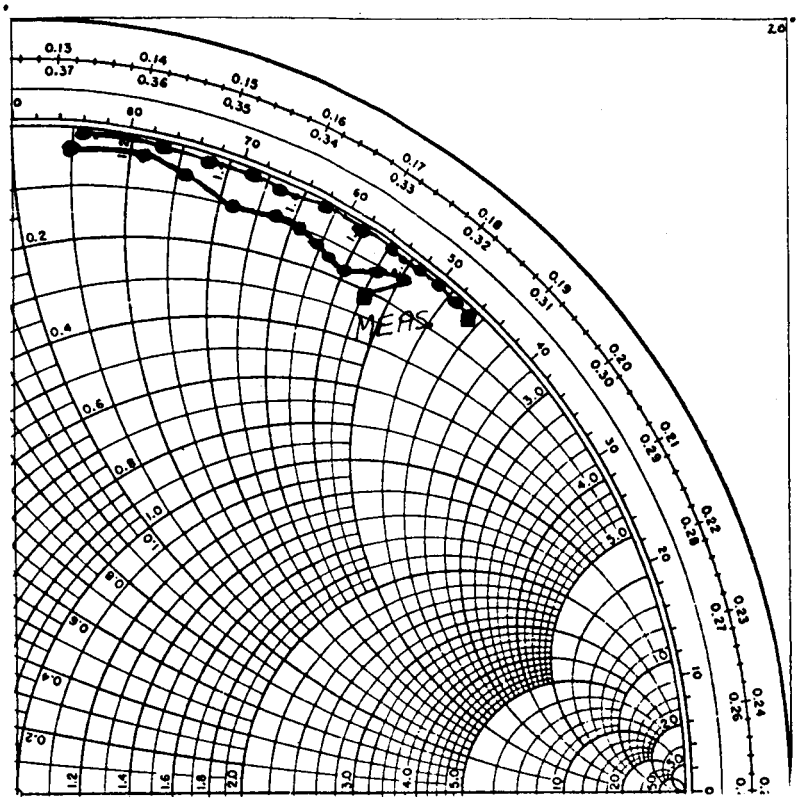

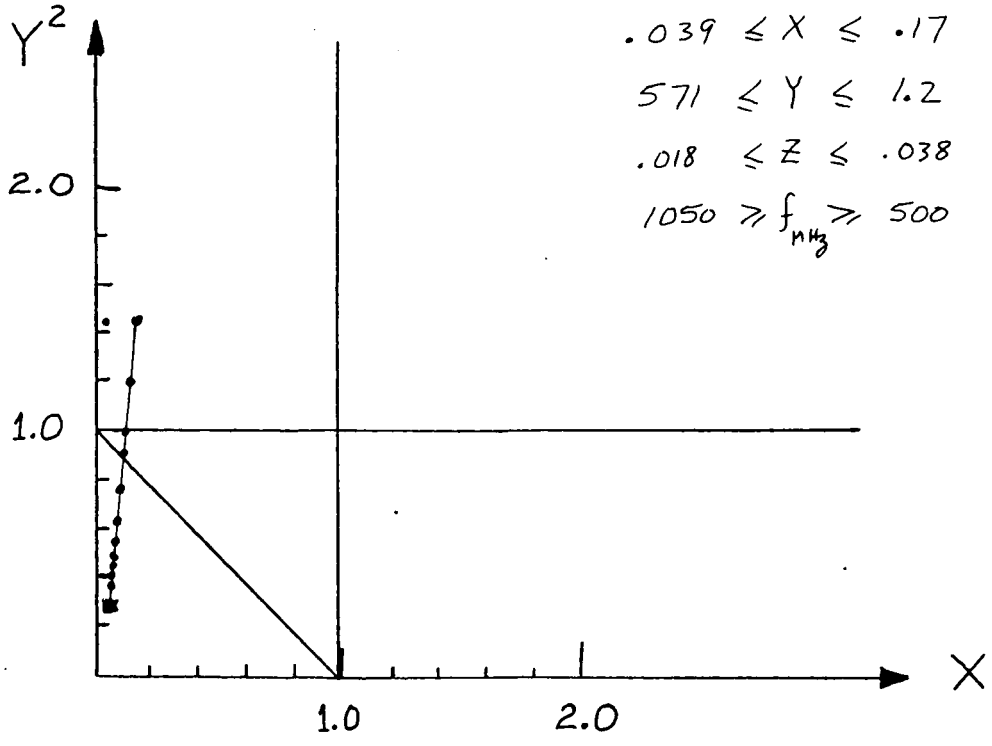

$.039 \leq X \leq .17$

$571 \leq Y \leq 1.2$

$.018 \leq Z \leq .038$

$1050 \geq f_{MHz} \geq 500$

Figure 41 Measured Results Compared to Theory;
$\overline{B}_o$ Parallel to the Loop, No. 5

impedance loci were predicted by the theory as in Figures 38, 39, and 40, i. e. when X and Y fell in the hyperbolic region, the measured loci exhibited unusual behavior as well. The qualitative behavior of the measured impedance agrees well in some cases, and not so well in others.

It is clear, however, that the measured loop impedance for this orientation was indeed plasma dependant.

CHAPTER 12 CONCLUSIONS

12.1 $\bar{B}_o$ Normal to the Loop

The loop impedance was derived in two different ways. The first was using the quasi-static approximation, which yielded the free space result. A first order correction term was a function of both K_1 and K_o. The second method was to consider the medium to be uniaxial, which resulted in a simpler derivation and the impedance turned out to be a function of K_1, but not K_o.

It would be helpful to know which approximation corresponded best with the measured loop impedance. Because both methods predicted essentially the free space impedance for the range of plasma parameters attained in the measurement program, no conclusive statement as to which approximation is better can be made.

However, the following conclusions can be drawn.

(i) Both approximations predicted essentailly the free space result for the plasma parameters used and the measured results verify this fact in all but one case (Figure 31); (the behavior of the impedance followed the behavior predicted for $X \gg 1$, $Y > 1$ although Y was a little less than 1).

(ii) No distinction between the "quasi-static plus first order correction term" method and the uniaxial method could be made from the measured results.

12.2 $\overline{B}_o$ Parallel to the Loop

For this orientation, the loop impedance was calculated under the uniaxial approximation.

The following conclusions can be drawn.

(i) The impedance of the loop in this orientation is a much more complex function of plasma parameters X and Y than for $\overline{B}_o$ normal to the loop.

(ii) Moderate values of X and Y are required to produce a loop impedance which is significantly different than the free space value.

(iii) The measured loop impedance locus was smooth in cases where the theory predicted a smooth locus.

(iv) The measured impedance locus was not smooth in cases where the theory predicted a locus that was not smooth.

(v) The qualitative behavior of the measured smooth impedance loci corresponded well to that of the theoretical smooth impedance loci, and the quantitative behavior agreed fairly well (within 15% as far as null shifts were concerned).

(vi) Qualitative agreement of the theory and the measured values was not good in the case of the unsmooth impedance loci, although qualitative agreement was better, and sometimes was excellent from a <u>local</u> standpoint. (Figure 38).

12.3 General Conclusions

By comparing the results of this study to those of Balmain (1963), one can conclude that a "short magnetic dipole" is affected by an anisotropic plasma to far less a degree than the short electric dipole.

The loop impedance measurement program corroborated the gross behavior predicted by the theory. In several instances (particularly for $\overline{B}_o$ normal to the loop) the measured results agreed very well.

The impedance formulae are presented in a relatively simple form and the general behavior of the impedance as a function of ω, ρ_o, δ, X, Y, and Z is displayed in these formulae in a rather simple fashion.

BIBLIOGRAPHY

Bateman, H., (1954), Tables of Integral Transforms, McGraw-Hill.

Cobine, J. D., (1958), Gaseous Conductors, Dover.

Kaplan, W., (1959), Advanced Calculus, 5th printing, Addision-Wesley.

Ratcliffe, J. A., (1959), The Magneto-Ionic Theory and Its Applications to the Ionosphere, Cambridge Press.

Churchill, R. V., (1960), Complex Variables and Applications, 2nd edition, McGraw-Hill.

Collins, R. E., (1960), Field Theory of Guided Waves, McGraw-Hill.

Harrington, R. F., (1961), Time Harmonic Electromagnetic Fields, McGraw-Hill.

Jordan, E. C., (1962), Electromagnetic Waves and Radiating Systems, 8th edition, Prentice-Hall.

Luke, Y. L., (1962), Integrals of Bessel Functions, McGraw-Hill.

Wilf, H. S., (1962), Mathematics for the Physical Sciences, Wiley and Sons.

Balmain, K. G., (1963), The Impedance of a Short Dipole Antenna in a Magnetoplasma, Antenna Lab. Report, E. E. Department, University of Illinois, May, 1963.

Wu, C. P., (1963), Radiation From Dipoles in a Magneto-Ionic Medium, IEEE Trans., PGAP, November, 1963.

Kostelnicek, R. J., (1964), The Admittance and Resonance Probe Characteristics of a Spherical Plasma Probe, M.S. Thesis, E. E. Department, University of Illinois.

Persson, K. B., (1964), The Brush Cathode Plasma - A Well - Behaved Plasma, NBS Rpt. No. 8452, September, 1964.

Duff, G. L., Mittra, R., (1965), The Input Impedance of a Small Loop of Electric Current in a Cold Anisotropic Plasma. Presented at the International Symposium on Antennas and Propagation, Washington, D.C., September, 1965. Also Electronics Letters, July, 1965.

Mittra, R., Duff, G. L., (1965), A Systematic Study of the Radiation Patterns of a Dipole in a Magnetoplasma Based on a Classification of the Associated Dispersion Surfaces. Vol. 69D, No. 5, May, 1965, Radio Science, NBS.

Duff, G. L., Mittra, R., (1965), Input Impedance of a Small Loop of Uniform Electric Current in an Anisotropic Cold Plasma, Electronics Letters, July, 1965, Vol. 1, No. 5.

Weil, H., Walsh, D., (1965), Radiation Resistance of an Elementary Loop Antenna in a Magneto-ionic Medium, IEEE, PGAP, Ap. 13, No. 1, pp. 21-26, 1965.

VITA

The author, Graham Lyman Duff, was born on August 28, 1939 in Montreal, in the Province of Quebec, Canada.

After completion of Ontario Senior Matriculation in 1957, he entered McGill University in the Department of Electrical Engineering. He graduated in 1961 with First Class Honours, ranking 4th in a class of 103, and received the degree of Bachelor of Engineering (B. Eng.) in Electrical Engineering. During his undergraduate years at McGill, he was elected to the Honorary Engineering Fraternity at McGill University as well as to the Scarlet Key Society, an honorary men's society at McGill University. He was also elected Vice-President of his chapter of the Psi Upsilon Fraternity.

With the help of a four year Province of Quebec Scholorship, the author entered the University of Illinois Graduate School in 1961 in the Department of Electrical Engineering and received the degree of Master of Science (M. S.) in 1963. He then continued in his studies and received the Ph. D. degree in Electrical Engineering in 1966. While at the University of Illinois, the author worked as a Research Assistant and a Teaching Assistant.

In 1966 the author accepted a three year appointment as Assistant Professor in the Department of Electrical Engineering at the University of Washington, Seattle, Washington.

The author's general field of interest is in electromagnetic theory and experiments.

The following is a list of publications and papers by the author.

Dyson, J. D. and Duff, G. L. (1963), Near Field Measurement on the Conical Logarithmic Spiral Antenna. A paper presented at the 1963 PTGAP International Symposium, July, 1963, Boulder, Colorado.

Mittra, R. and Duff, G. L. (1964), A Classification of the Dispersion Surfaces in a Magneto-Ionic Medium and a Study of the Associated Radiation Patterns. Scientific Report No. 2, E. E. Department, University of Illinois.

Mittra, R. and Duff, G. L. (1965), A Systematic Study of the Radiation Patterns of a Dipole in a Magnetoplasma Based on a Classification of the Associated Dispersion Surfaces. Vol. 69D, No. 5, May 1965, Radio Science, NBS.

Duff, G. L. and Mittra, R. (1965), Input Impedance of a Small Loop of Uniform Electric Current in an Anisotropic Cold Plasma Electronics Letters, July, 1965, Vol. 1, No. 5.

Duff, G. L. and Mittra, R. (1965), The Input Impedance of a Small Loop of Uniform Electric Current in an Anisotropic Cold Plasma, A paper presented at the 1965 International Antenna and Propagation Symposium, Washington, D.C., September, 1965.